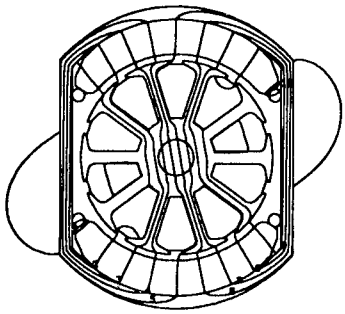

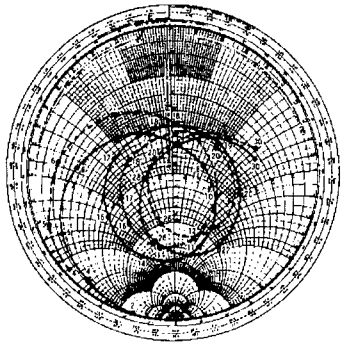

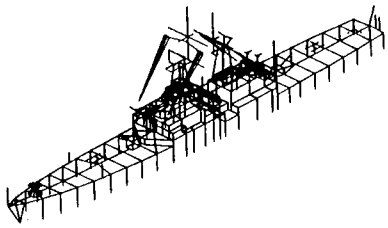

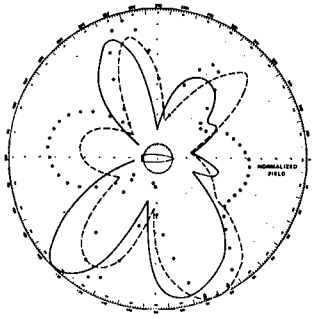

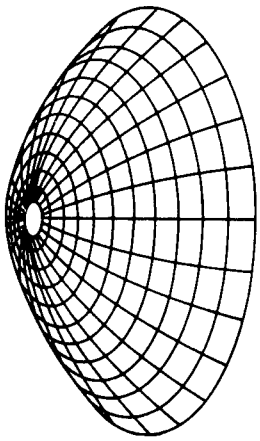

APPLIED COMPUTATIONAL ELECTROMAGNETICS SOCIETY JOURNAL

SPECIAL ISSUE ON GENETIC ALGORITHMS

GUEST EDITORS
RANDY HAUPT
AND
J. MICHAEL JOHNSON

2000
Vol. 15 No. 2

ISSN 1054-4887

GENERAL PURPOSE AND SCOPE. The Applied Computational Electromagnetics Society Journal hereinafter known as the ***ACES Journal*** is devoted to the exchange of information in computational electromagnetics, to the advancement of the state-of-the-art, and to the promotion of related technical activities. A primary objective of the information exchange is the elimination of the need to "re-invent the wheel" to solve a previously-solved computational problem in electrical engineering, physics, or related fields of study. The technical activities promoted by this publication include code validation, performance analysis, and input/output standardization; code or technique optimization and error minimization; innovations in solution technique or in data input/output; identification of new applications for electromagnetics modeling codes and techniques; integration of computational electromagnetics techniques with new computer architectures; and correlation of computational parameters with physical mechanisms.

SUBMISSIONS. The ***ACES Journal*** welcomes original, previously unpublished papers, relating to **applied computational electromagnetics**.

Typical papers will represent the computational electromagnetics aspects of research in electrical engineering, physics, or related disciplines. However, papers which represent research in **applied computational electromagnetics** itself are equally acceptable.

Contributions may be sent to the Editors-in-Chief, Dr. Ahmed Kishk or Dr. Allen Glisson

Department of EE
University of Mississippi
University, MS, 38677 USA
Phone: 601-232-5385 (Ahmed)
Phone: 601-232-5353 (Allen)
Fax: 601-232-7231
email:ahmed@olemiss.edu
email:aglisson@mail.olemiss.edu. See "Information for Authors" on inside of back cover.

SUBSCRIPTIONS. All members of the Applied Computational Electromagnetics Society (**ACES**) who have paid their subscription fees are entitled to receive the ***ACES Journal*** with a minimum of three issues per calendar year.

Visit us on line at: www.emclab.umr.edu/aces, and http://aces.ee.olemiss.edu

Back issues, when available, are $15.00 each. Subscriptions to **ACES**, orders for back issues of the ***ACES Journal*** and changes of addresses should be sent to:

Dr. Richard W. Adler
ACES Executive Officer
ECE Department, Code ECAB
Naval Postgraduate School
833 Dyer Road, Room 437
Monterey, CA 93943-5121 USA

Allow four week's advance notice for change of address. Claims for missing issues will not be honored because of insufficient notice or address change or loss in mail unless the secretary is notified within 60 days for USA and Canadian subscribers or 90 days for subscribers in other countries, from the last day of the month of publication. For information regarding reprints of individual papers or other materials, see "Information for Authors".

LIABILITY. Neither ACES or the ***ACES Journal*** editors are responsible for any consequence of misinformation or claims, express or implied, in any published material in an ***ACES Journal*** issue. This also applies to advertising, for which only camera-ready copies are accepted. Authors are responsible for information contained in their papers. If any material submitted for publication includes material which has already been published elsewhere, it is the author's responsibility to obtain written permission to reproduce such material.

APPLIED COMPUTATIONAL ELECTROMAGNETICS SOCIETY Journal

July 2000
Vol. 15 No. 2

ISSN 1054-4887

The ACES Journal is abstracted in INSPEC, in Engineering Index, and in DTIC.

The second, third, fourth, and fifth illustrations on the front cover have been obtained from Lawrence Livermore National laboratory.

The first illustration on the front cover has been obtained from FLUX2D software, CEDRAT S.S. France, MAGSOFT Corporation, New York.

THE APPLIED COMPUTATIONAL ELECTROMAGNETICS SOCIETY

JOURNAL EDITORS

EDITORIAL

Randy Haupt
Utah State University
ECE Department
4120 Old Main Hill
Logan, UT 84322-4120
haupt@ieee.org
435-797-2841

J. Michael Johnson
North Shore Associates
153 Antigua Court
Reno, NV 89511
jmjohnson@ieee.org
775-849-3085

We are happy to present a special issue of the ACES Journal on Genetic Algorithms and hope readers enjoy the interesting applications presented. The first paper uses a GA to design low sidelobe nonuniformly spaced arrays over a wide bandwidth. The next paper shows the power of the evolutionary algorithms applied to five design examples in integrated optics, optical communication technology, and dielectric, and dielectric material modeling. Paper number three explains how to apply a genetic algorithm to find the weightings in an array to generate a plane wave in the near field of a planar array. The fourth paper shows how a hybrid GA/local optimizer can reduce the number of function calls needed in the optimization of wire antennas via a method called clustering. A fifth paper proves that a parallel GA provides an excellent solution to the problem of bandwidth reduction of sparse matrices encountered in computational electromagnetics. Finally, a controversial paper is included that advocates the use of small population sizes and relatively high mutation rates for optimization with GAs. We would like to thank the authors for their response to this very fast publication deadline.

Introduction to Genetic Algorithms in Electromagnetics

Randy L. Haupt
Utah State University
Electrical and Computer Engineering
4120 Old Main Hill
Logan, UT 84322-4120
Haupt@ieee.org
435-797-2841

This special issue of the ACES Journal is devoted to new developments in Genetic Algorithm (GA) applications in computational electromagnetics. Genetic Algorithms have become extremely popular in the computational electromagnetics literature. The papers included in this special issue are very arcane, so I decided to include an unreviewed tutorial overview at the last minute as an introduction for those of you who are at a more basic level. GAs model natural selection and genetics on a computer to optimize a wide range of problems. Some of the advantages of a genetic algorithm include that it

- Optimizes with continuous or discrete parameters,
- Doesn't require derivative information,
- Simultaneously searches from a wide sampling of the cost surface,
- Deals with a large number of parameters,
- Is well suited for parallel computers,
- Optimizes parameters with extremely complex cost surfaces,
- Provides a list of semi-optimum parameters, not just a single solution,
- May encode the parameters so that the optimization is done with the encoded parameters, and
- Works with numerically generated data, experimental data, or analytical functions.

These advantages have inspired many people working in computational electromagnetics. For a nice historical development of applications of genetic algorithms in electromagnetics, see [1].

A genetic algorithm is relatively simple compared to many of the local optimizers used. As an example, consider the very simple MATLAB code presented in [2]:

```
% This is a simple binary GA

N=8;      % # bits in a chromosome
M=16;     % # chromosomes
last=20;  % # generations
M2=M/2;

% creates initial population
chromo=round(rand(M,N));

for ib=1:last

   ************************
   * insert subroutine to calculate
   * objective function output
   *   cost=function(chromo)
   *   cost is a Nx1 array
   ************************

   % ranks results and chromosomes
```

```
    [cost,ind]=sort(cost);
    chromo=chromo(ind(1:M2),:);

    %mate
    cr=ceil((N-1)*rand(M2,1));

    % pairs chromosomes
    % performs crossover
    for ic=1:2:M2
chromo(M2+ic,1:cr)=chromo(ic,1:cr);
chromo(M2+ic,cr+1:N)=chromo(ic+1,cr+1:N);
chromo(M2+ic+1,1:cr)=chromo(ic+1,1:cr);
chromo(M2+ic+1,cr+1:N)=chromo(ic,cr+1:N);
    end

    %mutate
    ix=ceil(M*rand);
    iy=ceil(N*rand);
    chromo(ix,iy)=1-chromo(ix,iy);

end %last
```

This small code has inspired many people to try genetic algorithms and is given to students taking a computational electromagnetics course at Utah State University. If you have never tried a GA, then this one is a good starter program.

Figure 1 shows the components of a GA. Compare this approach to a typical line search approach shown in Figure 2. The GA usually loses to a local optimizing line search in a race to the bottom of a bowl. On the other hand, the GA has the ability to jump out of a bowl into another bowl within the search area whereas a line search is much more constrained. Often times a local optimizer is worth using after a GA finds the bowl containing the desired minimum.

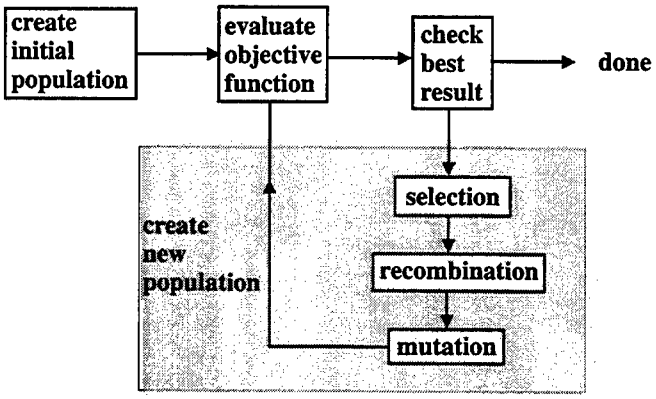

Figure 1. Flow chart of a genetic algorithm. Numerical simulation of genetics and evolution occurs in the gray box.

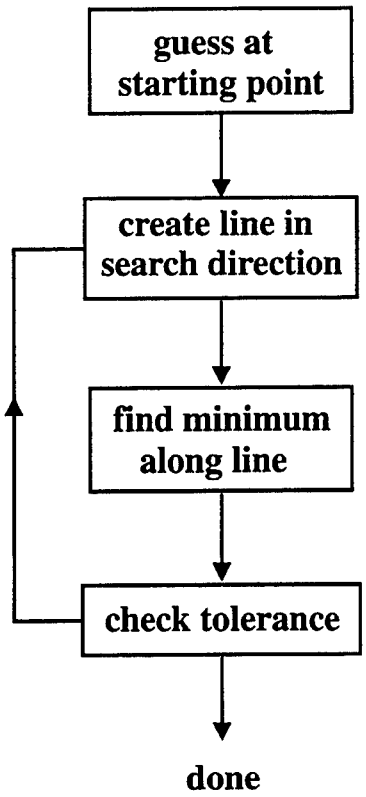

Figure 2. Flow chart of a typical line search optimizer.

A GA can work with either continuous parameters or binary encodings of the continuous parameters. In some cases, the parameters are naturally binary. In either case, the GA begins by creating a random set of parameters called a population. Each member of the population is a chromosome and contains all the information necessary as an input to an objective function that creates an output of interest. This first part is a random search. Next, the algorithm enters the gray box in Figure 2. Here, parents are selected to generate offspring by taking part(s) of one chromosome parent selected and combining with part(s) of one or more other parents. Natural selection occurs by weighting the probability of a chromosome being selected as a parent in proportion to its fitness. Also, inferior solutions or chromosomes with low fitness values are usually discarded from the population. Finally, random mutations are introduced to the population by randomly changing parameter values or bits in the binary encoding.

For the reader interested in pursuing introductory material on genetic and evolutionary programming, see the nice articles by Fogel [3] and Holland [4]. Goldberg has been a leader in the field and his book [5] is an excellent overview. For a practical introduction with a more tutorial, handholding approach to writing and using GAs see [6].

[1] D.S. Weile and E. Michielssen, "Genetic algorithm optimization applied to electromagnetics: a review," IEEE AP-S Trans., Vol. 45, No. 3, Mar 97, pp. 343-353.
[2] R.L Haupt, "An introduction to genetic algorithms for electromagnetics," IEEE Antennas and Propagation Magazine, Vol. 37, No. 2, Apr 95.
[3] D.B. Fogel, "Evolutionary computing," IEEE Spectrum, Vol. 37, No. 2, Feb 00, pp. 26-32.
[4] J.H. Holland, "Genetic algorithms," Sci. Am., Jul 92, pp. 66-72.
[5] D.E. Goldberg, *Genetic Algorithms in Search, Optimization, and Machine Learning*, Reading, MA: Addison-Wesley, 1989.
[6] R.L. Haupt and S.E. Haupt, *Practical Genetic Algorithms*, New York: John Wiley & Sons, 1998.

THE APPLIED COMPUTATIONAL ELECTROMAGNETICS SOCIETY

JOURNAL

SPECIAL ISSUE ON GENETIC ALGORITHMS

Vol. 15 No. 2 July 2000

Editorial - Randy L. Haupt and J. Michael Johnson

Introduction to Genetic Algorithms in Electromagnetics - Randy Haupt

---

SPECIAL ISSUE PAPERS

REGULAR PAPERS

A Genetic Algorithm Optimization Procedure for the Design of Uniformly Excited and Nonuniformly Spaced Broadband Low Sidelobe Arrays

Brian J. Barbisch
The Pennsylvania State University
Applied Research Laboratory
P.O. Box 30
State College, PA 16804-0030

D. H. Werner
The Pennsylvania State University
Department of Electrical Engineering
211A Electrical Engineering East
University Park, PA 16802
dhw@psu.edu

P. L. Werner
The Pennsylvania State University
Department of Electrical Engineering
University Park, PA 16802
plw7@psu.edu

ABSTRACT. This paper presents a systematic methodology for designing uniformly excited broadband low sidelobe linear and planar antenna arrays by varying interelement spacings. In the past, attempts to develop a robust array broadbanding design technique have been only marginally successful because of the large number of possible spacing combinations involved, coupled with the theoretical limitations surrounding the problem. The genetic algorithm (GA) has recently proven to be a very effective design tool for nonuniformly spaced low sidelobe antenna arrays with uniform excitation intended for operation at a single frequency. This paper introduces an approach for extending previous applications of GA to include the design of optimal low sidelobe arrays that are operable over a band of frequencies. In addition, it will be demonstrated that designing for low sidelobe operation over a bandwidth adds significant array steerability that can be described by a simple mathematical relation. Finally, it will be shown that the GA objective function is no more complicated to evaluate for broadbanding purposes than it is in the single frequency case. Several examples of GA-designed broadband low sidelobe arrays will be presented and discussed.

1. Introduction

In recent years, genetic algorithms have found a fairly strong presence in electromagnetics optimization problems involving antenna design. The difficulty in solving many antenna design problems is that very often there are many parameters and no practical analytical methods available to optimally determine them. Such difficulties make robust search strategies, like genetic algorithms, very important. The main advantages of using the GA over other search strategies are: 1) the GA can search from any number of random points to find a solution, 2) the GA works with a coding of the parameters and not the actual parameters, 3) GA's use random, not deterministic, transition rules, and 4) the GA does not require the evaluation of derivatives [1]. Several books have been written which discuss genetic algorithms and demonstrate many useful applications [2-4]. Among the first applications of genetic algorithms in antenna design was the thinning of large arrays [1]. Some other varieties of antenna arrays to which the GA has been applied include planar arrays [1,5], multiple beam arrays [6], and Yagi-Uda arrays [7]. There have also been several excellent review articles and books written about GA's and their application to solving complex engineering electromagnetics problems [4], [8-11].

The capability of GA's to produce optimal low sidelobe designs for linear arrays of uniformly excited isotropic sources (at a single frequency) by allowing only the interelement spacings to vary was first demonstrated in the pioneering work of [8]. Interelement spacings were decided by using a 3 bit parameter such that they could vary in increments of $\lambda/8$ with a minimum interelement spacing of $\lambda/4$. In this paper, we will demonstrate that GA's are also an extremely useful tool for broad-banding of uniformly excited, unequally spaced antenna arrays. There are three major advantages of the technique employed in this paper when compared to previously published methods, such as those described in [8]. These advantages are that 1) a much finer discretization ($\approx \pm 0.01\,\lambda$) will be used, 2) the GA-designed

arrays will have minimal sidelobes over a band of frequencies instead of at just one frequency, and 3) these arrays will typically have a much wider angular region over which the main beam can be steered compared to those optimized for low sidelobe performance at a single frequency. The steady-state genetic algorithm with uniform crossover [12] was chosen for use in optimizing the array designs discussed in this paper.

Although many traditional analytical techniques exist for placing elements in unequally spaced arrays for broad-banding purposes, *viz.* [13-15], none of these methods are capable of producing significantly low sidelobe levels over the entire band. The focus of many of these methods is to place elements in an array such that the minimum separation between elements is greater than or even much greater than a wavelength. The advantage of such large interelement spacings is that a larger bandwidth can be achieved because a lower minimum frequency is possible. The disadvantage, however, is that a theoretical lower bound exists on the sidelobe level when average interelement separations exceed a wavelength [16]. This theoretical minimum is usually not low enough for practical applications. Keeping in mind this theoretical limitation, a design optimization technique will be introduced in this paper which attempts to place elements such that the average interelement spacing in the array is always less than a wavelength.

Another important consideration in the design of antenna arrays is their steerability. Broad-band arrays have the property that they may exhibit perfect steerability at lower frequencies of operation, but steerability is reduced when moving to higher frequencies. The fact that steerability changes with frequency can be quantified by the bandwidth-steerability product of the array [16].

A useful conversion factor will be introduced in Section 2 that permits design tradeoffs to be made between bandwidth and (minimum) element separation. Steerability issues will also be briefly discussed in Section 2. Section 3 begins by considering an example of an optimized low-sidelobe array design intended for operation at a single frequency. Following this, four examples of genetic algorithm produced broadband low sidelobe array designs are presented and discussed– two linear arrays (Section 3) and two planar arrays (Section 4). In addition, the GA objective function used to produce each design is given in the respective sections. All array designs considered in this paper were specified to have a maximum possible bandwidth with a minimum element separation of $\lambda/4$ and the lowest possible sidelobe level throughout the band.

2. Some Considerations for Broad-Banding Arrays

In designing a broadband array for low sidelobe performance, it is sufficient to design for the highest desired frequency of operation f_2. Having done this, the frequency may then be varied from f_2 to any f_1, provided $f_1 \le f_2$, without the appearance of any higher sidelobes. The bandwidth for such an array is defined to be $B = f_2 / f_1$. Furthermore, we note that if a minimum separation between two elements exists at the lowest design frequency f_1 that is considered too small for practical purposes, then that spacing can be made larger at the expense of a smaller bandwidth $B' < B$ (i.e., $f_2' < f_2$). This property is best illustrated by the following useful transformation:

$$s' = \left(\frac{f_2}{f_2'}\right) s = \left(\frac{B}{B'}\right) s \qquad (1)$$

where

$B' = f_2' / f_1$

s = the set of original element locations $\{s_n = d_n \lambda_1 : n = 1,2,...,N\}$

s' = the set of new element locations $\{s_n' = d_n' \lambda_1 : n = 1,2,...,N\}$

Hence, the array configuration need only be optimized for a desired maximum bandwidth B, subject to some specified tolerance on the minimum element separation. Once this optimal array design has been found using the GA then, if desired, the transformation given in (1) may be employed to find modified designs which tradeoff larger element separations for smaller operating bandwidths.

Another notable characteristic of broadband arrays is how steerability is affected with increasing bandwidth. It can be shown that the bandwidth and steerability of a linear array are related by the following formula, which is known as the bandwidth-steerability product [15]:

$$B(1+\cos\theta_0) = \frac{2w_0}{d_{ave} / d_{\min}} \qquad (2)$$

where

B = bandwidth

θ_0 = steering angle

w_0 = the maximum value of $(d_{ave} / \lambda)\cos\theta$ that can be used before a sidelobe will exceed the desired sidelobe level

d_{ave} = average interelement separation in the array

d_{min} = smallest interelement separation in the array

The right-hand side of this equation is a constant, and is characteristic of the individual array. Note that at a 1:1 bandwidth, the right-hand side of the equation must be at least two to guarantee perfect steerability. When a bandwidth of larger than 1:1 is desired, the left-hand side of this equation limits steerability at some of the higher frequencies in the band. Thus, while a broadband array may exhibit perfect steerability at lower frequencies of operation, steerability may become limited at higher frequencies of operation. In addition, arrays designed to operate at only one frequency when interelement spacings are small may not exhibit any steerability.

3. Linear Broadband Array Designs

The array factor expression for the far-field radiation pattern of a symmetric linear array of isotropic sources can be written in the following form:

$$AF(\theta) = 2\sum_{n=1}^{N} I_n \cos[2\pi(f/f_1)d_n \cos\theta + \alpha_n] \quad (3)$$

where

$$\alpha_n = -2\pi(f/f_1)d_n \cos\theta_0 \quad (4)$$

and

$2N$ = the total number of elements in the array

I_n = excitation current amplitude of the nth element in the array

α_n = excitation current phase of the nth element in the array

$s_n = d_n \lambda_1$ = total distance of the nth element from the origin (note that the parameter d_n is unitless)

θ = angle measured from the line passing through antenna elements

θ_0 = steering angle

f_1 = base (minimum) frequency of operation

f = desired frequency of operation

The objective function used by the GA in this paper is based on the array factor expression given in (3), where the desired goal is to minimize the maximum relative sidelobe level (RSLL) of the array over some prescribed bandwidth. In other words, each gene has an associated RSLL calculated from

$$F(\theta) = \max\left|2\sum_{n=1}^{N} I_n \frac{\cos[2\pi B d_n \cos\theta]}{AF_{max}(\theta)}\right| \quad (5)$$

where

$AF_{max}(\theta)$ = peak of the main beam (for normalization)

$B = f_2/f_1$ = desired bandwidth of the array ($f_2 \geq f_1$)

The parameters d_n were selected by the GA to minimize the maximum sidelobe level with I_n set to unity for all values of n. The discretization of d_n was made relatively fine, such that it could be varied in increments of approximately ±0.01 between zero and some maximum selected value. The use of any finer discretization was found to yield little improvement in the overall results. It was also found that, in the case of broadband array optimization ($B>1$), the GA objective function need not be any more complicated to evaluate than it is for optimization of array performance at a single frequency ($B=1$). This is one of the attractive features of the technique presented here, since it means that the overall design optimization time required by the GA will be essentially the same regardless of whether single-frequency or broadband array configurations are being considered.

Previous attempts to design low sidelobe linear antenna arrays using the GA have been limited to operation at a single frequency (i.e., for $B=1$) [1,5]. The GA approach introduced in this paper is also able to produce low sidelobe designs for $B=1$ as a special case of a more general procedure which is valid for $B>1$. For example, given a uniformly excited 40 element array with a minimum element separation requirement of a quarter-wavelength (i.e., $\Delta_n = (d_{n+1} - d_n) \geq 0.25 \ \forall\, n = 1,2,\ldots,N-1$), the GA was able to generate an array with maximum sidelobe levels as low as –28.86 dB (see Figure 1a). Figure 1b shows the array factor of the same array with the main beam steered from 90^0 (broadside) to 91^0. Notice that steering the beam by even such a small amount as 1^0 in this case causes sidelobes to rise above the broadside maximum sidelobe level of –28.86 dB. This property is a direct consequence of the fact that the array is not designed to operate over a significant bandwidth, as predicted by the bandwidth-steerability product (2). It will be demonstrated in this paper, however, that significant steerability is possible for broadband arrays where $B>1$.

The first broadband design that will be considered is also a uniformly excited 40 element array. The minimum element separation requirement will be a quarter-wavelength at the lowest design frequency ($f = f_1$). In this case, the GA was able to optimize interelement spacings so that a bandwidth of $B = 3.5$ was possible for broadside operation with a maximum sidelobe level of -19.41dB throughout the entire band (see Table 1). Figures 2a–2c show plots of the array factor at the

low-band ($f = f_1$), mid-band ($f = (f_1 + f_2)/2$), and high-band ($f = f_2$) design frequencies. The radiation patterns of an un-optimized, uniformly spaced 40 element array at the same three frequencies are shown in Figures 3a-3c for comparison purposes. Note that, as expected, the

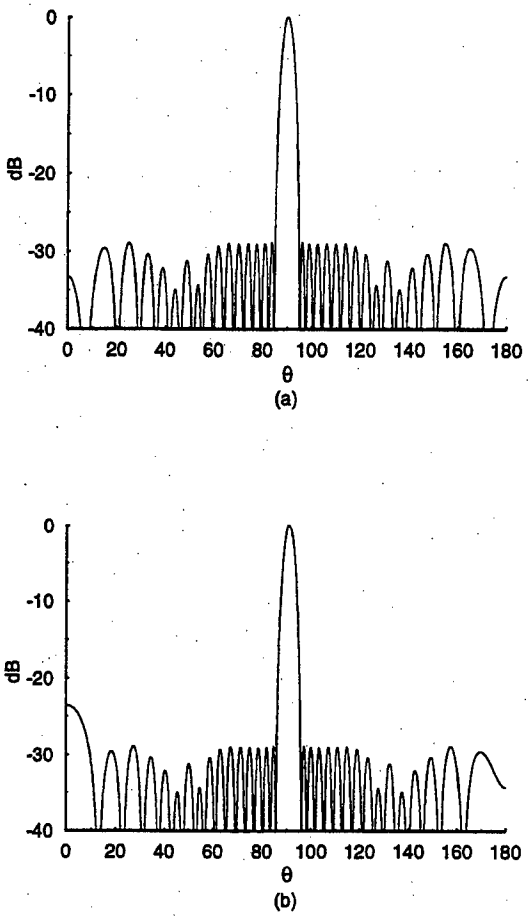

Figure 1. Array factor for a uniformly excited and nonuniformly spaced 40 element linear array of isotropic sources with (a) a broadside mainbeam and (b) the mainbeam steered to 91^0 (one degree from broadside). The maximum sidelobe level at broadside is –28.86 dB with a bandwidth of $B = f_2 / f_1 = 1$

maximum sidelobe level under these conditions is about –12.5 dB. In addition, Figures 4a-4c show the optimized 40 element array from Figures 2a-2c with the main-beam steered to 60^0 also at low-band, mid-band, and high-band design frequencies. These figures demonstrate that, for the low-band ($f = f_1$) and mid-band ($f = 2.25 f_1$) frequencies, it is possible to steer the main-beam to 60^0 without any increase in the synthesized sidelobe level. However, for the high-band frequency ($f = 3.5 f_1$), we see that the synthesized sidelobe level can no longer be maintained when the beam is steered to 60^0. Further investigation reveals, as predicted by (2), that there is almost no steerability for this array when $f = f_2 = 3.5 f_1$. The maximum frequency at which this array exhibits perfect steerability was found to be $f = 1.75 f_1$.

Table 1. Element separations at $f = f_1$ for the GA-optimized 40 element linear array (see Figures 2a-2c).

Element Number (n)	Element Separation (s_n / λ_1)	Element Number (n)	Element Separation (s_n / λ_1)	Element Number (n)	Element Separation (s_n / λ_1)	Element Number (n)	Element Separation (s_n / λ_1)
1	0.125	6	1.375	11	2.625	16	3.955
2	0.375	7	1.625	12	2.885	17	4.215
3	0.625	8	1.875	13	3.135	18	4.475
4	0.875	9	2.125	14	3.435	19	5.625
5	1.125	10	2.375	15	3.695	20	6.485

Table 2. Element separations at $f = f_1$ for the GA-optimized 100 element linear array (see Figure 5).

Element Number (n)	Element Separation (s_n / λ_1)	Element Number (n)	Element Separation (s_n / λ_1)	Element Number (n)	Element Separation (s_n / λ_1)	Element Number (n)	Element Separation (s_n / λ_1)
1	0.125	14	3.375	27	6.865	40	11.355
2	0.375	15	3.625	28	7.115	41	11.615
3	0.625	16	3.875	29	7.365	42	12.105
4	0.875	17	4.125	30	7.615	43	12.355
5	1.125	18	4.375	31	7.865	44	13.115
6	1.375	19	4.625	32	8.115	45	13.365
7	1.625	20	4.875	33	8.365	46	14.095
8	1.875	21	5.365	34	9.095	47	14.345
9	2.125	22	5.615	35	9.345	48	14.595
10	2.375	23	5.865	36	9.595	49	15.085
11	2.625	24	6.115	37	9.845	50	15.585
12	2.875	25	6.365	38	10.105		
13	3.125	26	6.615	39	10.865		

Larger sized arrays were found to be capable of producing wider bandwidths. For example, using $\lambda_1 / 4$ as the minimum nterelement separation for a 100 element array, it was possible to optimize the array configuration using the GA to yield a bandwidth of $B = 3.97$ and a maximum sidelobe level of -20.32 dB (see Figure 5 and Table 2). The maximum frequency at which this array is steerable to 60^0 is at $f=2.64f_1$, and the maximum frequency at which this array exhibits perfect steerability is at $f = 1.98 f_1$ (see Figure 6). If larger interelement spacings are desired, then (1) may be used to determine the corresponding reduction in bandwidth that would result. For instance, increasing the $\lambda_1 / 4$ minimum interelement separation to $0.49625\,\lambda_1$ reduces the bandwidth from 3.97 down to 2. On the other hand, the bandwidth of the array can be doubled to $B = 7.94$ by allowing the minimum element separations to be as small as $\lambda_1 / 8$. Reducing the minimum element separation to $\lambda_1 / 8$ also doubles the bandwidth over which the array is steerable – i.e., in this case the above array would be perfectly steerable over a bandwidth of $B = 3.96$ with a maximum sidelobe level of –20.32 dB.

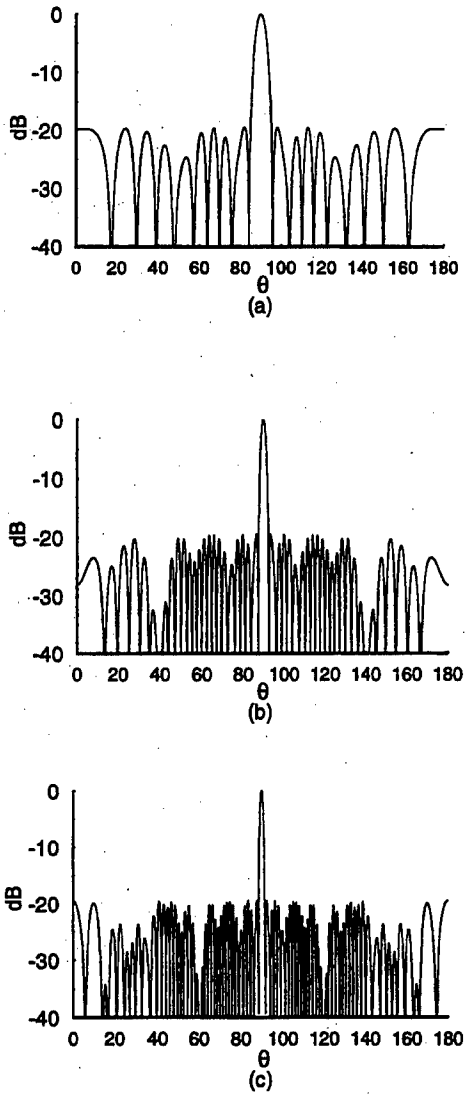

Figure 2. Plots of the array factor for an optimized broadside $(\theta_0 = 90^0)$ uniformly excited and nonuniformly spaced 40 element linear array of isotropic sources at (a) $f/f_1 = 1$, (b) $f/f_1 = 2.25$, and (c) $f/f_1 = 3.5$. The maximum bandwidth for this array is $B = f_2/f_1 = 3.5$.

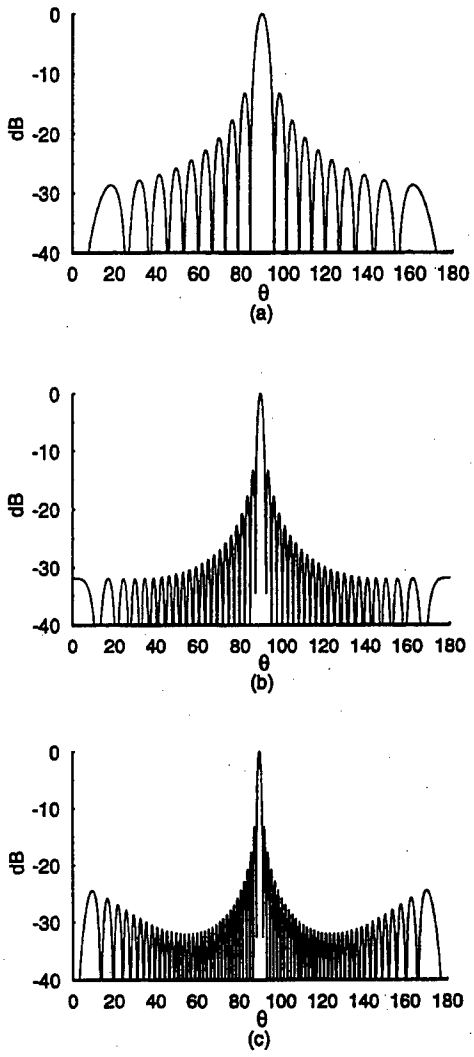

Figure 3. Plots of the array factor for a broadside $(\theta_0 = 90^0)$ uniformly excited and uniformly spaced 40 element linear array of isotropic sources at (a) $f/f_1 = 1$, (b) $f/f_1 = 2.25$, and (c) $f/f_1 = 3.5$.

4. Planar Broadband Array Designs

The GA optimization procedure described in the previous section for broadbanding linear arrays will be generalized in this section to include planar array configurations. In particular, the GA design approach will be developed for rectangular arrays as well as for concentric circular arrays with variable element spacings. The array factor for a non-uniformly spaced symmetric rectangular array of isotropic sources may be represented in the following form:

$$AF(\theta,\phi) = 4\sum_{n=1}^{N}\sum_{m=1}^{M} I_{mn}\cos[2\pi d_{xn}(f/f_1)\sin\theta\cos\phi] \cdot \cos[2\pi d_{ym}(f/f_1)\sin\theta\sin\phi] \tag{6}$$

where

$2M$ = total number of elements in the y-direction

$2N$ = total number of elements in the x-direction

$s_{xn} = d_{xn}\lambda_1$ = element locations in the x-direction with respect to the origin

$s_{ym} = d_{ym}\lambda_1$ = element locations in the y-direction with respect to the origin

The corresponding RSLL in this case is calculated from

$$F(\theta,\phi) = \max\left|4\sum_{n=1}^{N}\sum_{m=1}^{M} I_{mn}\frac{\cos[2\pi d_{xn}B\sin\theta\cos\phi]\cos[2\pi d_{ym}B\sin\theta\sin\phi]}{AF_{\max}(\theta,\phi)}\right| \tag{7}$$

The GA uses (7) to determine the set of parameters d_{xn} and d_{ym} that yields the lowest possible sidelobe level over a specified bandwidth *B*, assuming that the array is uniformly excited (i.e., $I_{mn} = 1$ for all values of m and n). In order to accomplish this, a spacing scheme was designed such that rows and columns were treated the same. For example, the GA selects a set of spacings $s = \{d_1, d_2, d_3, \ldots, d_n\}$, where n is the number of rows and columns in the array (i.e., $N = M = n$ where N and M are from (6)). The number d_i, $1 \le i \le n$, then represents the interelement spacing between elements (i, j) and $(i-1, j)$ and the elements (j,i) and $(j,i-1)$ $\forall j \ni 1 \le j \le n$, where the indices $(0, j)$ and $(j,0)$ are the y and x axes respectively. This scheme makes the objective function very simple to evaluate because the maximum sidelobe level will always be located in the $\phi = 0^0$ and $\phi = 90^0$ planes. Figures 7a-7c show radiation pattern cuts at $\phi = 0^0$, $\phi = 45^0$, and $\phi = 90^0$, respectively, for a 4,096 element array which was designed to produced a bandwidth of $B = 3.5$ and a maximum sidelobe level of –19.41dB with a minimum specified element separation of $\lambda_1 / 4$.

Next we will consider an alternative design optimization approach based on concentric circular arrays which results in a more spatially uniform distribution of sidelobes. The RSLL in this case is calculated from

$$F(\theta,\phi) = \max\left|\frac{\sum_{m=1}^{M}\sum_{n=1}^{N_m} I_{mn}\exp[j2\pi B a_m\sin\theta\cos(\phi-\phi_{mn})+j\alpha_{mn}]}{AF_{\max}(\theta,\phi)}\right| \tag{8}$$

where

$$AF(\theta,\phi) = \sum_{m=1}^{M}\sum_{n=1}^{N_m} I_{mn} \cdot \exp[j2\pi(f/f_1)a_m\sin\theta\cos(\phi-\phi_{mn})+j\alpha_{mn}] \tag{9}$$

$$\alpha_{mn} = -2\pi(f/f_1)\sin\theta_0\cos(\phi_0-\phi_{mn}) \tag{10}$$

and

$r_m = a_m\lambda_1$ = radius of the m*th* ring array

M = total number of concentric ring arrays

N_m = total number of elements in the m*th* ring

The spacing scheme was designed such that elements were placed on arcs spaced $\lambda_1 / 4$ apart, where λ_1 corresponds to the wavelength at the lowest design frequency f_1. In addition to this, the elements in each quadrant were assumed to be arranged symmetrically about their respective diagonal axis (e.g., the elements in the first quadrant are symmetric with respect to the $\phi = 45^0$ axis). Figure 8 shows one quadrant of a concentric circular array in the equally spaced case that could be constructed using this spacing scheme. For this example, the minimum arc length between any two consecutive array elements was set to $\lambda_1 / 4$. Figure 9 shows the radiation pattern produced over the $\phi = 45^0$ cut by a 308 element concentric circular array with element spacings optimized to yield a bandwidth of $B = 3.5$ with a maximum sidelobe level of –21.91dB throughout the band.

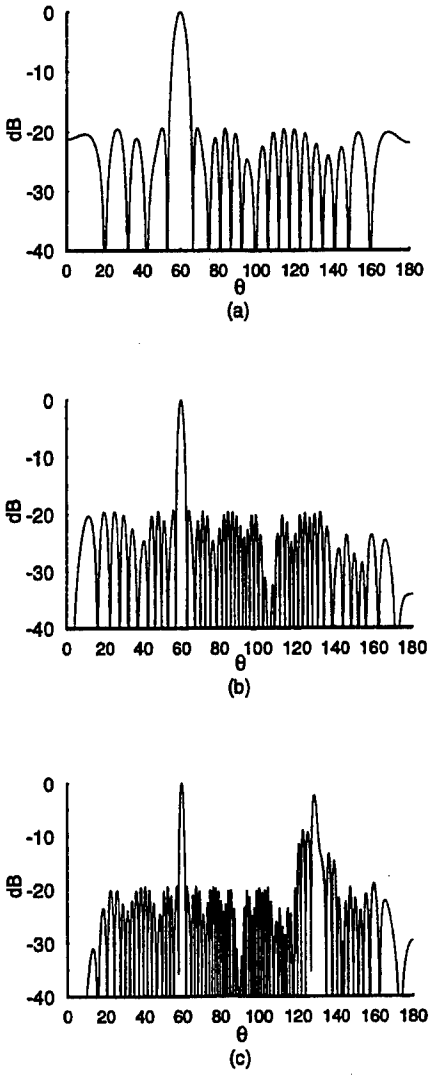

Figure 4. Plots of the array factor for an optimized uniformly excited and nonuniformly spaced 40 element linear array of isotropic sources with $\theta_0 = 60^0$ at (a) $f/f_1 = 1$, (b) $f/f_1 = 2.25$, and (c) $f/f_1 = 3.5$.

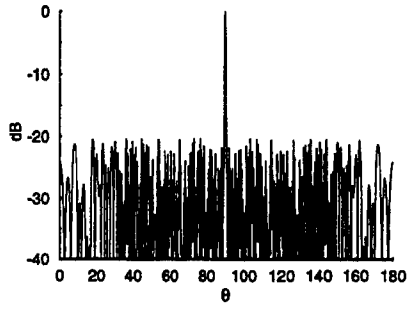

Figure 5. Array factor for an optimized uniformly excited and nonuniformly spaced 100 element linear array of isotropic sources with $f/f_1 = 3.97$.

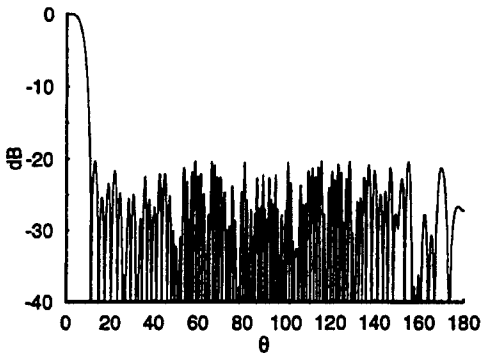

Figure 6. Array factor for an optimized uniformly excited and nonuniformly spaced 100 element linear array of isotropic sources with $\theta = \theta_0$ and $f/f_1 = 1.98$.

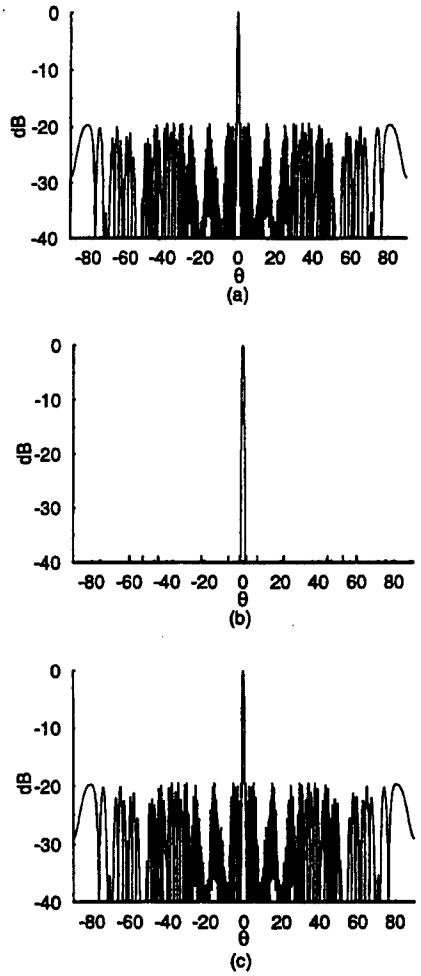

Figure 7. Radiation pattern cuts at $\phi = 0^0$ (Figure 7a), $\phi = 45^0$ (Figure 7b), and $\phi = 90^0$ (Figure 7c) of an optimized 4,096 element square planar array with $f/f_1 = 3.5$.

5. Conclusions

Uniformly excited array broad-banding has been achieved using a genetic algorithm optimization procedure with bandwidths as large as $B = 3.97$ for linear arrays and $B = 3.5$ for planar arrays with a minimum element separation of $\lambda_1/4$. Minimum element separation can easily be made larger to avoid mutual coupling effects, or it can be made smaller to increase bandwidth by using the convenient conversion factor given in (1). Array steerability issues have also been addressed in this paper. Steerability varies with operation frequency as predicted by (2) – it is greater at lower frequencies of operation and lesser at higher frequencies of operation. In addition, the bandwidth over which the array is steerable improves proportionally as (1) is used to increase bandwidth. It should also be noted that in order to include steerability within the optimization scenario (in the sense of a multi-objective constraints synthesis procedure), we could adopt a more general definition of the objective function that includes the right-hand side of (2). Finally, we point out that even lower sidelobe levels might be achieved in some cases by including the element pattern in the optimization scheme.

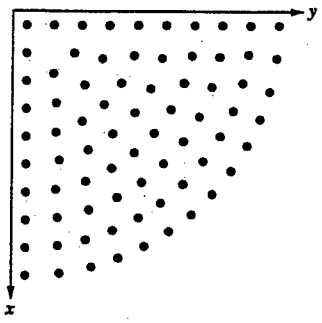

Figure 8. One quadrant of an equally spaced concentric circular ring array that is arranged symmetrically about its diagonal axis.

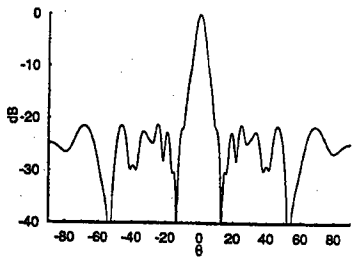

Figure 9. Radiation pattern cut at $\phi = 45^0$ for an optimized broadband concentric circular ring array with $f/f_1 = 3.5$.

References

[1] R. L. Haupt, "Thinned Arrays Using Genetic Algorithms," *IEEE Trans. Antennas Propagat.*, Vol. 42, No. 7, pp. 993-999, July 1994.

[2] D. E. Goldberg, *Genetic Algorithms: In Search, Optimization & Machine Learning*. New York: Addison-Wesley, 1989.

[3] L. Davis, Editor, *Handbook of Genetic Algorithms*. New York: International Thomson Computer Press, 1996.

[4] R. L. Haupt and S. E. Haupt, *Practical Genetic Algorithms*. New York: Wiley, 1998.

[5] D. Marcano and A. Nieto, "Genetic Algorithms for the Synthesis of Planar Arrays, "*USNC/URSI Radio Science Meeting Abstracts*, Baltimore, MD, USA, July 21-26, 1996, Vol. 1, pp. 584-587.

[6] D. Marcano, F. Durán, and O. Chang, "Synthesis of Multiple Beam Linear Antenna Arrays Using Genetic Algorithms," *1995 IEEE Antennas and Propagation Society International Symposium Digest*, Newport Beach, CA, June 1995, pp. 938-941.

[7] E. A. Jones and W. T. Joines, "Design of Yagi-Uda Antennas Using Genetic Algorithms," *IEEE Trans. Antennas Propagat.*, Vol. 45, No. 9, pp. 1386-91, September 1997.

[8] R. L. Haupt, "An Introduction to Genetic Algorithms for Electromagnetics," *IEEE Antennas and Prop. Magazine*, Vol. 37, No. 2, pp. 7-14, April 1995.

[9] M. J. Johnson and Y. Rahmat-Samii, "Genetic Algorithms in Engineering Electromagnetics," *IEEE Antennas and Propagation Magazine*, Vol. 39, No. 4, pp. 7-25, August 1997.

[10] E. Michielssen, D. Treyer and D. S. Weile, "The Application of Novel Genetic Algorithms to Electromagnetic Problems," Proceedings of the 13th Annual Review of Progress in Applied Computational Electromagnetics (ACES), Vol. 2, Monterey, CA, March 1997, pp.1382-1386.

[11] Y. Rahmat-Samii and E. Michielssen, *Electromagnetic Optimization by Genetic Algorithms.* New York: Wiley, 1999.

[12] G. Syswerda, "Uniform Crossover in Genetic Algorithms," *Proceedings of the Fifth International Conference on Genetic Algorithms,* pp. 2-9, 1988.

[13] D. D. King, R. F. Packard and R. K. Thomas, "Unequally-Spaced, Broad-Band Antenna Arrays," *IRE Trans. on Antennas Propagat.*, Vol. AP-8, No. 4, pp. 382-384, July 1960.

[14] A. Ishimaru and Y. S. Chen, "Thinning and Broadbanding Antenna Arrays by Unequal Spacings," *IEEE Trans. Antennas Propagat.*, Vol. AP-13, pp. 34-42, Jan. 1965.

[15] J. H. Doles III and F. D. Benedict, "Broad-Band Array Design Using the Asymptotic Theory of Unequally Spaced Arrays," *IEEE Trans. Antennas Propagat.*, Vol. 36, No. 1, January 1988.

[16] M. G. Andreasen, "Linear Arrays with Variable Interelement Spacings," *IRE Trans. Antennas Propagat.*, Vol. AP-10, pp. 137-143, March 1962.

APPLICATION OF EVOLUTIONARY OPTIMIZATION ALGORITHMS IN COMPUTATIONAL OPTICS

Daniel Erni[1,2], Dorothea Wiesmann[1,3], Michael Spühler[1,2], Stephan Hunziker[1,2], Esteban Moreno[1,2], Benedikt Oswald[2], Jürg Fröhlich[4] and Christian Hafner[2]

[1]*Optical Signal Processing Group* of the
[2]Laboratory for Electromagnetic Fields and Microwave Electronics,
and the [3]Electronics Laboratory,
Swiss Federal Institute of Technology, ETH-Zentrum,
Gloriastrasse 35, CH-8092 Zürich,
[4]Institute for Operartions Research, University of Zürich
Moussonstrasse 15, CH-8044 Zürich
contacts: erni@ifh.ee.ethz.ch

ABSTRACT – The spatial and spectral treatment of electromagnetic fields express an essential operation regarding, e.g., the functionality of dense integrated optical devices. Such molding of fields can hardly be handled without sophisticated heuristic optimization tools. By means of five design examples we have demonstrated that evolutionary algorithms (EA) are highly qualified to solve "real world" inverse problems considering various applications in the field of planar integrated optics, optical communication technology, and dielectric material modeling as well. In comparison to other optimization schemes EAs are even able to deliver structural and temporal information of the device under optimization which is an important feature when targeting computer guided engineering and virtual design platforms.

1. INTRODUCTION

Evolutionary algorithms (*EA*) [1] are computer codes which emulate the search process of natural evolution. This class of optimization algorithms rests upon the collective learning process within a population of individuals, each of which represents a search point in the space of potential solutions to the given problem. Because of an implicit parallelism in the search behavior they avoid the common pitfalls of local optimization algorithms, but hold the promise of finding novel solutions perhaps not thought to exist.

The latter aspect – i.e., the structural optimization feature – has successfully been applied to several different types of design problems in planar integrated optics [2], such as single longitudinal mode multi-cavity laser diodes [3], [5]-[10], ultra-short non-periodic segmented spot-size converters for highly efficient chip-to-fiber coupling [9]-[13] and concatenated Bragg gratings for apodized add/drop filters in wavelength division multiplexing (*WDM*) network nodes [14]. In earlier contributions [15], [16], *evolutionary algorithms* have also been considered as very efficient regarding their *parameter estimation* features in the context of speeding up costly computational electromagnetics simulations. They have also been applied when optimizing frequency channel distributions in fiber optic *SCM*-links [17] and for the determination of analytical dispersion models for complex and highly lossy dielectric materials [18].

In the paper presented here, we will outline all design examples mentioned above. Therefore, the remainder of the paper is organized as follows: In Section 2, we briefly explain our special type of *evolutionary algorithm* which is then used for the optimization of an active waveguide device namely a non-periodic coupled-cavity semiconductor laser diode. Section 3 is dedicated to the design of realistic apodized concatenated Bragg gratings as highly selective add/drop filters for wavelength division multiplexing (*WDM*) applications. The spatial treatment of guided modes by a non-periodically segmented waveguide structure leading to a very compact and efficient spot-size converter is reported in Section 4. Section 5 describes the optimization of frequency channel distributions in fiber optic *SCM*-links and the determination of an analytical dielectric material model is given in Section 6.

After these elucidations, a brief outlook is given, focusing on some algorithmic prospects (Section 7) and tracing two aspects towards computer guided engineering (Section 8) as well. We conclude our contribution with a short summary in Section 9.

2. MULTI-CAVITY LASER TOPOLOGIES

An economically priced monolithic GaAs/AlGaAs laser diode with an emission wavelength around *852 nm* represents an attractive light source for low-cost high-precision time and distance metrology. Such single-longitudinal-mode laser operation usually relies on distributed Bragg reflector (*DBR*) laser topologies or distributed feedback (*DFB*) lasers respectively. Both utilize a fine-scale grating mostly having periods on the orders of a few hundred nanometers. This puts high demands even on the state-of-the-art lithographic reproduction, resulting in very high costs.

In order to focus on simple laser processing, we restrict our design to large-scale non-periodic perturbations in the form of multi-section cavity structures. Such irregular topologies are now to be optimized with respect to given laser specifications.

The type of *breeder genetic algorithm* (see also [4]) presented here works on fixed-length bit-strings. It starts by initializing a population of $N = 50$ bit-strings randomly. Then the population evolves by using probabilistic *genetic operators* for reproduction purposes. Within this frame, two parent-strings are selected by the *fitness*-proportional *roulette-wheel selection* process. Two off-spring are then generated using *two-point crossover* and *mutation*. Referring to the forward problem a laser simulator is activated, delivering all characteristic data needed for the quality

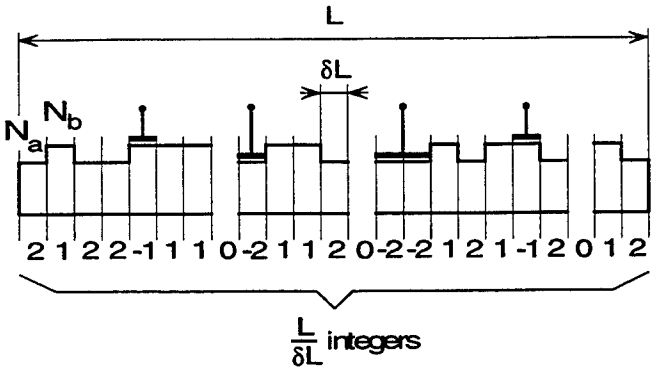

Fig.1: Representation of the non-periodic multi-cavity laser structure (phenotyp) by a 5-valued integer string (genotyp) including contact electrodes for current injection.

rating of each off-spring. After judging the quality (*fitness*) of these new individual two advantageous aspects of our implementation should be mentioned [5], [6]: *1.)* every new individual is checked whether it is already included in the population. Allowing no duplicates guarantees a certain diversity and avoids premature convergence. *2.)* only better individuals than the worst enclosed in the population are inserted, e.g., a *strict breeding* is done. The whole reproduction process defines a loop which is carried out until the number of calculated individuals reaches a certain predefined value.

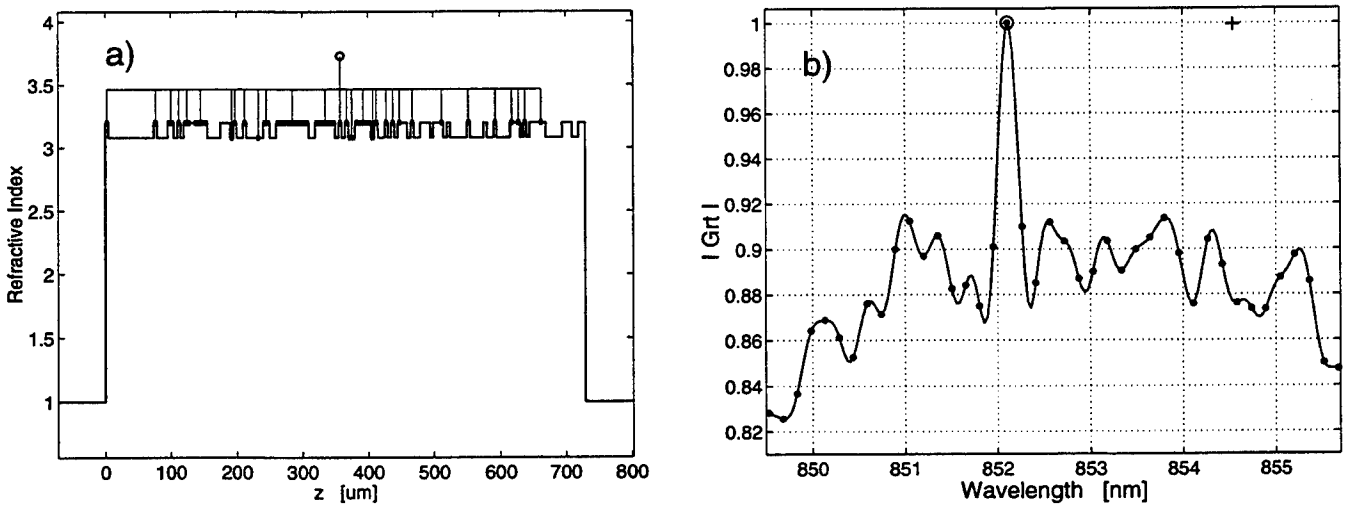

Fig.2: Best performing laser solution. a) The effective refractive index distribution along the cavity shows 59 sections at a total length of 730 μm. The position of current injection is sketched by its corresponding electrode (labeled as a bold line). b) Corresponding round-trip gain spectrum G_{rt}. Lasing occurs at the circle, all round-trip phase zeros are marked with dots and the small cross indicates the material gain maximum. The distinct mode selectivity should be considered in the context of the very low effective refractive index contrast of the perturbed laser cavity.

In order to judge the quality of each search point a *fitness* value has to be defined, relying on the forward solver's specific output. As the main validation criterion within all further simulations the round-trip gain G_{rt} is taken in terms of a potential mode-selectivity at lasing threshold. The round-trip gain G_{rt} represents the oscillation condition itself. According to our laser structure, the overall *fitness* is defined as a sum of three different *fitness* numbers: one concerns the side-mode suppression within the round-trip gain spectrum. A second term validates the coincidence between the position of the material gain peak and the specified wavelength of *852 nm*. The third term measures the wavelength-difference between the lasing point and this specification.

Following [8], a *representation scheme* (*Fig.1*) of the multi-cavity laser structures is obtained using a fine-scale discretization. Assuming a maximal laser length of $L = 1000\ \mu m$ and a discretization's resolution of $\delta L = 5\ \mu m$, the laser topology can be described as an array with $L/\delta L = 200$ integers each representing one segment within the potential laser cavity. Each segment having an effective refractive index N_a or N_b is assigned to an integer value of *2* or *1* respectively. A *"don't care"* represented by an integer value of *0* does not influence the decoding operation when mapping the integer array (*genotype*) into its corresponding physical representation (*phenotype*).

In combination with genetic operators such as *crossover* and *mutation* the optimization procedure has the ability to build up lasers with different lengths. Further we allow the optimizer to *"decide"* how the current injection into the laser structure has to be performed when searching for appropriate numbers and positions of contact electrodes. A contacted segment may simply be marked by a reversed sign of its corresponding integer (*allele*) leading to a 5-valued *genotype* and therefore to a tremendous large search space of $200^5 \approx 10^{140}$ search points.

The performance of the multi-cavity laser structure is evaluated by applying the well known transfer-matrix analysis [19]. All material properties involved such as material gain and the carrier induced refractive index change are obtained from optical gain measurements and are implemented as an appropriate spectral model [5]. The effective refractive index difference representing the perturbation is assumed $1.92 \cdot 10^{-2}$.

Our optimization scenario [8] after *33'720* evaluated individuals yields a maximal performing structure (*Fig.2a*) with a *fitness* of $1.056875 \cdot 10^6$. The spread of *fitness* values within the optimized population is around *4%*. It should be noted that good solutions (*fitness* $> 4 \cdot 10^5$) are already achieved after less than *700* iterations. The round-trip gain spectrum G_{rt} of the best performing laser structure (*Fig.2b*) shows the desired distinct wavelength selectivity permitting single longitudinal mode lasing operation at *852.10 nm*. Here the current injection reaches a threshold value of *11.98 mA* when lasing.

3. CONCATENATED GRATING FILTERS

Wavelength division multiplexing (*WDM*) at wavelengths of *1520-1570 nm* in optical fiber networks for, e.g., *2.488 Gb/s* data rates demands (integrated) optical filters for adding and dropping single wavelength channels at certain network nodes. Bragg grating based filters become very attractive, when the requirements for intra-channel crosstalk are stringent. Unfortunately, uniform Bragg gratings suffer from poor sidelobe suppression in their spectral response. If only a certain inter-channel crosstalk, i.e. a certain sidelobe level at the neighboring channel, is allowed the high sidelobe results in a large channel spacing and thus in a small bandwidth utilization. In order to circumvent this deterioration apodized grating structures – i.e., gratings with longitudinally varying mode coupling constants according to a bell-like weighting function – are strongly recommended.

An obvious way to alter the coupling strength of surface corrugated gratings consists of a correspond-

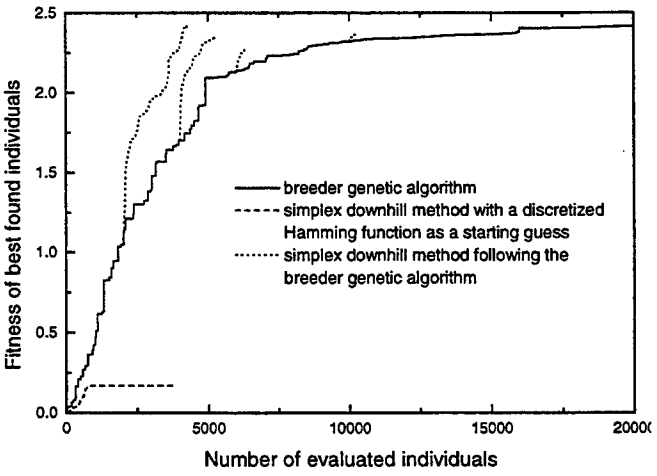

Fig.3: Fitness evolution of different grating filter optimization attempts as a function of evaluated individuals. A discrete valued Hamming distribution of the coupling constant acts here as a starting guess for the initial SDH.

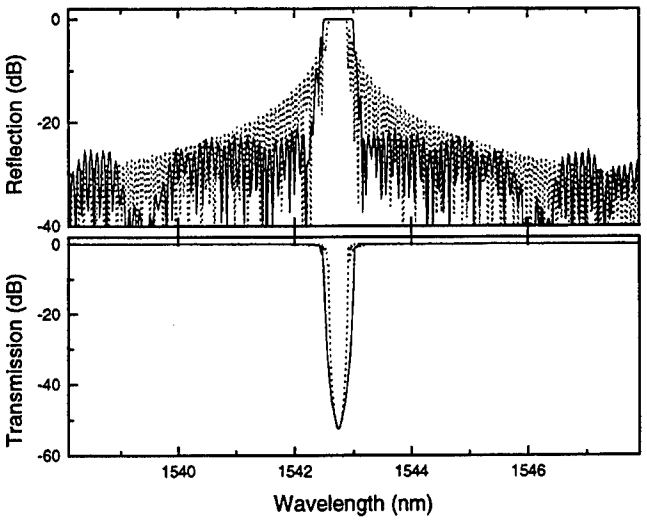

Fig.4: Simulated spectral response of a concatenated grating (solid line) and of the equivalent uniform grating (dotted line). Both gratings are 11 mm long.

ing change in etch depth of the periodic ridge waveguide corrugation (another attempt using a direct UV-writing technology [20], [21] to locally change the planar glass waveguide's effective refractive index is still under investigation). However, to preserve process reproducibility a binary grating, e.g., a constant etch depth is preferred. One apodization method obeying this constraint exploits the dependence of the coupling coefficient on the grating duty cycle [22]. In this approach the minimum coupling coefficient is

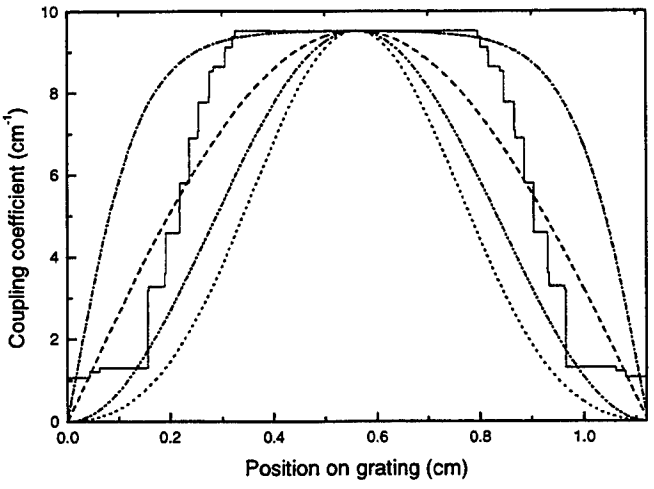

Fig.5: Coupling strength distribution along the grating for the optimized concatenated grating (solid line) and several conventional taper functions (Blackman function (dotted line), raised sine (dash-double dotted line), sine (dashed line), positive hyperbolic-tangent profile (dash-dotted line)).

determined by the most extreme duty cycle that is producible, i.e., the one deviating most from *50%*, which has to be found experimentally. We found a minimum duty cycle of about 10% to be a typically achievable value for glass waveguides with grating periods of about *500 nm* [14]. In consequence, any apodization function realized within our production technology will be truncated. Classical windowing functions of, e.g., a Hamming (or a raised cosine) shape, suppress all sidelobes below a certain level (e.g. *–50 dB*) that is given by the function itself and the accurateness of its practical realization. Thus, all classical windowing schemes tend to perform unsatisfactory when truncated (for the Hamming window the sidelobe level raise up to *–14 dB* when this apodization function has to comlpy with a minimal available duty-cycle of 10%). We have therefore decided to look for apodization functions that are optimized, taking experimental constraints into account with the more pragmatic goal to just suppress all sidelobes outside a certain bandwidth.

The choice of the optimization scheme was also influenced by the discrete nature of the actual problem representation: the gratings are usually implemented by a vector scan electron beam lithography system with a discrete address grid. The set of producible duty cycles and hence the set of realistic coupling coefficients is thus given once the writing field size has been chosen. The only parameters that are available when optimizing the coupling strength profile are the lengths of the different grating regions. Furthermore, each length should be an integer multiple of its corresponding grating period. Therefore, finding an appropriate apodization scheme – i.e., to trace an appropriate concatenation of different subgratings – always represents a crucial combinatorial optimization problem which is efficiently solved only by a *genetic algorithm* [5], [6], [8].

To evaluate the gratings we first have to define the desired crosstalk levels, e.g., an intra-channel crosstalk better than *-30 dB* within a bandwidth of *0.4 nm* and an inter-channel crosstalk of *-25 dB* outside a bandwidth of *0.8 nm*. According to [23] the inter-channel crosstalk requirements for neighboring channels is less strict and amounts to *–20 dB*. We use the larger value to give the optimizer a larger margin. In each iteration step the grating response is calculated using the well known transfer-matrix method [24]. According to the given filter specification, the overall *fitness* is consequently defined as a sum of two different fitness constituents: One number validates the actual spectral filter response with respect to the desired inter-channel crosstalk and a second term measures the spectral deviation with regard

to the given intra-channel crosstalk specifications. *Fig.3* shows the fitness evolution for a grating consisting of *40* grating sections with corresponding duty cycles. In order to compare our *breeder genetic algorithm* (solid line) with alternative optimization schemes we have also plotted the evolution when enabling a specific *simplex downhill* (*SDH*) optimization working on discrete number spaces (dotted line). As starting guess for the coupling strength distribution we used a discrete valued Hamming function. Referring to the corresponding trace in *Fig.3* it is clearly visible that the *simplex downhill* method gets caught in a local optimum. Additionally, we have stopped our *genetic algorithm* after a certain number of evaluated individuals and have it followed by a *simplex downhill* optimization (several dashed lines). The *simplex downhill* usually tends to accelerate the down tracking of promising parameter sets nearby a fitness landscape's local optimum. But it is noteworthy to realize that a prior global optimization procedure is always mandatory.

After *2000* iterations (and additional *1300 down hill simplex* iterations) a representative design has led to *50* grating solutions where the best performing one has a potential bandwidth-utilization-factor of *50%* at an intra-channel crosstalk of *-30 dB* and an inter-channel cross-talk of *-21 dB* close to the Bragg resonance which complies well with the requirements (*Fig.4*).

As shown in *Fig.5* the *3 μm* wide ridge waveguide Bragg gratings consist of *40* different subgrating sections having an overall length of *11 mm*. All of them are producible in an inexpensive planar *SiO_2/SiON* glass technology with an available etch depth of *100 nm*. Comparing our design approach to, e.g., commonly used thin-film interference filter synthesis methods [25], our *evolutionary optimization* procedure potentially reveals an objectionable computational effort. But from the viewpoint of a *realistic* design, this sobering prospect should be reassessed into a promising one especially with regard to our design procedure's feasibility while including all critical nonidealities of the technological production process.

4. ULTRA SHORT SPOT-SIZE CONVERTER

In the last two sections we described how our *evolutionary algorithm* can be used to comply with the *spectral* specifications within a design procedure of integrated optical devices. The example being now under consideration is dedicated to the *spatial* treatment of optical fields regarding the functionality of such devices. Because of its large refractive index difference ($\delta n \approx 0.02$) the planar *SiO_2/SiON* glass waveguide technology has the

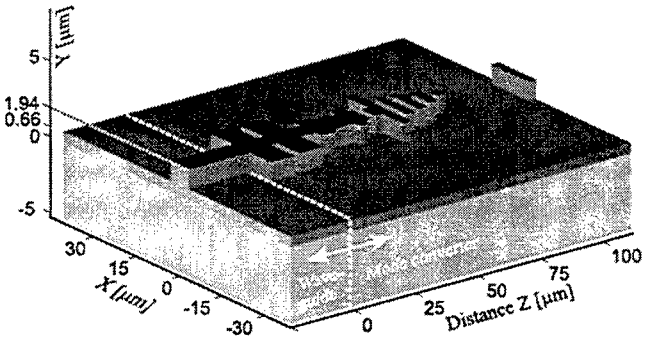

Fig.6: Example of a planar spot-size converter. For visualization purposes the upper cladding is not shown. Only changes in the width and segmentation are supported. Such structures can be manufactured as simply as a normal waveguide.

benefit of allowing small bending radii on the order of *1 mm*. Therefore, this inexpensive technology meets the requirements for dense integrated optics. But such strong waveguiding has inevitably its drawback considering the mode mismatch at an optical transition between chip and single mode fiber. Direct butt-coupling would cause losses of more than *3.5 dB*. In order to reduce these losses, the modal shape of the integrated waveguide's fundamental mode has to be converted into a shape as close as possible to the fundamental fiber mode.

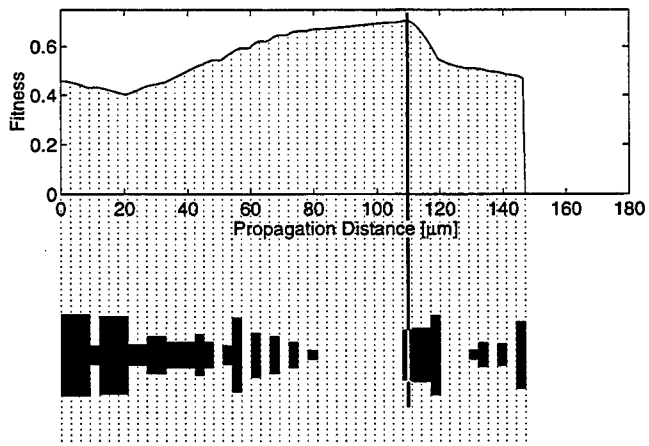

Fig.7: The fitness evolution through the converter is shown here. The real structure will be cut at the position where the highest fitness is obtained. Therefore the implemented converter is usually considerably shorter than the total structure. The fitness is calculated after each BPM propagation step. The best fitness ever encountered (here at about 110μm, shown by the vertical line) is retained as the overall fitness of the converter.

Several approaches how to transform the modal properties are already known [26]. Because of the difficulty to produce vertical tapering, a structure must be found that does not require such kinds of additional fabrication steps.

A converter structure, which is easy to fabricate within a rigorous planar waveguide concept, consists of a segmented waveguide with or without lateral tapering. By general means, such spot-size converters do not have to be periodically segmented (*Fig.6*). Our approach [9]-[13] leaves an *evolutionary optimizer* to "decide" himself how much tapering and segmentation is needed to obtain an optimal mode conversion.

The actual problem to be optimized hence contains a chip to fiber coupler at an operational wavelength of *1550 nm* where the width of the ridge waveguide is *3 μm* with a residual layer thickness of about *1 μm*, and the single mode fiber has a core diameter of *9 μm*. The coupling loss L_C (including scattering losses within the spot-size converter structure) is defined as

$$L_c = 1 - \left| \int_A \Psi_a \Psi_F^* \, dA \right|^2 \Big/ \left(\int_A |\Psi_i|^2 dA \cdot \int_A |\Psi_F|^2 dA \right)$$

where Ψ_i is the fundamental mode of the ridge waveguide, Ψ_a is the optical field after the spot-size converter, Ψ_F is the fundamental mode of the fiber and the integration is performed along the waveguide's cross-sectional plane A. The optimization goal is to find a suitable structure that minimizes the coupling loss L_C. The *fitness* of the structure is therefore defined as $F = 1 - L_C$ and has apparently to be maximized.

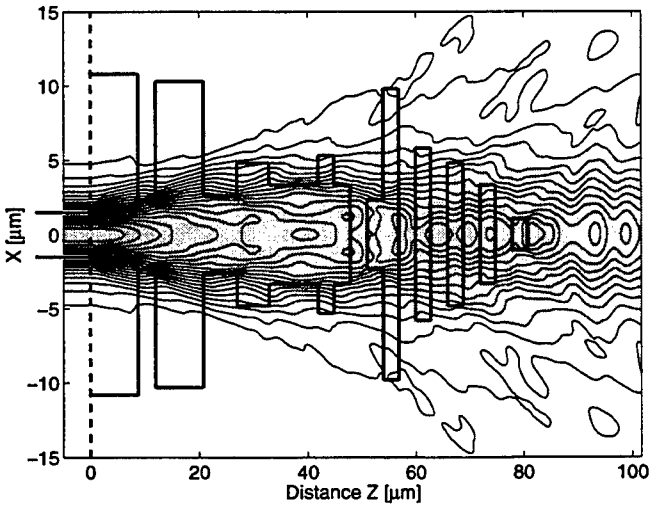

Fig.8: $|E_y|$-field distribution (TM-polarization) within a converter structure. Left of the dashed line the width of the original waveguide is shown. A horizontal slice of the ridge waveguide is superposed. The expansion of the propagating field is clearly visible.

Similar to the laser problem a *genotype* is defined as follows: The converter is divided into N sections of *2.7 μm* length (a choice which is motivated mainly by technological reasons). Each section's width is represented by a multi-valued bit, where each bit can hold *42* different values. Values from *0* to *40* correspond to the real width of the waveguide in steps of *0.5 μm* and *-1* stands for *"don't care"*. The *"don't care"* bits are needed to leave the total converter length variable. Each converter is then calculated using a *FD-BPM* (finite difference beam propagation method) based code. The fundamental modes of both the waveguide and the fiber are calculated with the *imaginary distance BPM* [27].

The *evolutionary algorithm* is initialized with a starting population of *100* individuals each having a maximum length of *70* sections. The *fitness* value F is evaluated after each propagation step. The best *fitness* ever encountered along the structure is taken as the nominal *fitness* of the corresponding converter. An example of the *fitness* distribution within an optimized structure is shown in *Fig.7*. For these *BPM* simulations, the propagation step size is chosen *0.25 μm* by means of stability.

The best performing of our *evolutionary* optimized converter topologies was achieved after evaluating only *10350* out of totally $4.24 \cdot 10^{113}$ possible solutions. It consists of *15* different ridge waveguide segments and reduces the coupling loss from *3.5 dB* down to about *1.3 dB*. A *0 dB* coupling loss is hardly possible because the residual layer in the waveguide structure severely handicaps the vertical expansion of the optical field.

The optimal converter structure corresponds to the topology given in *Fig.6* and the optical field distribution is shown in *Fig.8*. The scattering loss through the converter structure is estimated to be less than *0.2 dB* and the principal neglect of power reflection in our simulation model has been affirmed by measurement [12], [13] of a very low value of *-40 dB*.

The final converter device has an overall length of *138 μm*, which to our knowledge represents the shortest spot-size converter ever built for such large refractive index steps.

5. FREQUENCY CARRIER DISTRIBUTION

Today, fiber optic links are substantial parts of modern communication systems [28]. It is therefore important to know their distortion and noise properties [29]. Systems with subcarrier multiplexing (*SCM*), in which often equally spaced *rf* carriers with different amplitudes lie within a narrow band, have very low intermodulation-distortion (*IM*) specifications, as do common antenna television systems (*CATV*). In optical transmission links with standard fibers and directly intensity-modulated lasers at *1.3 μm*, the main contribution to the distortion is due to mixed – static and dynamic – laser nonlinearity [30]. In such communication systems only odd orders of the nonlinearity have to be considered when a weak nonlinearity is assumed.

It is rather the resulting 3^{rd} order *IM* which is of technical relevance [31]. Having, e.g., a transmission band of $f_1,\ldots,f_n$ equally spaced *rf* carrier frequency channels, where M_C is assumed to be the set of operational carrier indices, then 3^{rd} order IM generates mixing products of the following kind: $f_i+f_k-f_\ell$, $f_i-f_k+f_\ell$, $-f_i+f_k+f_\ell$, $\forall\ i, k, \ell \in M_C$. All mixing products which coincide with a frequency f_r within the transmission band obey $i+k-\ell = r$ or $i-k+\ell = r$ or $-i+k+\ell = r$, $\forall\ i, k, \ell \in M_C$.

In order to propose M_C as an optimal carrier distribution, one has to look for operational *rf* carrier frequencies within the transmission band whose *IM* products do minimally interfere amongst themselves as well as with their engendering carriers, respectively.

In an ideal case, where one simply wants to prevent a carrier to overlap with those *IM* products stemming from the remaining ones, all distances between pairs of carrier frequencies should be different like $i-\ell \neq r-k$. A set M_C with such properties is also called *"Golomb ruler"* [17] when containing *0* as an additional element. Therefore, placing N operational carriers within a minimal transmission bandwidth of $n > N$ channels, means nothing else than looking for a preferably short *Golomb ruler* whose largest element should be as small as possible.

Computational solutions are only available for $n >> 16 \geq N$. Thus, considering dense carrier distributions inevitably leads to a combinatorial optimization procedure, where a minimal intermodulation-to-carrier-ratio (*IM/C*) should be aspired for occupied

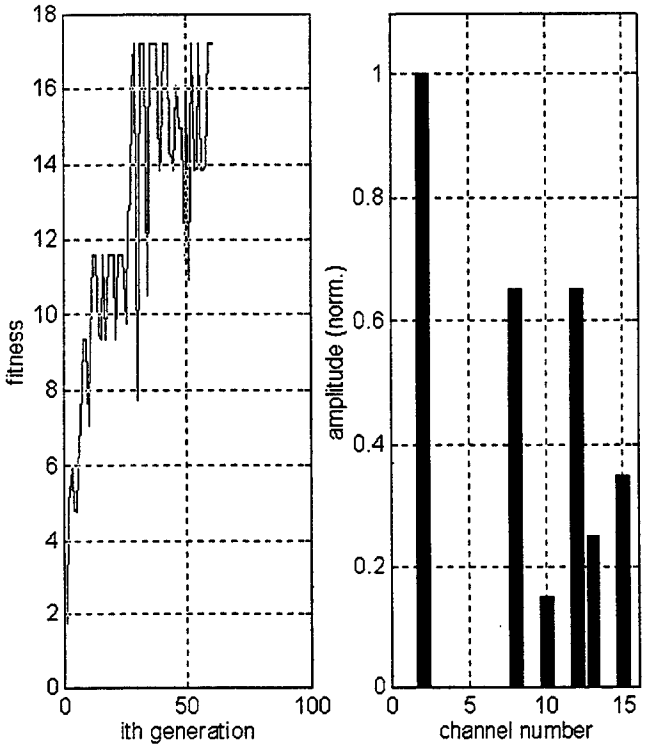

Fig.9: Optimal distribution of 6 different carriers within 15 equally spaced transmission frequency channels. (Left) fitness evolution during optimization, (right) transmission band with optimally placed carriers (shown as bars).

channels as well. The optimization task becomes even more severe when taking into account different carrier amplitudes. There are

$$M_1 = \binom{n}{N}$$

combinations of how to distribute N operational carriers within n transmission channels. Assuming a given set of N different amplitudes within each distribution pattern additional $M_2 = N!$ permutations of carrier amplitudes have to be taken into account. As *genotype* of a particular carrier distribution, we define a bit-string representation for a pair of ordinal numbers (m_1, m_2) $\forall\ m_1 \in [1, M_1]$, $m_2 \in [1, M_2]$, where the first of them addresses the combination state of the particular pattern and the second characterizes its permutation state respectively. The *fitness* of a particular pattern is then calculated with respect to the worst *IM/C* of all occupied transmission channels involved.

Our exemplary *evolutionary optimization* problem [17] includes a set of *6* given carrier amplitudes to be placed within a transmission band of *15* equally spaced frequency channels. As optimizer we use a standard *genetic algorithm* (generation based *genetic algorithm*: traditional *one-point crossover, 60% selection probability, 1% mutation rate*) which operates on a population size of *300* individuals. A best performing solution was found after *30* of totally *60* generations. *Fig.9* shows the optimal carrier distribution leading to a minimal 3^{rd} order *IM* distortion of the fiber optic *SCM*-link.

The optimization problem presented here is also of prime importance regarding the design of very advanced optical *WDM*-systems. For high-speed *WDM*-systems the simultaneous requirements of high launched power and vanishing fiber dispersion lead to the generation of new optical frequencies by four-photon mixing. These generated waves can interfere with system operation while degrading the system capacity by intermodulation distortion and additional noise generation in band limited erbium doped fiber amplifiers (*EDFAs*). In order to prevent phase matching of these waves one is tempted to allow a small amount of fiber dispersion at an additional expense of system capacity [32]. Hence, an optimization of optical carrier distribution enables the reduction of intermodulation distortion without need of any dispersive fiber.

6. DIELECTRIC MATERIAL MODELS

In this section, we report an *evolutionary optimization* based method for the determination of the dispersive dielectric properties $\underline{\varepsilon}_r(f)$ of natural materials exhibiting high dielectric and ohmic losses over a wide frequency range. Accurate information on the dependence of dielectric properties of (mixtures of) natural materials on content of, e.g., water or hydrocarbons, and also on temperature is of considerable importance in a number of applications, e.g., in environmental engineering, geophysics, mathematical geology and chemical process engineering. The microstructure of such multiphase mixtures are generalized by a structural material matrix representing the characteristic distribution of its constituents. This concept of *structural units* [33] – which is a picture for capturing the microstructural and compositional information of the randomly distributed constituents within a dielectric host material – becomes particularly attractive when linked to an accurate spectral dispersion

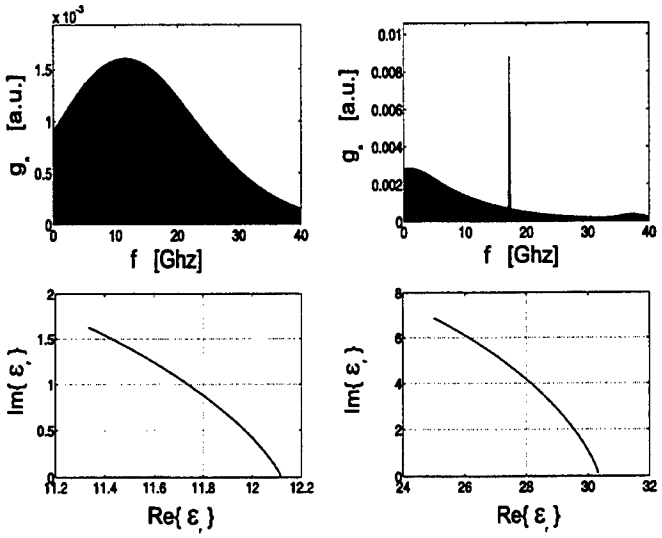

Fig.10: (Top) relaxation spectra $g_n(f_r^n)$ and (bottom) Cole-Cole plot of $\underline{\varepsilon}_r(f)$ for a volumetric water content of (left) Θ = 0, and (right) Θ = 15% where the relaxation frequency of free water is clearly reproduced by the proposed model. The frequency range of the measured scattering data is f = 10 MHz...3 Ghz.

model in an effective medium approach. Hence, disposing of such an accurate macroscopic description of dielectric mixtures could even have a seminal impact on advanced topics in physical optics such as wave localization phenomena due to random scattering, photon diffusion, coherent backscattering and has yet led to the *diffusive wave spectroscopy* as a new optical measurement technique in material science and food engineering [33].

The analytical material model presented here is extracted from electromagnetic scattering data of a corresponding coaxial transmission line measurement setup. Following the classical *Debye* model for the relative permittivity we propose a weighted linear superposition of *N* different *Debye* models

$$\underline{\varepsilon}_r(f) = \varepsilon_\infty + (\varepsilon_s - \varepsilon_\infty) \cdot \sum_{n=1}^{N} \frac{g_n(f_r^n)}{1 + i\left(\frac{f}{f_r^n}\right)} - i\frac{\sigma_{diel}}{2\pi\varepsilon_0 f}$$

where ε_s stands for the static limit, ε_∞ for the high frequency limit, ε_0 describes the vacuum permittivity, σ_{diel} accounts for the ohmic conductivity of the material involved, f_r^n represents the relaxation frequency of the *n*-th *Debye* model and $g_n(f_r^n)$ defines a normalized relaxation weighting function which on itself is composed by a finite set of *G* different *Gaussian* relaxation functions. Choosing such a finite base of the relaxation

spectra $g_n(.)$ mainly helps to circumvent the *ill-posedness* of the model estimation problem. The *genotype* consists of an appropriate binary representation of all parameter values to be optimized. The parameters include the weightings, the relaxation frequencies and bandwidths of the numerous *Gaussian* relaxation components, the conductivity σ_{diel} and both limits, ε_s and ε_∞ of the permittivity model. We can define the *fitness* of a potential solution as the quality of the approximation of calculated and measured scattering spectrum respectively. Referring to the matching of the scattering phase between analytical model and measured data the resulting *fitness* function behaves like a jagged multimodal landscape provoking serious pitfalls for commonly used optimization algorithms.

As an *evolutionary* optimized example we present the analytical description of *Bentonite*, a highly lossy, very complex clay like material with and without volumetric water content Θ [18] at a temperature of *23°C*. The behavior of our estimated model is shown in *Fig.10*, whereas the corresponding parameters can be obtained from the following table *Tab.1*.

	$\Theta = 0$	$\Theta = 15\%$
# individual	*21'373*	*21'552*
ε_s [–]	*12.1236*	*30.4155*
ε_∞ [–]	*3.00012*	*2.18958*
σ_{diel} [*mS*]	*18.314*	*99.9847*

Tab.1: Optimized parameter set for Bentonite at two different humidity states.

To conclude we derived a very general analytical material model for complex and highly lossy dielectric materials which outperforms commonly used *Debye* models in terms of flexibility and accuracy as well. Our approach is able to cover different distinct relaxation phenomena which are not easily tractable within a straight forward *ab initio* dispersion formula.

7. PROBLEM-BASED ALGORITHMIC PROSPECTS

We have demonstrated *evolutionary algorithm's* applicability to various optimization problems within the field of computational optics and electromagnetics. After all, this is because most of such real-world problems could easily be transformed into combinatorial problems as well, where *evolutionary algorithms* and especially *genetic algorithms* are claimed to belong to the best suited ones compared to other heuristic optimization codes. In addition, this kind of optimization scheme delivers much more general information about what actually leads to a good solution. Therefore, it permits us to implement superior meta-optimization strategies which rely on, e.g., a population based *information gathering*. Such an *information gathering* procedure includes *structural information* concerning typical patterns [8] within optimized individuals as well as *temporal information* [11] of the evolution process itself. In the following, both types of *information gathering* will be elucidated in the context of a corresponding application.

7.1 STRUCTURAL INFORMATION PROCESSING IN THE CONTEXT OF MULTI-CAVITY LASER DIODE OPTIMIZATIONS

All optimization scenarios presented in Section 2 appear to converge to an optimal laser structure and it seems that not even a continuation of the optimization process up to some higher iteration number enables the generation of better performing individuals. In addition, most of the statistically available information concerning a "final" state of a population's evolution (e.g., the decreasing spread of fitness values) usually lacks in reproducing the optimizer's potential for a further improvement.

Therefore a structural analysis of all individuals, i.e., searching for frequent and successful patterns within this optimized population could probably answer two questions: First, is such an *information gathering* procedure capable of delivering a novel population whose prospects look more promising within a further optimization attempt? Second, is it also possible to formally acquire insight as to what actually leads to well performing laser structures?

The *information gathering* based on pattern analysis [8] is simply done by evaluating the frequency of appearance of characteristic Q bit-pattern ($Q < L/\delta L$) within the population. By stepping a Q bit wide window along each individual's genotype a corresponding number of different Q bit-strings can be extracted. All these strings are then sorted according to their pattern label, thus assigning each pattern to its frequency of appearance (*Fig 11b*). A similar procedure delivers the

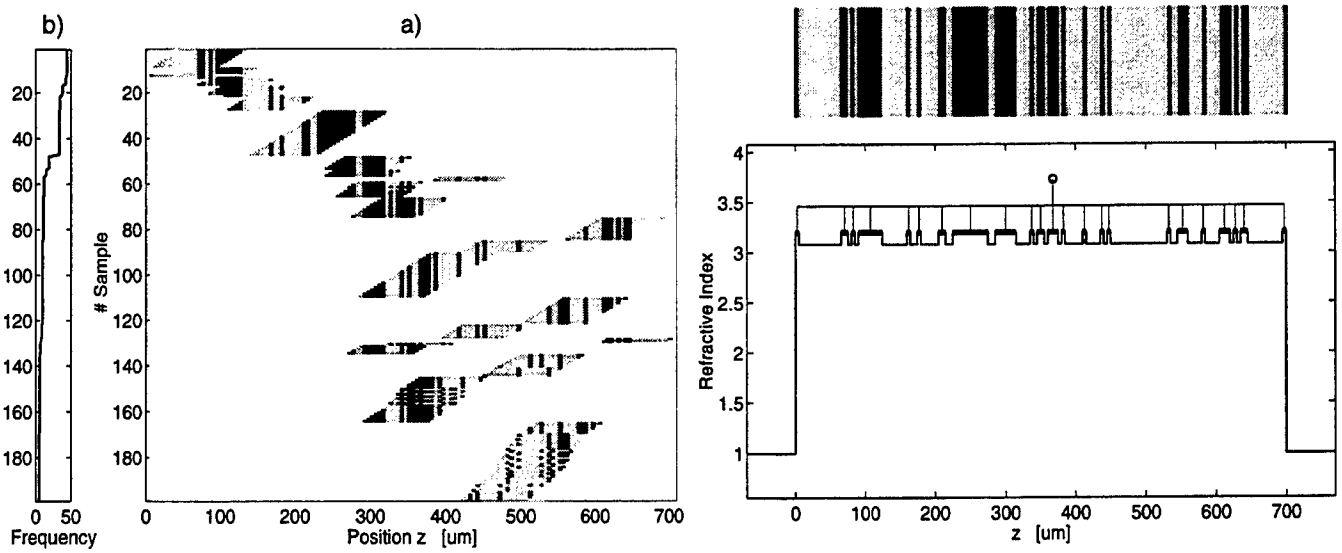

Fig.11: Pattern analysis considering the final population of the optimization scenario described in Section 2: a) Distribution of characteristic 18-bit-patterns along the laser structure and ranked by its frequency of appearance. b) Corresponding frequency of appearance of these patterns. For visualization purposes the pattern analysis has been restricted only to the high and low refractive index segments of the decoded cavity structure (left). Typical cavity refractive index pattern deduced from the 18-bit-pattern distribution (top right). The corresponding non-periodic coupled cavity laser structure (bottom right) consists of 45 sections and has a total length of 700 μm.

most frequent position for every Q bit-pattern within this ranking, leading to the distribution scheme shown in *Fig.11a*). Finally, the distribution of characteristic Q bit-patterns enables us to deduce a typical laser structure which is believed to gather all the specific information needed to qualify as a good solution. The typical laser structure of *Fig.11* is obtained by counting each specific allele value of all pattern sequences at the considered segment position. The counting procedure itself employs a weighting which is proportional to the pattern's frequency of appearance. Therefore, the most frequent parts of patterns will always obtain recognition. Choosing pattern lengths between $Q = 3$ bit and $Q = 90$ bit up to *88* different typical laser structures can be obtained contributing partly to a novel starting population for a further optimization.

In order to validate a population's diversity D a particular non-binary definition of the Hamming-distance [6] has to be specified. We therefore investigate the distribution $\delta D(m)$

$$\delta D(m) = \frac{2}{N \cdot (N-1)} \cdot \sum_{i=1}^{N-1} \sum_{j=i+1}^{N} \rho_H\left(\vec{b}_i(m), \vec{b}_j(m)\right)$$

which measures the average number of appearance of incongruous alleles at the m-th genotype position considering all N integer strings of the population, whereas ρ_H values the incongruity between string $\vec{b}_i$ and $\vec{b}_j$ at position m. The summation of $\delta D(m)$ over the total string length immediately yields the diversity D mentioned above.

Within the optimization scenario presented in Section 2 different population stages have been analyzed according to the appearance of common patterns. As an example, the *information gathering* procedure has yielded 15 typical laser structures, forming a novel population, with some individuals performing even better, and whose diversity is around *13* bit. This represents a distinct increase compared to the *8* bit of the considered underlying population. Further details of the re-optimization process including such typical laser structures are elaborated in [8].

Coming back to the typical laser structure shown in *Fig.11* it can be noted that especially the regions neighboring the two laser facets are strongly correlated and imply a certain robustness against optimization interferences. Thus, changing segments from inner regions of the cavity has proved as a more successful policy while tracking down well performing laser topologies. This assumption is clearly confirmed when investigating the distribution $\delta D(m)$. Inspecting the configuration shown in *Fig 12*

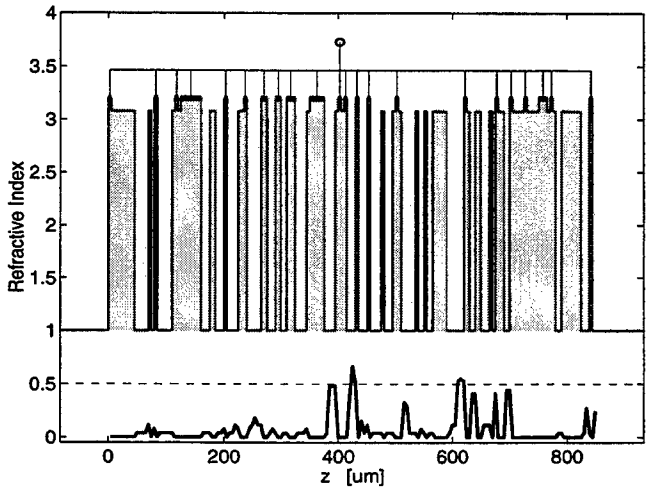

Fig.12: Diversity distribution δD (bold line) mapped along a corresponding decoded cavity configuration considering all genotypes of the underlying final population i.e. of the optimization scenario. The shaded sections indicate locations, where the congruence of all genotypes tends to be exact and the optimizer's interference is therefore believed to be negligible whereas the gaps stand for the position of distinct incongruity within the genotypes involved. The summation of δD over the total string length z immediately yields the diversity D.

one may be tempted to allocate the shaded regions to resistant characteristic patterns. But, because of its different algorithmic background neither the structure given by the shaded regions in *Fig.12* nor the typical cavity topology of *Fig.11* are rigorously comparable to each other. The typical cavity topology is generated when gathering the common pattern information within a population whereas the structure given in *Fig.12* puts the focus on all its differences.

In conclusion, our characteristic pattern analysis reveals a noteworthy feature: Nearly independent of the state of a population's convergence the proposed *information gathering* procedure delivers mostly one individual whose fitness exceeds that of the best performing structure of the underlying population. Therefore we suggest our *information gathering* be used as a sort of meta-optimization strategy. Increasing a population's diversity without degrading the corresponding fitness could be regarded as a useful mean to *revitalize* a population's prospect when looking forward to a further optimization attempt [8].

7.2 TEMPORAL EVOLUTION ASPECTS IN THE SPOT-SIZE CONVERTER DESIGN

Our evolutionary optimization scenario presented in Section 4 also delivers *temporal information* which may be reassessed in the framework of a superior solution strategy. One of the main differences between classical heuristic optimization procedures such as, e.g., *Monte Carlo* or simple *hill-climbing* methods and evolutionary optimization procedures is their implicit parallel search mechanism. As it is demonstrated later, any successful converter contains characteristic substructures that significantly contribute to good performance. In our procedure it is possible to keep track of such substructures during evolution. In order to obtain the corresponding data of the traces, substructures of 10 segments length were compared using a sort of relaxed structural correlation scheme: If no more than 3 segments of that substructure differ from one individual to another, both individuals are considered to be part of the same trace. The iteration index within the evolution process and the fitness of all individuals taking part of a trace are stored.

We can think of three different types of traces questioning the following: *(1) Traces from the initial population:* Are substructures of the initial population still persistent in a later evolution stage? *(2) Backward traces from distinct fitness jumps:* Which trace is mainly responsible for the increase in performance, or which characteristic substructure is part of this best performing individual? *(3) Backward traces from the final population:* How many traces and which substructures constitute the final population?

Referring to the survivability of the initial population's substructures it is observed within our specific example [11], that, even when most of the patterns die out within the first 25% of the optimization process, there are still two traces that play a major role during the overall evolution. This shows that proper initialization – i.e., the initial population's quality of diversity – may have a considerable impact on the evolution's outcome. Different initialization schemes (e.g., using deterministic or heuristic number generators instead of standard pseudo-random processes) are now under extensive investigation.

The history of substructures which provoke distinct fitness jumps reveals the coexistence of different competing patterns within the evolving population. Some substructures will temporarily be at

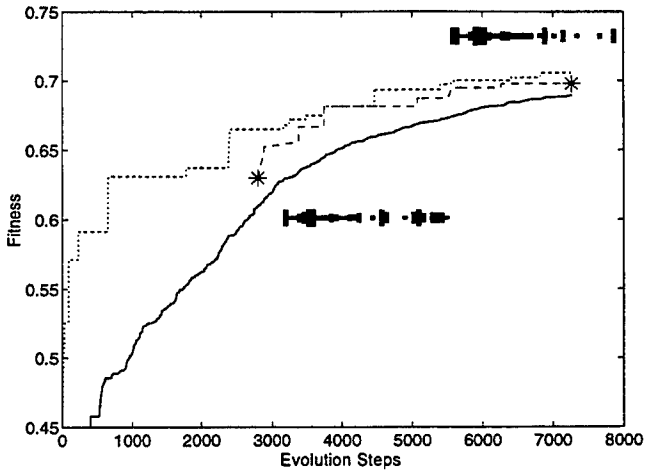

Fig.13: To observe if there are still different sub-populations in the actual or final population, a trace back to earlier stages of the population's evolution may be created. By doing so, it is possible to observe how the evolution of sub-populations takes place. Therefore the parallelism in the evolution is clearly visible. For these examples, the backward traces are shown for a population at 7300 evolution steps.

the top of the population's fitness ranking, while others are successful another time [11].

Considering the traces that constitute a final population (as depicted in *Fig.13*) this competition of patterns turned out to be a mean measure when qualifying an optimizer's potential termination state:

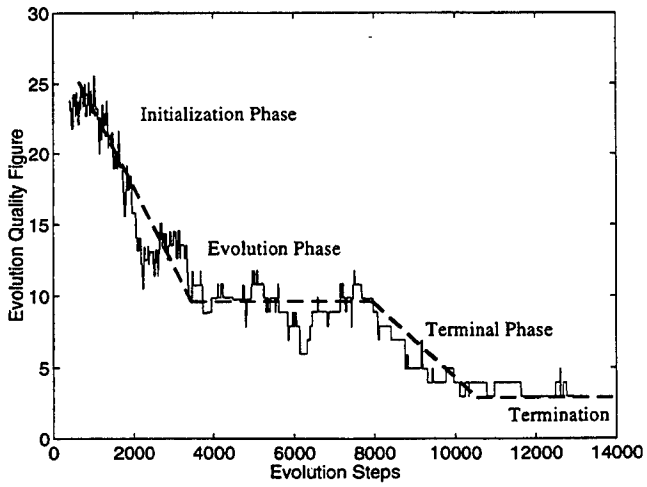

Fig.14: Value of the evolution figure during the optimization. Four phases may be distinguished where the labelling is proposed for visual purposes only.

qualifying an optimizer's potential termination state: Each substructure may be interpreted as a part of a sub-population of individuals containing this unique pattern, exemplifying as well that parallel optimization of different structures takes place even in a final evolution state. To dispose of different sub-populations at such stages underpins the impact of cross-over at the expense of mutation, indicating the optimization being still in an efficient operation mode compared to a purely statistically driven random search process. Thus, quantifying the *vitality* of a population after n iteration steps a *state variable* may be defined as follows [11]

$$C_P(n) = \frac{1}{F(n)} \sum_{i=1}^{N^{SP}(n)} F_i^{SP}(n)$$

where $F(n)$ stands for the temporal maximum fitness, N^{SP} represents the total number of sub-populations and $F_i^{SP}(n)$ assigns the maximum fitness within the i-th sub-population. *Fig14* shows the evolution of $C_p(n)$, whereas a categorization containing four different phases in the evolution process has been proposed. Here, $C_p(n)$ may be viewed as a specific representation of the number of competing patterns within the population involved.

7.3 EPILOGUE

We believe, when provided with both *structural* and *temporal* information of a population's evolution one should be able to define certain measures [8], [11] concerning, e.g., the vitality of the population or even a specification of its actual state of evolution. In order to underpin such ventured conjectures extensive statistical investigations are strictly inevitable, including also a much broader spectrum of examples than presented here. However, a lack of generality considering all attempts when formalizing the evolutionary algorithm's learning process will always remain. Therefore, other promising combinatorial optimization methods have to be compared when relying on an evolutionary paradigm. For the assessment of problem specific search space characteristics, hybridization of *evolutionary algorithms* with other methods should be investigated as well.

8. TOWARDS COMPUTER GUIDED ENGINEERING

Apart from the algorithmic considerations depicted in the previous Section 7 we will now briefly sketch two lines, where our research on evolutionary optimization in computational optics is about to advance. Within both strategies we always rely on the gathering of specific information regarding, e.g., the actual shape of the structure involved, the simulator's peculiarities and even the functional dependencies on the circuit level.

8.1 IMPROVEMENTS WITHIN ADVANCED DEVICE OPTIMIZATION PROBLEMS

At present we are strongly involved in the design of complex smart planar optical transducer elements for (bio-)chemical and physical sensor systems. Within these activities we believe we will obtain a deeper insight into the mechanisms of optical coupling and for the design of new grating couplers [35], especially of ultra-compact highly non-periodic coupler topologies. A rigorous design of such dense electromagnetic field coupling configurations usually represents an inverse scattering problem, which can only be solved with a combination of highly sophisticated codes for computational electromagnetics coupled to, e.g., an *evolutionary optimizer*.

When one links such optimization procedures with such simulation tools, one faces several difficult problems. As its main task the code for computational electromagnetics solves a so-called *forward problem* for the optimization procedure. Even when the time spent for the *forward problem* is long, the results have a limited accuracy. This may cause some noise within the data, which considerably disturbs the search process. Thus, the forward problem has to be solved many times. Referring to these issues, three different specifications should be respected when carefully looking for an appropriate forward solver: *1.)* The simulation program should be as *efficient* as possible, *2.)* it should maintain a *complete robustness* while possibly treating solutions not even thought to exist, and *3.)* it is mandatory that the solver delivers an *error measure* in order to guarantee a certain *accurateness* of the search process.

The *multiple multipole* (*MMP*) method [34] is a well-established, semi-analytical tool for solving time-harmonic 2D and 3D scattering problems within piecewise linear, homogeneous and isotropic domains. It is based on the *generalized multipole technique* (*GMT*). With *MMP*, the field f_D within individual domains D is approximated by a sum of N cylindrical or spherical multipole expansion functions f_{Dj}

$$f_D = f_{D0} + \sum_{j=1}^{N} A_{Dj} \cdot f_{Dj} + Error$$

which are themselves analytical solutions of the Helmholtz equation, where f_{D0} stands for the excitation.

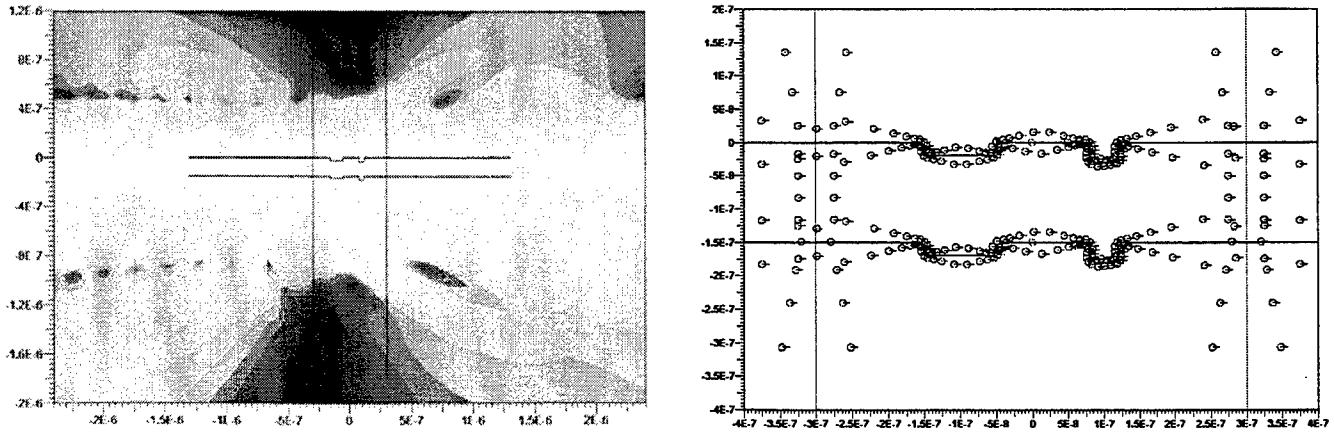

Fig.15: MMP calculation of a single slab waveguide perturbation pattern: (left) Intensity plot of the time-averaged Poynting field for TE-excitation from the left side. (right) Distribution of the corresponding multipole expansions (each multipole location is indicated by a small circle, boundaries are drawn as solid lines). The slab waveguide system consists of a TiO_2 core layer (thickness 150 nm), a H_20 upper cladding layer and polycarbonate as lower cladding respectively. The two grooves (1: width 100 nm, depth 20 nm; 2: width 40 nm, depth 30 nm) are separated by 200 nm. The operating wavelength is 785 nm (vacuum).

The origins for multipole expansions are usually set along the boundary of the domains in which the field is to be calculated. For the field around voluminous domains *Hankel*-type expansions are used whilst *Bessel*-type expansions are preferred inside. Other special functions are included as well, e.g., propagating and evanescent plane waves. The coefficients A_{Dj} are obtained by enforcing the boundary conditions for the field components at discrete matching points on the boundary. Since more matching points are introduced than necessary, the *MMP* method leads to an overdetermined system of equations. This system is solved in the least-square sense which is equivalent to an error minimization technique. Thus, an adequate *error measure* is inherently delivered by the method itself.

In order to maintain *robustness* during an optimization scenario, *MMP* should be insensitive to all parameter variations involved. Here, the most challenging task is to successfully adapt the simulation to repeated changes of the coupler's grating shape. For that reason we have developed a fully automatic pole-setting procedure which allocates all multipole expansions needed along their corresponding boundaries. The proper setting takes into account several properties of the actual shape as well as it considers implicit portions such as, e.g., the curvature and its context within the boundary's devolution. The *MMP* calculation shown in *Fig.15* is fully based on the automatic pole distribution procedure and it concerns a preliminary perturbation pattern which may constitute a grating coupler within our typical sensor configuration.

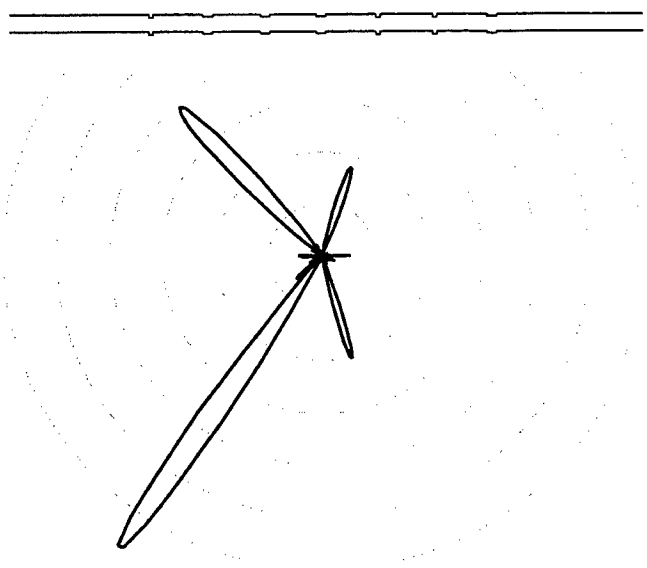

Fig.16: Non-periodic grating: Polar plot of the radiated far-field (time-averaged Poynting field) for TE-excitation from the left side. The inset shows the 7 fold concatenation of various single perturbations as described in Fig.15.

Besides the semi-analytical nature of *MMP*, there are further algorithmic potentialities when improving the program's *efficiency*. The *parameter estimation technique* (*PET*) is a very powerful technique that can be applied to numerical codes based on dense matrices as a power booster for the computation of the response of electromagnetical or optical problems at, e.g., different frequencies. It is applied to the *multiple multipole* (*MMP*) method in conjunction with the method of *conjugate gradients* (*CG*) for iteratively and efficiently solving the rectangular *MMP* matrix. The general idea of the *parameter estimation technique* (*PET*) is the evolutionary recycling of knowledge. Since all the expansion parameters $A_{Dj}^{(k)}$ (and functions f_{Dj}) are usually known from previous $1 \ldots k$ runs while, e.g., sweeping the wavelength λ, recycling of knowledge means nothing else but a pertinent extrapolation technique for estimating the parameters $A_{Dj}^{(k+1)}$ to be computed in the current run k. This speedup technique has already been detailed in earlier contributions to *ACES* publications [15], [16].

The most powerful mean to economize computational effort can be achieved, when focusing solely to characteristic portions of the overall coupler structure. Hence, we have developed a *near-to-far-field transformation* which allows the radiation field of a waveguide perturbation being approximated simply by a single particular multipole expansion. Each partial perturbation pattern can be analyzed within minutes and is then at the optimizer's disposal. Having available a library of such generic far-field expansions, the radiation field of the overall coupler topology is immediately calculated when placing the particular expansions accordingly. *Fig.16* depicts the far-field of a grating structure consisting of a seven fold concatenation of the perturbation analyzed in *Fig.15*. Within the scope of a realistic optimization scenario, the scalability due to the problem's complexity may be less severe, inasmuch a speedup of around two orders of magnitudes has become achievable. Constituting the field solution of highly-non-periodic grating structures as to the same degree of simplicity like in periodic ones (treating the

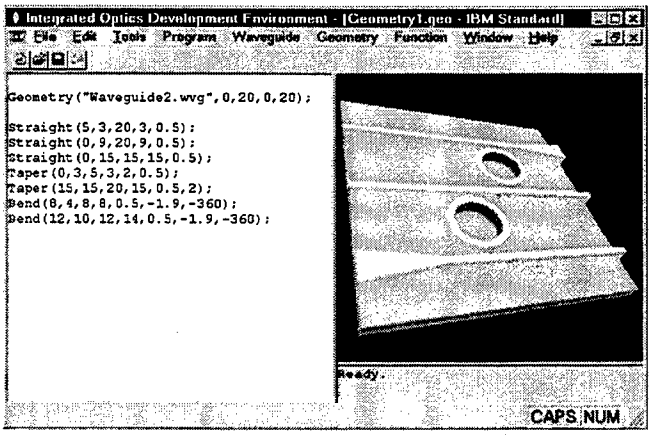

Fig.17: User interface of the developed design platform. (left) Formal description of the waveguide elements. (right) View of the corresponding planar integrated optical circuit topology.

grating's unit-cell with periodic boundary conditions) [36] reveals an unique attractiveness especially when targeting irregular topologies. This allows us to face novel design scenarios leading probably to unexpected topological coherence and implying readjusted representation schemes.

8.2 MOVING TOWARDS THE CIRCUIT LEVEL

On the system level, we are facing yet one of the most demanding *inverse problems:* designing an entire integrated optical circuit based solely on optical specifications. Resting on the expertise of the optimization examples presented earlier, our research is now focused to the development of a design platform for planar integrated optics devices. This

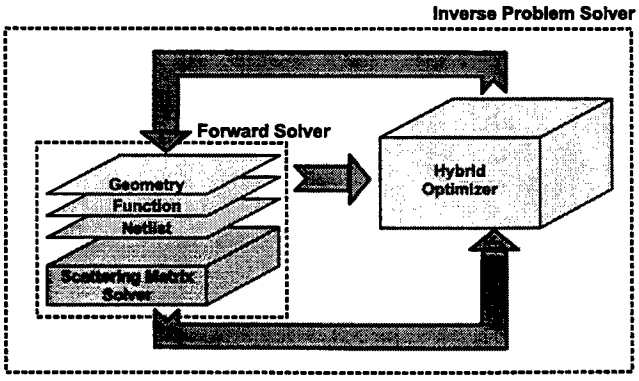

Fig.18: General architecture of the developed design and optimization platform.

design environment whose user interface is imaged in *Fig.17* relies on sophisticated representation schemes for device *geometries* based on elementary waveguide structures (e.g., straight waveguides, bends and tapers). While performing a *semantic analysis* the program is able to identify the potential *functionality* of a combination of such elements leading to "auto generated" optical circuits including, e.g., directional couplers and splitters of different shapes. For a rapid evaluation of each device topology under optimization a fast *scattering-matrix* approach is primarily used. *Fig.18* shows the general architecture of our optimization platform where the forward solver is allocated by the hierarchical representation scheme of the underlying problem.

As an optimizer we consider a kind of *evolutionary strategy* (*ES*) scheme. In order to formalize the optimizer's interference during optimization several *interference operators* have been designed. Looking for appropriate schemes on how to distort a circuit geometry or how to accordingly modify an element's functionality represents the most demanding part of our implementation. Besides translational and rotational distortion of the circuit while maintaining connectivity other operators such as scaling, and the introduction of predefined functional building blocks are under extensive investigation.

Some simple preliminary test cases like, e.g., the optimization of a multi-stage resonant-coupler add-drop device have clearly shown that the optimization problem posed here reveals an enormous search space. Even when assessing a 2D circuit topology to its inherent functionality has major influence on the problem's complexity, we still rely on our approach: Including semantic information like the circuit's intrinsic interrelations within an optimization process seems the only way to keep the problem tractable. Nevertheless, we believe our evolutionary design environment [37] to be very flexible because it does not necessarily require a preliminary design as a starting configuration and even allows modifications of the problem representation during the optimization process itself.

9. CONCLUSION

By means of five design examples we have demonstrated why *evolutionary algorithms* are highly qualified to solve "real world" inverse problems considering various applications in the field of planar

integrated optics, optical communication technology, and dielectric material modeling as well. The modal treatment of optical fields by an appropriate underlying structure is an essential operation regarding the characteristic functionality of the resulting device. Therefore, we have presented examples related to both the *spectral* shaping of the optical field (single mode multi-cavity laser diodes and concatenated Bragg grating filters) and the *spatial* molding of the light (spot-size converter).

Leaving the field of *structural optimization* we focused then on two examples stemming both from an applied engineering background.

First, a purely *combinatorial* optimization problem solution has been drawn when improving the performance of modern optical communication systems (e.g., fiber optic SCM-links and high-speed WDM-systems) according to a more adapted frequency (or wavelength) carrier distribution. In the second example we report the *evolutionary algorithm's* parameter estimation feature on the determination of the dispersive properties of highly lossy, very complex dielectric materials starting from scattering parameter measurements.

After illustrating the various examples, the focus of this paper has changed towards a more prospective view where the *evolutionary algorithm's* ability to gather problem-related information during optimization is addressed. Here, we propose to benefit from *structural* interdependencies within a population of potential solutions as well as to trace different *temporal* evolution aspects in order to establish corresponding superior meta-optimization strategies.

One obvious area for future research on *evolutionary optimization* has already been annotated by the improvement of the *forward solver* with respect to speedup, robustness and accuracy. Moving then to the circuit level we tried to use the optimizer as a proper design tool for planar integrated optics devices. Here, we have faced one of the most demanding inverse problems. It seems only tractable when including the circuit's intrinsic interrelations (by a *semantic analysis*) within the problem representation as well as implementing the optimizer's interference operators accordingly. Hence, extensive investigations are still mandatory. Nevertheless, we propose *evolutionary algorithms* being highly valuable candidates when evaluating codes for computer *guided* engineering and virtual design platforms.

10. REFERENCES

[1] On terminology: We call our *genetic algorithm* (*GA*) based optimization scheme *evolutionary algorithm* (*EA*) because of its *non-binary* genotype representation. Instead of the classical *GA's* binary chromosome we use *integer strings* in our *EA* implementation. Furthermore, the classical *GA* is a *generation based* scheme, where successful features are presumably transferred to a sequential part of the underlying population (the next generation) whereas our *EA* scheme rely on a *breeder type* [4] of optimization where only two off-springs are generated and reintroduced into the population replacing the worst two individuals. This latter optimization process is usually attributed to a *steady state GA* scheme.

[2] D. Erni, D. Wiesmann, M. M. Spühler, S. Hunziker, B. Oswald, J. Fröhlich and Ch. Hafner, *Recent Research Developments in Optical Engineering, Research Signpost, chapter* "Evolutionary optimization algorithms in computational optics," Recent Research Developments Series, Publisher: Research Signpost, Trivandrum, India,1999, still in press.

[3] D. Erni, J. Föhlich, and O. J. Homan, "Analysis and optimization of non-periodic coupled-cavity laser diodes," *Latsis Symposium on Computational Electromagnetics*, 19-21, Zürich, Switzerland, pp. 248-254, Sept. 1995.

[4] H. Mühlenbein, D. Schlierkamp-Voosen, "Predictive models for the breeder genetic algorithm," *Evolutionary Computation*, vol. 1, no. 1 pp. 25-49, Spring 1993.

[5] D. Erni, *Periodische und nichtperiodische Wellenleitergitter- und Laserkavitätskonzepte*. Diss. ETH, No. 11654, Zürich, 1996.

[6] J. Fröhlich, *Evolutionary Optimization for Computational Electromagnetics*. Diss. ETH, No. 12232, Zürich, 1997.

[7] D. Erni, "Nichtperiodische Konzepte in integrierten optischen Wellenleiterstrukturen," *Bulletin SEV/VSE 3/97*, vol. 88, no. 3, pp. 11-16, März 1997.

[8] D. Erni, M. M. Spühler, and J. Fröhlich, "Evolutionary optimization of non-periodic coupled-cavity semiconductor laser diodes," *Optical and Quantum Electronics (OQE), Special Issue: The 1997 International Workshop on Optical Waveguide Theory and Numerical Modelling*, vol. 30, no. 5/6, pp. 287-303, May 1998.

[9] D. Erni, M. M. Spühler, and J. Fröhlich, "A generalized evolutionary optimization procedure applied to waveguide mode treatment in non-periodic optical structures," *8th European Conf. on Integrated Optics ECIO'97*, April 2-4, pp. 218-221, Stockholm, Sweden, 1997.

[10] M. M. Spühler, D. Erni, and J. Fröhlich, "Topological investigations on evolutionary optimized non- periodic optical structures," *1997 International Workshop on Optical Waveguide Theory and Numerical Modelling*, Sept. 19-20, University of Twente, the Netherlands, 1997.

[11] M. M. Spühler, D. Erni and J. Fröhlich, "An evolutionary optimization procedure applied to the synthesis of integrated spot-size converters," *Optical and Quantum Electronics (OQE), Special Issue: The 1997 International Workshop on Optical Waveguide Theory and Numerical Modelling*, vol. 30, no. 5/6, pp. 305-321, May 1998.

[12] M. M. Spühler, B. J. Offrein, G.-L. Bona, R. Germann, I. Massarek and D. Erni, "A very short planar silica spot-size converter using a non-periodic segmented waveguide," *J. Lightwave Technol.*, vol. 16, no. 9, pp. 1680-1685, Sept. 1998.

[13] M. M. Spühler, B. J. Offrein, G.-L. Bona, R. Germann, and D. Erni, "Compact spot-size converter using non-periodic segments for high refractive index contrast planar waveguides," *European Conference on Lasers and Electro-Optics CLEO'98* Sept 13.-18., Glasgow, UK., CWN3, pp. 234, 1998.

[14] D. Wiesmann, D. Erni, J. Fröhlich, H. Rothuizen, R. Germann, G.-L. Bona, Ch. David and H. Jäckel, "Apodization of a grating filter by concatenation of Bragg gratings with different ridge patterns," *9th European Conf. on Integrated Optics ECIO'99*, April 14-16, Torino, Italy, WeG, pp. 159-162, 1999.

[15] Ch. Hafner, "MMP-CG-PET: The parameter estimation technique applied to the MMP code with the method of conjugate gradients," *ACES Journal.* vol. 9, no. 3, pp. 28-38, 1994.

[16] Ch. Hafner, J. Fröhlich, "The parameter estimation technique (PET): Speeding up dense matrix methods," *Proceedings of the 11th Annual Review of the Applied Computational Electromagnetic Society*, Monterey, CA, 1995.

[17] S. Hunziker, *Analyse und Optimierung faseroptischer SCM-Links*. Diss. ETH, No. 12604, Zürich, 1998.

[18] B. Oswald, D. Erni, H. R. Benedickter and W. Bächtold, "Dielectric properties of natural materials," *IEEE-AP Soc. Int. Symp., Conf. on Antennas and Propagation,* Atlanta, pp. 2002-2005, June 22-26, 1998.

[19] G. Björk, O. Nilsson, "A new exact and efficient numerical matrix theory of complicated laser structures: properties of asymmetric phase-shifted DFB lasers," *J. Lightwave Technol.*, vol. 5, no. 1, pp. 140-146, Jan. 1987.

[20] D. Wiesmann, J. Hübner, R. Germann, I. Massarek, H. W. M. Salemink, G.-L. Bona, M. Kristensen and H. Jäckel, "Large UV-induced negative index changes in germanium-free nitrogen-doped planar SiO_2 waveguides," *IEE Electron. Lett.*, vol. 34, no. 4, pp. 364-365, Feb. 1998.

[21] J. Hübner, D. Wiesmann, R. Germann, I. Massarek, B. J. Offrein, and M. Kristensen, "Strong Bragg gratings induced with 248 nm light in buried silicon oxynitride waveguides," *OSA Topical Meeting on Bragg Gratings, Photosensitivity, and Poling Glass Fibers and Waveguides: Applications and Fundamentals.* Williamsburg, VA, Oct. 26-28, 1997.

[22] H. Sakata, "Sidelobe suppression in grating-assisted wavelength-selective couplers," *Opt. Lett.*, vol. 17, no. 7, pp. 463-465-2043. April 1992.

[23] T. A. Strasser, P. J. Chandonnet, J. DeMarco, C. E. Soccolich, J. R. Pedrazzani, D. J. DiGiovanni, M. J. Andrejco, and D. S. Shenk, "UV-induced fiber grating OADM device for efficient bandwidth utilization," *Proc. Opt. Fiber. Commun. Conf., OFC'96*, vol. 2, Feb. 25 – March 1, San José, CA, USA, pp. 360-363, 1996.

[24] N. Matuschek, F. X. Kärntner, U. Keller, "Exact coupled-mode theories for multilayer interference coatings with arbitrary strong index," *IEEE J. Quantum Electron.*, vol. 33, no. 3, pp. 295-302, March 1997.

[25] J. A. Dobrowolski, "Numerical methods for optical thin films," *OSA Optics & Photonics News*, pp. 25-33, June 1997.

[26] K. De Mesel, I. Moerman, R. Baets, B. Dhoedt, P. Van Daele, and Jiri Stulemeijer, "Spot size converters for low cost PICs," *9th European Conf. on Integrated Optics ECIO'99*, April 14-16, Torino, Italy, ThC, pp. 253-258, 1999.

[27] S. Jüngling, J. C. Chen, "A study and optimization of eigenmode calculations using the imaginary-distance beam-propagation method," *IEEE J. Quantum Electron*, vol. 30, no. 9, pp. 2098-2105, Sept. 1994.

[28] S. Hunziker and W. Bächtold, "Cellular remote antenna feeding: optical fibre or coaxial cable?" *IEE Electron. Lett.*, vol. 34, no. 11, pp. 1038-1040, 28th May 1998.

[29] S. Hunziker and W. Bächtold, "Fiber dispersion induced nonlinearity in fiber-optic links with multimode laser diodes," *IEEE Photon. Technol. Lett.*, vol. 9, no. 3, pp. 371-373. March 1997.

[30] S. Hunziker, "Volterra analysis of second- and third-order intermodulation of InGaAsP/InP laser diodes: theory and experiment," *Opt. Eng.*, vol. 34, no. 7, pp. 2037-2043. July 1995.

[31] S. Hunziker and W. Bächtold, "Simple model for fundamental intermodulation analysis of RF amplifiers and links," *IEE Electron. Lett.*, vol. 32, no. 19, pp. 1826-1827. Sept. 1996.

[32] R. W. Tkach, A. R. Chraplyvy, F. Forghieri, A. H. Gnauck, R. M. Derosier, "Four-photon mixing and high-speed WDM systems," *J. Lightwave Technol.*, vol. 13, no. 5, pp. 841-849, May 1995.

[33] P. Sheng, *Introduction to Wave Scattering, Localization, and Mesoscopic Phenomena.* San Diego: Academic Press, 1995.

[34] Ch. Hafner, *Post-modern Electromagnetics – Using Intelligent Maxwell Solvers.* Chichester, West Sussex, UK: John Wiley & Sons, 1999.

[35] D. Erni, "MMP analysis of very short doubly perturbend waveguide structures," *7th European Conf. on Integrated Optics ECIO'95*, April 3-6, Delft, The Netherlands, pp. 387-390, 1995.

[36] Ch. Hafner, "Efficient MMP computation of periodic structures ," *Proceedings of the 10th Annual Review of the Applied Computational Electromagnetic Society*, March 21-26, pp. 303-310, 1994.

[37] M. M. Spühler, D. Erni, "Structural optimization in planar integrated optics," *1999 International Workshop on Optical Waveguide Theory and Numerical Modelling,* Sept. 23-25, The University Jean Monnet, Saint-Etienne, France, 1999.

Genetic-Algorithm Optimization of an Array for Near-Field Plane Wave Generation

Neil N. Jackson* and Peter S. Excell

University of Bradford, U.K.
*Now with Motorola P.L.C., Swindon, UK

Abstract

An alternative approach to the design of an array antenna to be used to generate plane waves in the near field is presented. The original array was designed on the basis of a triangular grid of seven elements arranged in a hexagon, to minimize the number needed to achieve approximately uniform illumination of the test zone, under the assumption of isotropic element radiation patterns. In the alternative approach, a genetic algorithm was used to discover more economical distributions of elements which could still generate acceptable approximations to a plane wave zone. It was found that considerable simplifications from the 'common sense' approach were possible.

1. Introduction

The desirable incident field distribution in a radiative susceptibility test is a plane wave, existing at least over a test zone large enough to enclose the equipment under test (EUT). A susceptibility test is intended to seek out the worst-case response of the EUT, equivalent to finding the main lobe amplitude of an antenna, and such a measurement is relatively tolerant of imperfections in the quality of the plane wave zone. Typical accuracy criteria for established electromagnetic compatibility tests of this type would correspond to a spread in the field amplitude of 3dB peak-to-peak (often up to 6dB) and a phase spread of 90° peak-to-peak. This is in contrast to the situation for precision antenna measurements, where deep nulls and low sidelobes have to be measured in close proximity to the main lobe: maximum amplitude uncertainties of 0.1dB and phase variations of 22° are then common criteria. The quality criterion on the plane wave zone for EMC testing is thus lower than that for antennas, but the desired bandwidth is likely to be greater and the pressure to constrain costs greater.

Test facilities for antennas which create a local plane wave region in the near field ('Compact Ranges') almost always use illuminating antennas that are variants on standard reflector antenna designs. The same principle has been extended to EMC testing, with the modified criteria discussed above, but its use of space is rather uneconomical for many purposes [1]. To overcome this deficiency, the use of array antennas for illumination of the range has been investigated, with some success [2]. The array was designed on the basis of a triangular grid of seven elements arranged in a hexagon. This arrangement was chosen intuitively as, in principle, it minimizes the number of elements needed to achieve approximately uniform illumination of the test zone, under the assumption of isotropic element radiation patterns. To achieve a high-quality plane wave zone, it is necessary to feed the elements with differing signals having non-intuitive ratios of relative amplitude and relative phase and this greatly adds to the cost and complexity of the scheme. These signal amplitudes and phases have to be found by optimization procedures based on a least-mean-squares method [2]. It is thus desirable that the number of elements in the array be reduced by a systematic procedure that can still guarantee maintenance of a

plane wave test zone that conforms to chosen criteria representing an acceptable approximation to a local plane-wave zone.

As an experiment in application of genetic algorithm (GA) methods to antenna design, such an approach was investigated as a way of producing a thinned array design for an EMC-quality compact range that would still be capable of generating an acceptable approximation to a local plane wave over a specified test zone. The method requires the running of numerical simulations of the antenna very many times over, and this can become costly in use of computer time. To minimize this requirement, the array elements in this experimental study were chosen to be simple dipoles: the behavior of an array of more directive elements, such as log-periodic antennas will not be significantly different in the direction of the test zone, since their main-lobe amplitude is relatively invariant with angle. Clearly, there will be great differences between the behavior of dipoles and directive antennas in other directions, but these are not of importance for the present application.

2. Genetic Algorithm Implementation

A genetic algorithm has the following general form [3,4]:

1. Create a population of N random individuals (chromosomes).
2. Assess the performance of each individual.
3. Rank individuals with respect to performance and assign a fitness value dependent on ranking.
4. Select M individuals (parents) from the population for breeding, the probability of being chosen being proportional to fitness.
5. Randomly pair parents and crossover parts of each chromosome (genes) to form N offspring.
6. Randomly mutate genes in the offspring chromosomes.
7. Assess the performance of each new individual in the population of offspring.
8. Record best individual.
9. Repeat from step 3 for required number of generations.

For applications in electromagnetics, steps 2 and 7 can represent vastly larger computational tasks than all of the rest put together. In the present work, the industry-standard program NEC-2 [5] was used for these steps.

2.1 Population Representation and Initialization

Genetic algorithms operate on a number of potential solutions called a population. The population is composed of a number of individuals (chromosomes), which contain an encoded description of the parameters (equivalent to 'phenotypes' in biological terminology) to be optimized. The most commonly used method of encoding phenotypes is as binary strings [3], which are concatenated to form a chromosome.

After devising a suitable encoding scheme, an initial population of chromosomes (typically around 100) is randomly generated.

2.2 The Objective and Fitness Functions

The chosen objective function, O(x), is used to provide a measure of how individuals have performed with respect to the problem space. The individual with the best value of O(x) is assigned a rank position of N and the worst O(x) is assigned a rank position of 1. Another function, called a fitness function F(x), is then used to transform O(x) into a measure of relative fitness. The fitness value is assigned according to the rank position, p_x of individual x. The fitness function is then derived from the rank position by application of a bias or selective pressure parameter, B, towards the most fit individuals. In the present case the following simple linear function was adopted:

$$F(x) = \frac{B(p_x - 1)}{N - 1} \tag{1}$$

Hence, best-fit individuals will have a fitness function equal to B and worst fit individuals will have a fitness function of zero.

2.3 Selection

Selection is the process of determining the number of times a particular individual is chosen for reproduction and, thus, the number of offspring that it will produce. The simplest selection method uses the fitness function values to reject a percentage of the population that performs badly [4]. A better selection technique [6] employs a roulette wheel selection (RWS) mechanism to select individuals probabilistically. In roulette wheel selection each individual in the population has a roulette wheel slot, sized in proportion to its fitness. In mathematical terms this may be expressed as shown in Equation (2):

$$\text{Prob(x selected)} = \frac{F(x)}{\sum_{i=1}^{N} F(i)} \tag{2}$$

A real-valued interval is determined as a sum (S) of the fitness values over all the chromosomes in the current population and individuals are then expressed as a proportion of this sum. To select an individual, a random number is generated in the range from zero to S and the individual whose segment spans the random number is the individual to be selected. This process is then repeated until the desired number of individuals has been selected.

2.4 Mating or Crossover

The basic operator for producing new chromosomes in genetic algorithms is that of crossover. Like its counterpart in nature, crossover produces new individuals that have some parts of both parents' genetic material. Several crossover strategies exist, each with their associated merits. The simplest form of crossover, and the one employed here, is that of single point crossover [6]. The chromosomes selected are randomly shuffled and then paired for breeding. A crossover point is randomly selected, dividing each parent chromosome into two gene strings which are then swapped to generate two new chromosomes (offspring).

To maintain the size of the original population, the new individuals, created by crossover of the selected individuals, must be reinserted into the old population. This was achieved by creating sufficient new individuals to replace the least-fit half of the old population. The most-fit half thus survives, and its children attempt to evolve to a superior form. Once a new population has been produced, its fitness may be determined.

2.5 Mutation

In natural evolution, mutation is a random process where a gene is altered to produce a new genetic structure. In genetic algorithms, mutation is randomly applied (with a low probability, typically in the range 0.001 to 0.01) to modify elements in the chromosomes. The role of mutation is to enable the recovery of good genetic material that may have been lost through the action of selection and cross-over [3]. Many variations on the mutation operator have been proposed, for example, biasing the mutation towards individuals with lower fitness values to increase the exploration in the search without losing information from the fitter individuals [7], or parameterizing the mutation such that the mutation rate decreases with the population convergence [8].

2.6 Termination

Because the genetic algorithm is a stochastic search method, it is difficult to specify convergence criteria. As the fitness of a population may remain static for a number of generations before a superior individual is found, the application of conventional termination criteria becomes problematic. A common practice [4] is to terminate the GA after a pre-specified number of generations and then test the quality of the best members of the population against the problem definition. If no acceptable solutions are found, the GA may be restarted or a fresh search initiated.

3. Optimization of the Geometry of an Array of Five Wire Dipoles

A computer program was developed which incorporated the major features of a GA, as outlined above. In addition, the software was developed to automatically generate input files in NEC format and then run NEC-2 [5] from within the programming environment. For computational speed, an array of five half-wavelength wire dipole antennas was initially chosen to demonstrate the use of a GA for minimizing the normalized error in plane wave synthesis.

The frequency was fixed at 1GHz and a test zone defined as a cube of side length 0.6m (2λ) with the front face positioned 0.4m from the array. Element locations were constrained to the nodes in a two-dimensional grid with 8×8 allowed locations and a spacing of 0.5λ (to avoid overlapping elements). The number of combinations in which it is possible to arrange five elements in the 64 locations, excluding any superpositions of elements and eliminating all patterns that are identical apart from a spatial transformation, is approximately 7.6×10^6 and hence use of an exhaustive search technique for finding an optimum arrangement was infeasible.

For this problem, the parameters to be optimized were the locations of each of the five array elements. A suitable chromosome structure therefore consisted of ten phenotypes as shown below:

$$\text{chromosome} = [(x_1,y_1)\ (x_2,y_2)\ (x_3,y_3)\ (x_4,y_4)\ (x_5,y_5)] \quad (3)$$

where x_n,y_n are the two-dimensional co-ordinates of the nth array element.

1. Setting the number of bits (genes) per phenotype to be 3 led to a problem space equivalent to an 8 × 8 grid and a total chromosome length of 30 bits.

2. Setting the restriction that the grid spacing was to be 0.5λ led to a problem space of dimensions 3.5λ × 3.5λ. A phenotype of value 000 was made to correspond to a value of -0.45m and a phenotype of value 111 made to correspond to 0.6m. The asymmetry is a function of the 3-bit resolution and the fact that it was considered desirable that one element had the potential to be located at the problem space origin.

3. The performance of each individual was determined by first calculating the excitation weightings of individual array elements using the synthesis methods described in [2] and then computing the normalized synthesis error (see below). This was adopted as the Objective Function and the results ranked from 'best' (lowest) to 'worst' (highest).

4. Selection of the most fit individuals (those having the lowest numerical value of the normalized synthesis error) was made using the roulette wheel method and using a selective pressure of B = 2 for defining the fitness function.

5. The mutation method used was to change the value of a randomly selected gene from a randomly selected chromosome at each generation.

6. The number of chromosomes per population was chosen to be 100 and the algorithm was terminated after 100 generations.

The near field synthesis procedure [2] involves the specification of a three-dimensional mesh of M points within the test zone. A set of excitations for the elements of the illuminating array, [f], is then derived by minimizing the deviations between the resulting electric field values at the nodes of the mesh and the values that would be present if the field distribution was a perfect plane wave. The process may be represented by the matrix equation:

$$[T][f] = [E] \approx [E_0] \quad (4)$$

where [f] is an n-element vector of complex excitations for the n elements of the array, [E] is an M-element vector of the resulting electric field values at the nodes of the grid in the test zone, $[E_0]$ is a similar vector for the desired plane wave and [T] is the interaction matrix, of size n × M. The elements of [T] can be found by using an electromagnetic field computation program, such as NEC. The synthesis algorithm finds values for the elements of [f] that minimize the deviation between [E] and $[E_0]$.

The normalized synthesis error is a measure of the quality of the fit of the synthesized field to the desired distribution. It is the normalized summation of the field deviations at all points in the discretisation mesh used by the synthesis algorithm within the test zone:

$$\text{Synthesis error} = \frac{\sum_{m=1}^{M} |E_m - E_{0m}|^2}{\sum_{m=1}^{M} |E_{0m}|^2} \tag{5}$$

where E_m and E_{0m} are arbitrary elements of the vectors [E] and [E_0] respectively.

3.1 Results Using Synthesis Method with Magnitude and Phase Specified

Using the synthesis method with magnitude and phase specified [2], a genetic algorithm, as described in previous sections, was initiated. Figure 1 shows how the synthesis error of the best-fit individual varied with generation. This figure highlights the difficulty in specifying convergence criteria since the synthesis error remains static for an unpredictable number of generations. The optimized element locations are shown in Figure 2 and the computed element excitations are listed in Table 1. The optimized geometry is two-dimensional and symmetrical about the origin with each element spaced at a distance of one wavelength from each other element. The resultant geometry is perhaps intuitively obvious; however, this may not necessarily always be the case for larger arrays or for different array patterns.

A sample of the computed x-component of the electric field in slices throughout the quiet zone is shown in Figure 3 and the resultant synthesis error and the worst case deviation in the field magnitude and phase throughout the entire test volume are also summarized in Table 1. The deviations are calculated with respect to an ideal plane wave.

Table 1 Summary of Element Excitations, Synthesis Error and Maximum Field Deviation for a Genetically Optimized Array using Magnitude and Phase Synthesis

Element Number	Magnitude (dB)	Phase
1	0.00	0.0°
2	-4.90	-41.8°
3	-4.90	-41.8°
4	-3.95	-8.9°
5	-3.95	-8.9°
Synthesis error	0.1530	
Magnitude Deviation	±4.9 dB	
Phase Deviation	±53°	

3.2 Results using Synthesis Method with Magnitude Only Specified

From previous studies [2] it was determined that a synthesis technique with magnitude only specified offered the best method for minimizing the synthesis error. The GA was thus used to determine if a more optimal geometry could be achieved using this procedure. As an aid to assessment of the performance of the genetic algorithm to optimize the plane wave quality, a benchmark problem was

proposed. The *cross* geometry shown in Figure 2 was considered suitable for comparison purposes and optimum element excitations determined, using the magnitude-only synthesis method, for the test zone specified.

Figure 4 shows how the synthesis error of the best-fit individual varied with generation. The synthesis error for the benchmark case is included for comparison purposes. It is clear that the genetic algorithm has been successful in reducing this error. The optimized element locations are shown in Figure 5 and the computed element excitations are listed in Table 2.

Table 2. Summary of Element Excitations and Synthesis Error for Benchmark and Genetically Optimized Arrays using Magnitude-Only Synthesis

	Benchmark Array (Cross)		Genetic Array	
Element Number	Mag (dB)	Phase	Mag (dB)	Phase
1	0.00	0.0°	0.00	0.0°
2	-9.34	-44.6°	0.00	0.0°
3	-9.34	-44.6°	-1.84	-2.9°
4	-8.87	13.6°	-1.84	-2.9°
5	-8.87	13.6°	-8.96	47.3°
Synthesis Error	0.0442		0.0239	
Magnitude Deviation	±4.24 dB		±3.08 dB	
Phase Deviation	±61°		±70°	

A sample of the computed x-component of the electric field in slices throughout the quiet zone is shown in Figure 6 for the benchmark case and in Figure 7 for the best-fit genetically optimized array. The resulting synthesis error and the worst case variation in the field magnitude and phase for the two cases are summarized in Table 2. Comparing the results for the cross geometry with those obtained in Section 3.1, where the excitations had been optimized using the magnitude and phase synthesis method, shows that an improvement in the normalized synthesis error and magnitude deviation is achieved by using the magnitude-only method. However, the phase performance is shown to degrade somewhat.

Comparing the results for the cross array with those for the magnitude-only genetically-optimized design shows that there is an improvement in the field magnitude error at the expense, however, of the phase uniformity. This is not unexpected since the optimization method, in this case, did not take phase into account when computing the synthesis error.

4. Conclusions

Genetic algorithms were shown to be able to derive simplified designs for an illuminating array antenna of a plane-wave generator for electromagnetic susceptibility testing. Traditional designs had used seven elements, whereas genetic optimization showed that adequate performance could, in principle, be achieved with five. The study was undertaken as a proof-of-concept exercise using plain dipoles as the array elements, whereas a practical array would use log-periodic elements. Use of dipoles would cause difficulties in practice due to generation of stray radiation away from the test zone,

but within the test zone itself the behavior of dipole and log-periodic elements would be broadly similar. The two genetically-derived designs studied both reached the optimum configuration in less than 60 generations.

The design that was derived by genetic optimization with magnitude and phase specified was of a cross-shaped configuration that was similar to a thinned version of the traditional hexagonal seven-element design, but inherently more economical due to the use of only five elements. The configuration optimized under a magnitude constraint only was closer in form to a linear array, with the result that phase errors in the test zone reached 70°, although the amplitude distribution was relatively constant, showing a lower maximum deviation than could be achieved with the cross geometry. The excitation pattern for the near-linear array might be seen to have advantages of simplicity in some realizations, in cases where the phase error can be tolerated. However, the cross-shaped geometry is likely to be more generally useful.

References

1. Rousseau, M. and Excell, P.S.: 'Computation of the Field Distribution in a Broadband Compact Range for EMC Applications', IEE Conf. Pub. No. 274, 'Antennas & Propagation', York University, UK, Vol. 1, pp. 395-398, 1987.

2. Excell, P.S., Jackson, N.N. & Wong, K.T.: 'A Compact Electromagnetic Test Range using an Array of Log-Periodic Antennas', IEE Proceedings, Part H, Vol. 140, No. 2, pp 101-106, 1993.

3. Goldberg, D.E.: 'Genetic Algorithms in Search, Optimization and Machine Learning', Reading MA: Addison-Wesley, 1989.

4. Haupt, R.L.: 'An Introduction to Genetic Algorithms for Electromagnetics', IEEE Antennas and Propagation Magazine, Vol. 37, No.2, pp. 7-15, 1995.

5. Burke, G.J. and Poggio, A.J.: 'Numerical Electromagnetics Code (NEC): Method of Moments', US Naval Ocean Systems Center, Rept. No. TD116, 1981.

6. Michalewitz, Z.: 'Genetic Algorithms + Data Structures = Evolution Programs', Berlin: Springer Verlag, 2nd edition, 1992.

7. Davis, L.: 'Adapting Operator Probabilities in Genetic Algorithms', Proceedings of the 3rd International Conference on Genetic Algorithms, pp.61-69, 1989.

8. Fogarty, T.C. 'Varying the Probability of Mutation in the Genetic Algorithm', Proceedings of the 3rd International Conference on Genetic Algorithms, pp. 104-109, 1989.

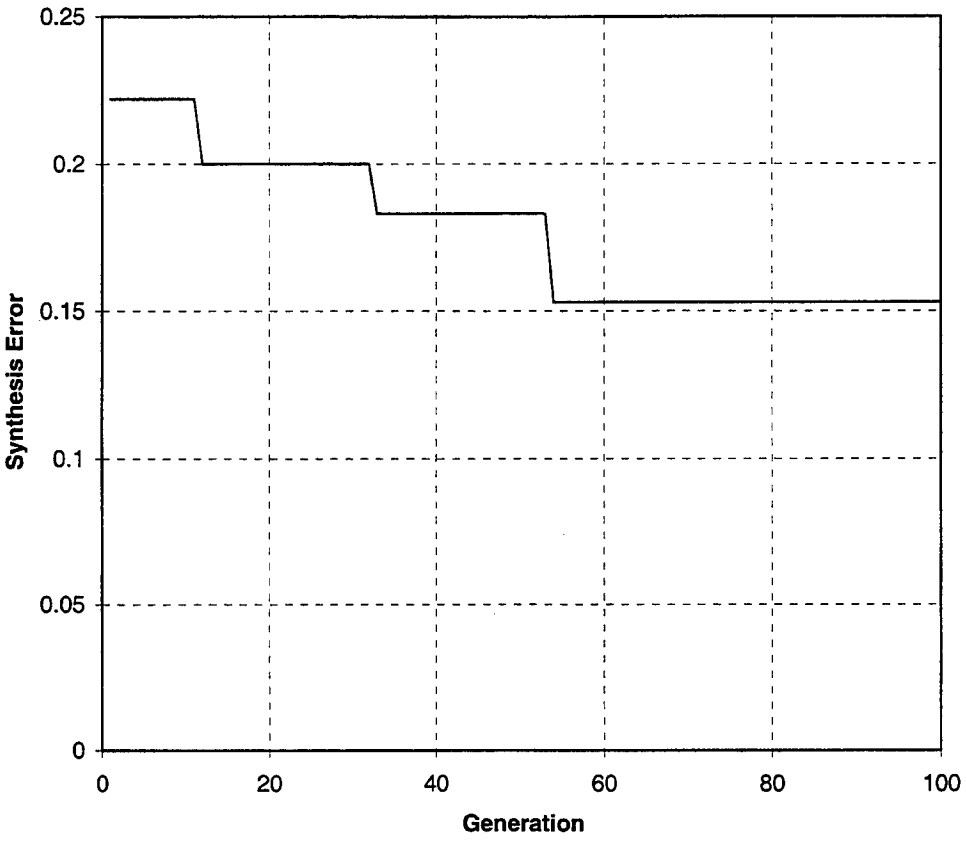

Fig. 1. Variation of best synthesis error with generation: magnitude and phase synthesis method.

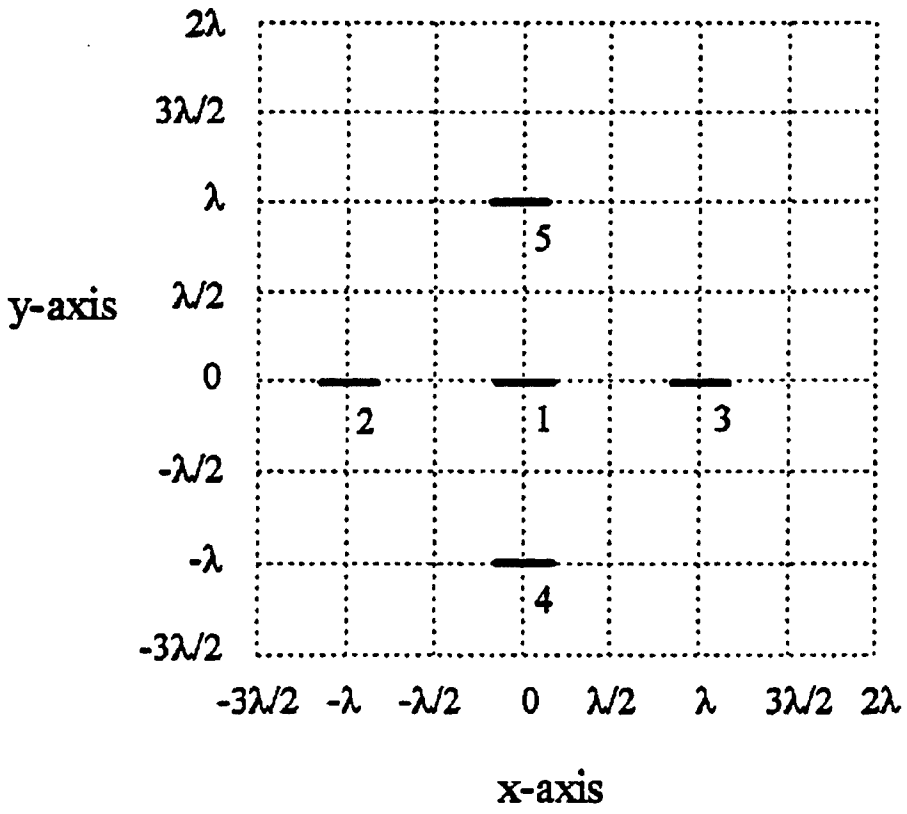

Fig. 2. Genetically optimized element locations using magnitude and phase synthesis method.

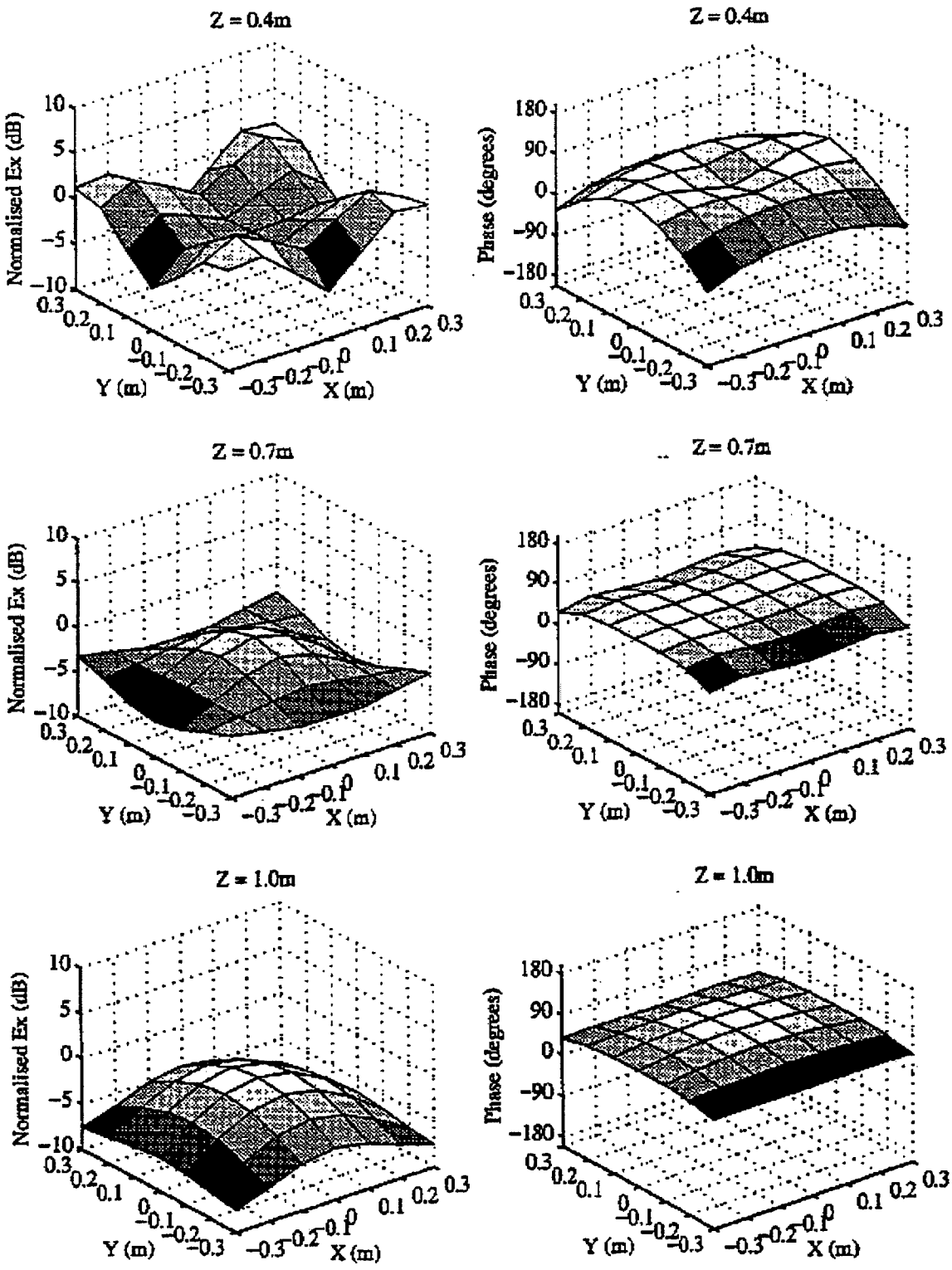

Fig. 3. Magnitude and phase variations of dominant (x) component of computed electric field strength due to array in Fig. 2, synthesized by magnitude and phase method.

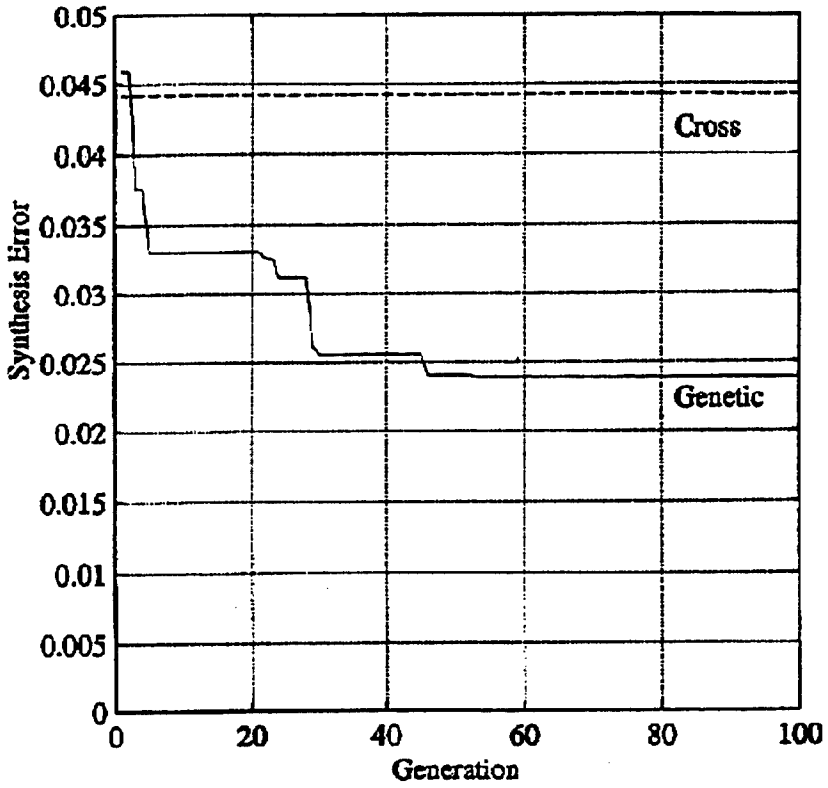

Fig. 4. Variation of best synthesis error with generation: magnitude-only synthesis method

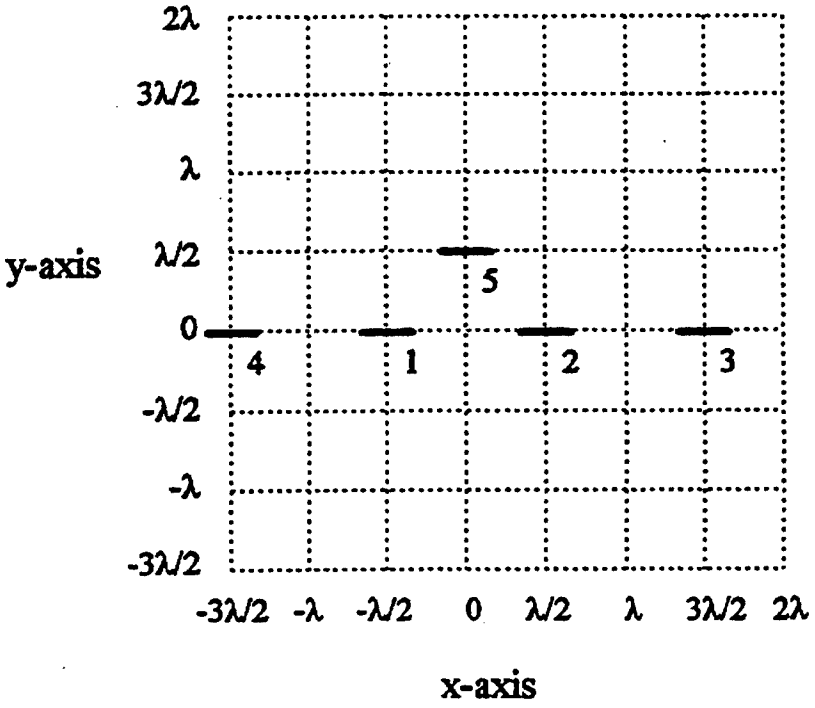

Fig. 5. Genetically optimized element locations using magnitude-only synthesis method.

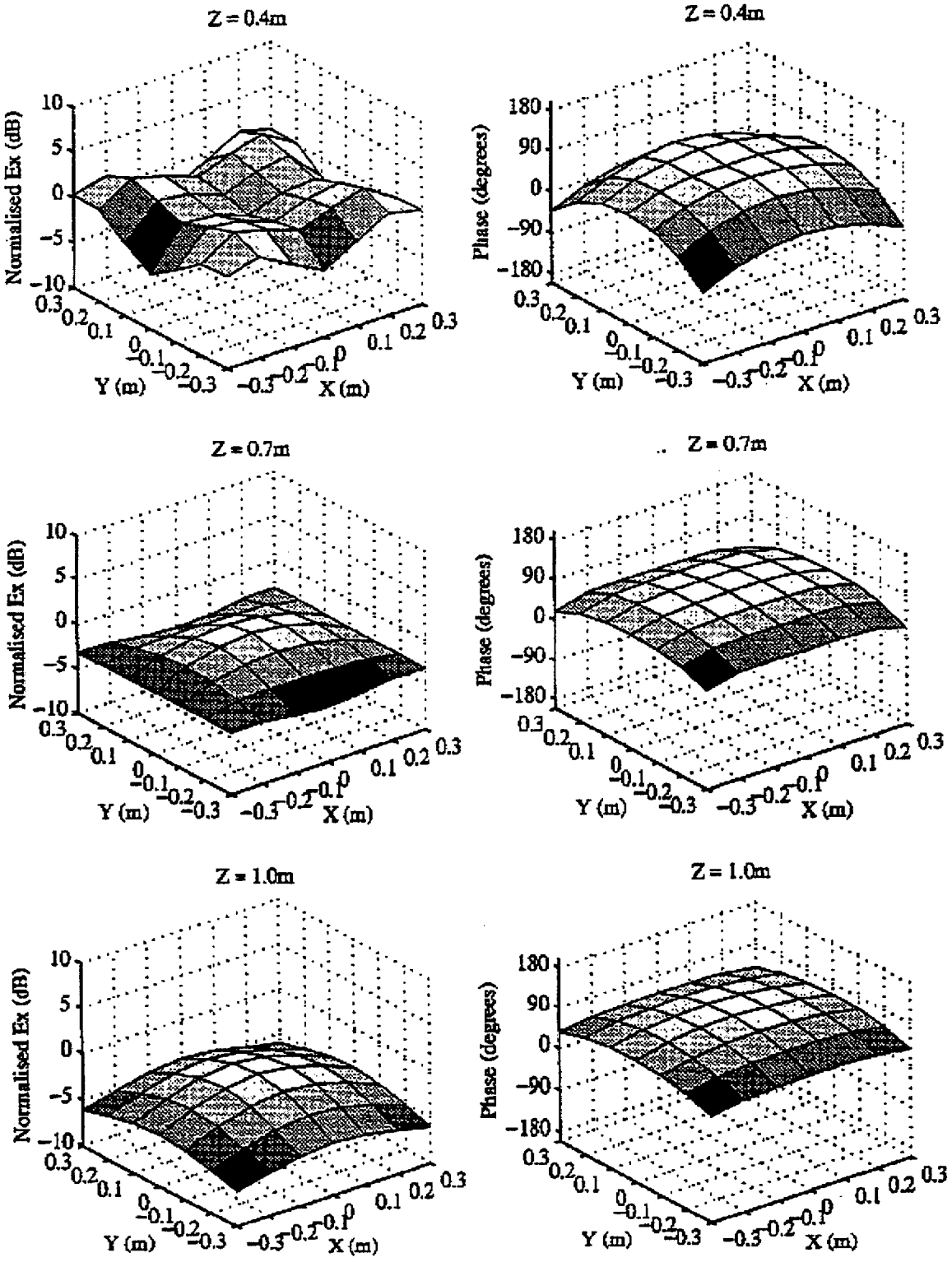

Fig. 6. Magnitude and phase variations of dominant (x) component of computed electric field strength due to cross-shaped array in Fig. 2, synthesized by magnitude-only method.

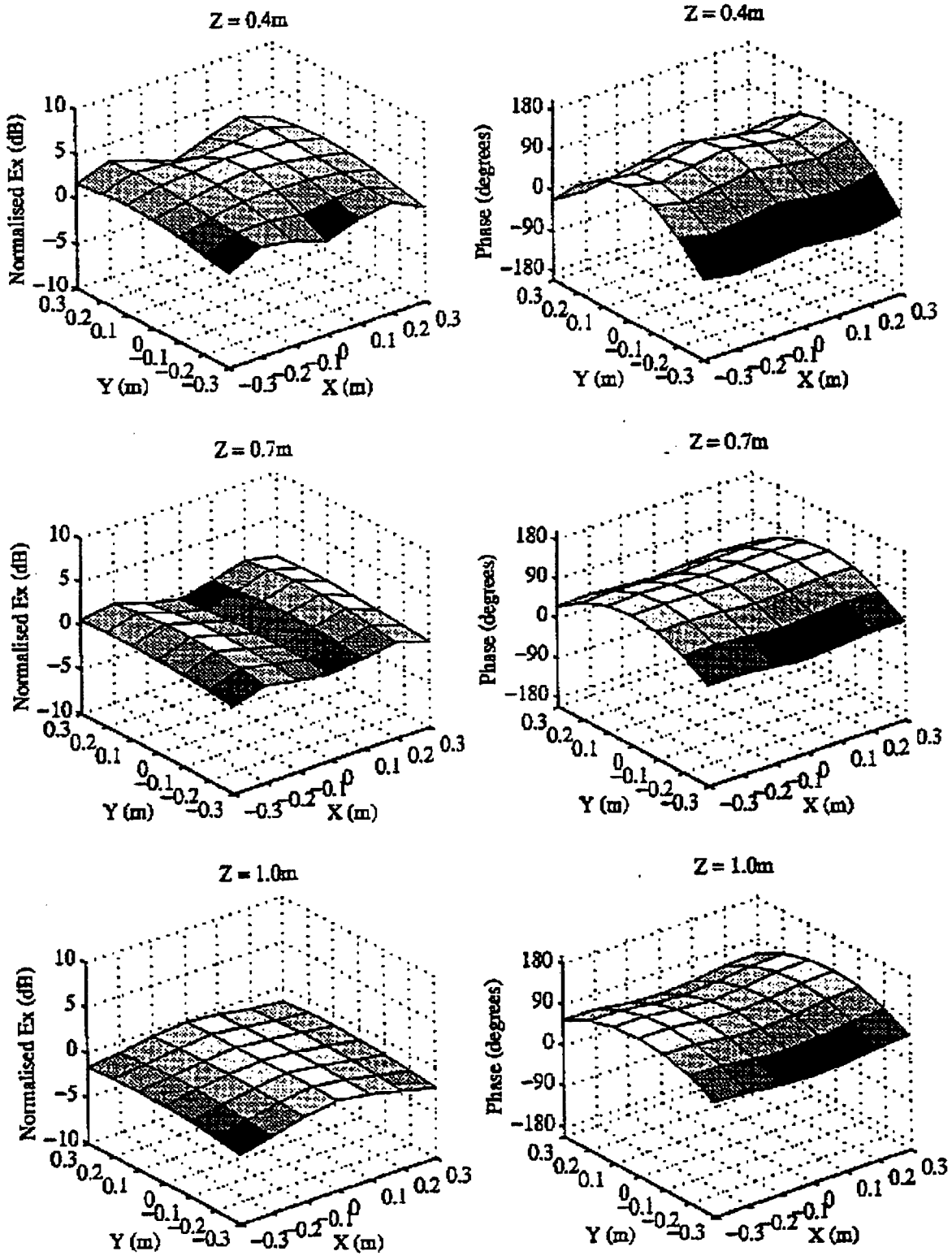

Fig. 7. Magnitude and phase variations of dominant (x) component of computed electric field strength due to near-linear array in Fig. 5, synthesized by magnitude-only method.

Increasing Genetic Algorithm Efficiency for Wire Antenna Design Using Clustering

D. S. Linden
R. MacMillan
Linden Innovation Research LLC
info@lindenir.com

Abstract

The Genetic Algorithm (GA) is a very robust, powerful technique that is capable of optimizing designs in very multimodal search spaces. However, it also requires significant numbers of simulations to perform such optimizations. If the simulations are expensive, as in the case of antenna design, GAs can be prohibitively expensive to use. A clustering technique has been investigated which cuts the required number of function calls 20-90% with minor or no degradation in the optimization quality. In this technique, a GA using real-valued genes is halted when the population has clustered around portions of the search space, and a local optimization technique completes the optimization quickly. This method has been applied to a variety of test functions and wire antenna designs, and the advantages of this technique seem to have broad applicability.

1.0 Introduction

Communication, radar and remote sensing systems employ thousands of different types of wire antennas, and there is an increasing need for high-performance, customized antennas. However, antenna design is a difficult field of engineering. Antenna designs have non-intuitive, complicated search spaces, and problems with even a few variables are highly multimodal. In addition, most antenna simulations require a significant amount of time to run. Typical simulations can take anywhere from a few seconds to several hours, so it is imperative to use an efficient yet robust method of optimization.

Genetic algorithms (GAs) [1, 2] are currently being explored with great success as a way to automate the antenna design process [3]. GAs are well suited to the multimodal, spiky search spaces of electromagnetic problems. Particularly useful is that the GA does not require an initial guess, and the amount of design information the engineer must supply can be very minimal.

In spite of their success, GAs with conventional convergence criteria require too many cost function evaluations for many antenna design problems. This research investigates using the clustering behavior of real-valued genes during a GA optimization as a way to determine convergence—a method that significantly enhances efficiency.

A GA begins with a random distribution of points across a search space. As the GA run progresses, order begins to appear in the population. For many optimization problems, the initial random distribution begins to cluster around certain points in the search space, and gene values begin to show organization, first in multi-modal, then unimodal, distributions as the GA converges. Once gene value distributions become clustered around points in the search space, the GA has probably found a number of hills which, barring unusually useful mutations, the GA will slowly begin to exploit. Members of the population that are fit enough to survive will generally be from one of these peaks. Peaks with individuals of greater fitness will gain more population members, and eventually the entire population will exist on a single peak and then a single point.

The GA can, however, be stopped as soon as the population has divided itself into a number of discrete clusters. A local optimizer can then be applied to each cluster. Because this clustering can occur early in the GA run, many cost function evaluations can be saved, usually with minor or no impact on the optimization results.

1.1 Real GAs and Adewuya's Method

The reader is probably familiar with binary GAs, in which all parameters are encoded into a string of bits called a chromosome. Any continuous parameters must be discretized, which means that resolution becomes a factor. The crossover processes for these GAs are also straightforward, involving swapping bits in some fashion to create children. However, previous research [4] has shown that real-valued GAs, where each gene in a chromosome is a real number, coupled with special crossover techniques, are much better at optimizing problems with all or nearly all parameters continuous.

These special crossover techniques involve the use of interpolation and extrapolation to create children. The method used by the authors was first investigated in [5], and is called Adewuya's method. Adewuya's method consists of a sequence of crossover methods applied to real genes. First, quadratic crossover is applied, where the child's gene is taken from a predicted minimum of a quadratic curve fit using three parents. If quadratic crossover fails, heuristic crossover is applied, which pulls the child's gene from a range predicted to be better than two parent's genes. See Figure 1 for a graphical representation of what happens in these two methods.

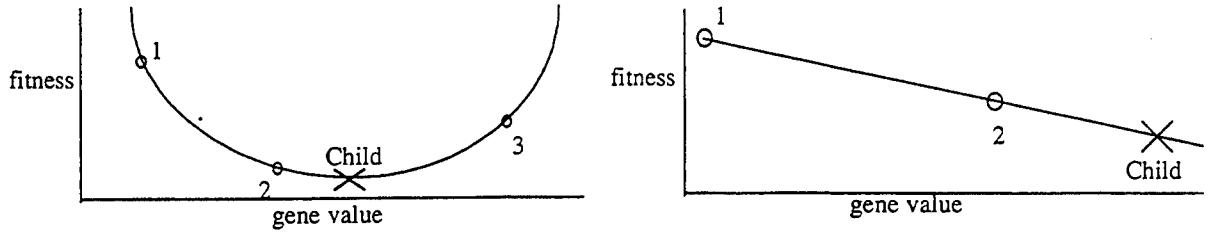

Figure 1. Quadratic and heuristic crossover. Fitness is to be minimized in these examples.

If both quadratic and heuristic crossover fail, the child's gene is one of the parent's genes taken at random. This process is applied gene by gene to create a new child. See [4, 5, 6] for a more complete explanation and comparisons with other methods. This method has been found to be particularly powerful in electromagnetics and mechanical engineering.

Mutation for the real valued GA can take many different forms. The one used here was Gaussian—mutated genes were pulled from a distribution with a mean equal to the unmutated gene, and a standard deviation of 0.1 of the full gene range.

Each gene varied over the same range. We chose this range to be from 0 to 1. Each gene is translated into parameter values as appropriate, and can cover very different ranges in the design space. However, normalizing the gene values in this way allows the accurate calculation of the genetic distance between individuals using Euclidean geometry, a very important quality when determining the clusters in a population.

Regarding other GA parameters, mating selection was accomplished via the weighted roulette wheel method of [2], and a steady-state GA was used, in which the parents of the next generation are the best of a specified percentage of the total population. This percentage is called the overlap, for it is the portion of each generation that carries over to the next. This type of GA has proved to converge quickly, a feature necessary to accommodate the costly simulation time of antenna designs. Fitness scaling was also used for the weighted roulette wheel, basing the amount of the roulette wheel given to an individual on the difference between the scores of that individual and the worst parent carried over from the previous generation.

1.2 Wire Antenna Design

Since F. Braun created the first wire antenna in 1898, a variety of wire antennas have appeared: monopoles (e.g., car whip antennas), log-periodic antennas (e.g., rooftop TV aerials), helix and spiral antennas, and a host of other types. In recent years, GAs have shown sufficiently powerful to optimize even very challenging designs for unusual applications [3,6,7,8]. Following is a definition of several antenna design terms that are important in this paper.

Directivity and *gain* are two related qualities in antenna design. Directivity is the ratio of power density being transmitted by an antenna in a particular direction to the average power density being transmitted in all directions. The gain is the directivity multiplied by the ratio of power radiated to power input. Gain takes into account the losses due to resistance in the antenna, which converts some of the input power into heat. When the losses are considered to be zero, as in this paper, the directivity and gain are equal.

Gain is usually expressed in decibels (dB), which relates to a ratio of power or power densities by the following expression: $dB = 10\log_{10}(P_1/P_2)$. In the case of gain, P_2 is the power density of an isotropic radiator that transmits power equally in all directions. The abbreviation dBi refers to gain compared with an isotropic radiator. However, the "i" is sometimes left off, and is understood from context.

A *gain pattern* or *antenna pattern* plots gain magnitude versus angle, showing the proportion of power an antenna transmits in a particular direction. For 2-D antennas, or antennas symmetric in the third dimension, this angle is simply the elevation angle θ. In 3-D, there are two angles that specify a direction: θ and the azimuth ϕ. Figure 2 shows these angles on a set of axes. An antenna is considered to be *directive* if its gain pattern is heavily weighted in one direction.

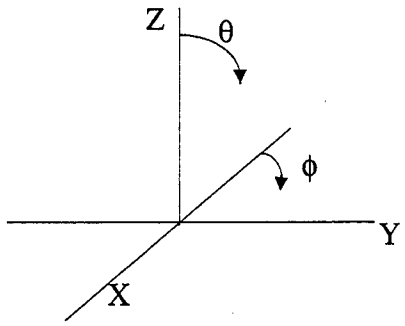

Figure 2. θ and ϕ on a 3-D axis system. Arrows begin where NEC2 defines 0 degrees for θ and ϕ.

A *ground plane*—at its simplest a large, flat metal plate underneath the antenna—is often used in conjunction with a wire antenna. It acts as a mirror for the antenna above it, and therefore changes the antenna gain pattern. A ground plane can decrease the height and/or simplify the construction of the wire antenna. The hood or roof of a car acts as a ground plane, and antennas that will be affixed to such places need to be designed for use with one.

There are several electromagnetic simulators that exist for wire antennas. One particularly suited to the task of creating a general antenna synthesis system is the Numerical Electromagnetics Code, Version 2 (NEC2) [9]. This code was used exclusively on this research. NEC2 has a simple file-interface for input and output that makes it ideal for using with an optimizer. The code is in the public domain, so obtaining and modifying the source code is cost-free and easy, as is copying the simulator between machines. But perhaps most important, it has a long track record of being accurate. The NEC2 code was produced in the early 1980s, and has been used it to simulate antenna structures for many years. It has shown itself to be in very good agreement with actual measurements, and thus one can have more confidence that answers received from simulation have validity.

There are three antennas that will be discussed in this paper: a two-wire Yagi antenna, a loaded monopole, and a 14-wire Yagi antenna.

1.2.1 The Two-wire Yagi

The Yagi antenna is a series of parallel wires, first proposed by Prof. Yagi and his student S. Uda in the late 1920s. One element is driven, one element is behind the driven element and is called the reflector, and, usually, there are other elements in front of the driven element called directors. The highest gain can be achieved along the axis and on the side with the directors. The reflector acts like a small ground plane, allowing power that would otherwise be sent backward to be reflected forward.

In this case, there are no directors—only the reflector and the driven element. This gives a two-dimensional problem, as shown in Figure 3. The chromosome for this antenna is two real genes, encoding length and separation respectively.

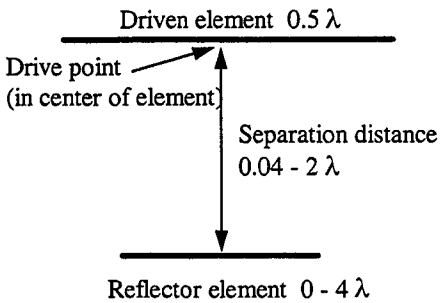

Figure 3. Two-element Yagi antenna search space. λ = 1 wavelength

In spite of the fact that there are only two variables, the response surface is very multi-modal, as shown. This behavior is typical for electromagnetic problems, which are usually filled with local minima. This behavior shows why GAs are one of the most powerful techniques for solving these problems—its parallel sampling of the search space makes it able to resist many of the local minima.

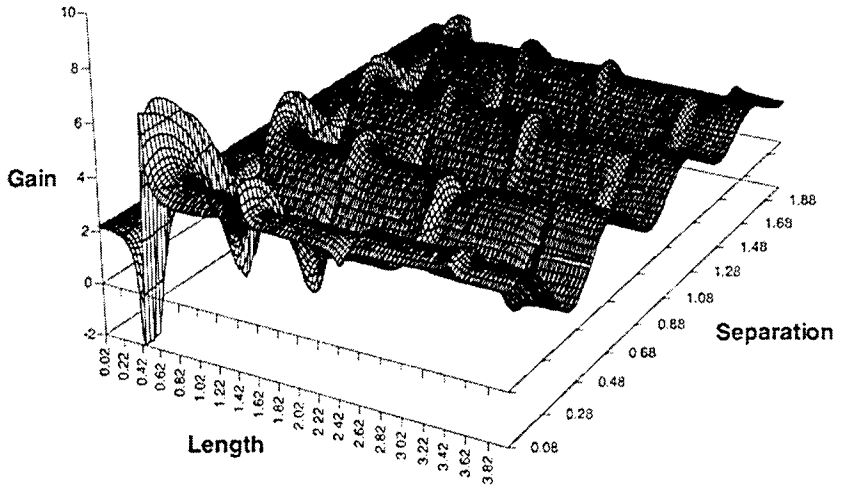

Figure 4. Response surface for gain vs. separation and reflector length.

The goal for this antenna is to maximize the forward gain, so the objective function for this antenna is simply the gain. As can be seen on the graph, the best parameter settings to maximize gain are a length of about 0.48λ and a separation of about 0.14λ. The figure below shows what the antenna pattern looks like near this maximum.

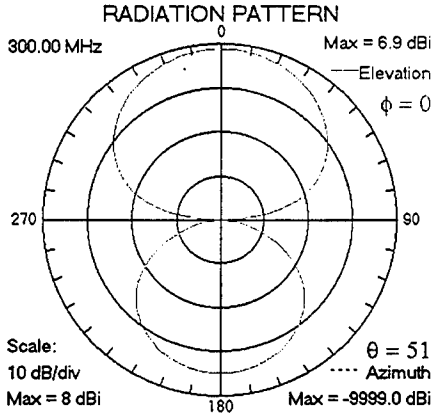

Figure 5. Radiation pattern of an antenna near the maximum

GAs optimizing this antenna show clustering in a very clear way, as will be described in the next section. But first, the other wire antennas, the loaded monopole and the 14-wire Yagi, need explanation.

1.2.2. The Loaded Monopole

A monopole loaded with a modified folded dipole has been previously investigated [10]. It has a search space as shown below.

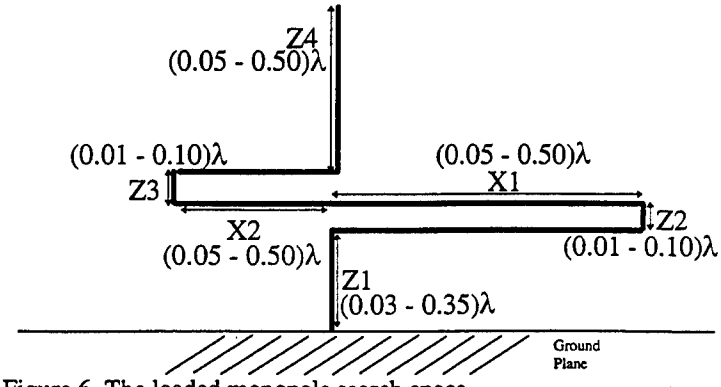

Figure 6. The loaded monopole search space

The chromosome for this antenna is six real-valued genes, encoding Z1 through Z4, then X1 and X2. However, the ordering makes no difference, because the crossover techniques described in section 1.1 are applied separately for each gene.

This antenna is capable of having even coverage over the upper hemisphere given the proper set of parameters [8]. The resulting pattern for one such configuration is shown in Figure 7.

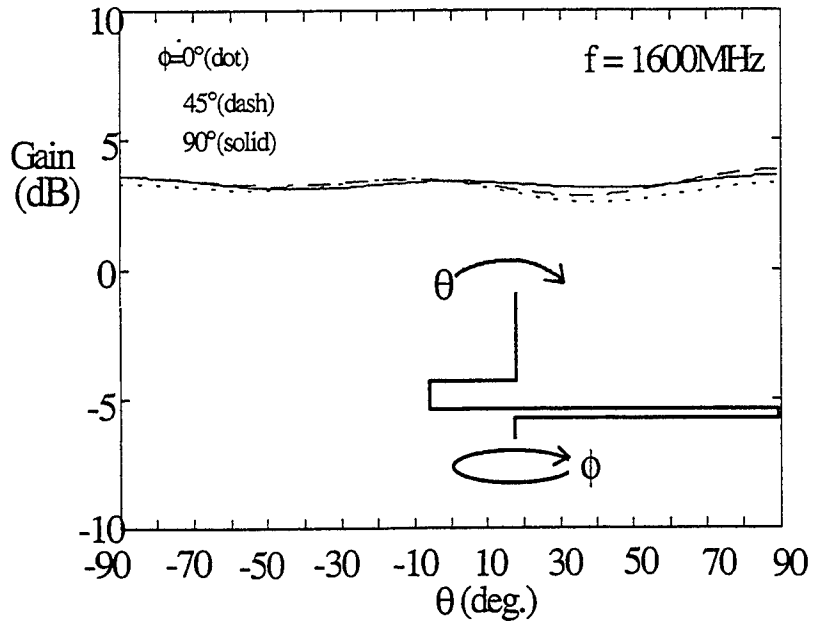

Figure 7. Folded monopole pattern and corresponding optimized design.

What is unusual is that the shape is so asymmetric. This asymmetry was an unexpected result, but further study showed it to be necessary to achieve the very flat pattern shown in Figure 7.

The objective function for this antenna is the sum of the squares of the deviation of all calculated gains from the mean. In equation form:

Fitness = $\Sigma_{\text{over all } \theta,\phi}(\text{Gain}(\theta,\phi) - \text{Avg. Gain})^2$.

The GA's goal is to minimize this function.

1.2.3. The 14-wire Yagi

The 14-wire Yagi antenna is a more traditional Yagi antenna than the two-wire Yagi above, with a reflector, driven element, and 12 directors as shown below. This antenna optimization is the most challenging of all the examples, with 28 variables, multiple criteria, and a difficult, sensitive search space. It will show whether the clustering technique described in the paper will work on a truly difficult problem.

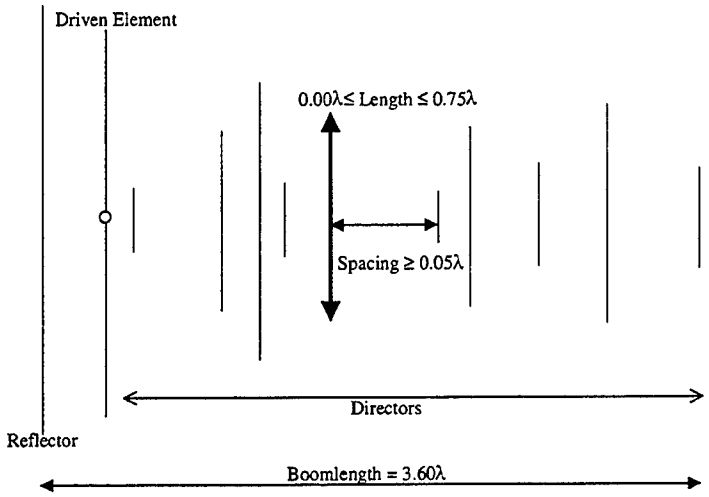

Figure 8. 14-wire Yagi design.

The real-valued chromosome consists of 14 length genes, 13 spacing genes, and a gene for wire diameter. Each wire length is allowed to vary between 0.0 λ (effectively removing the element) and 0.75λ. They are constrained to be symmetric.

The spacing between wires is constrained to be greater than 0.05λ. However, the boomlength is constrained to be 3.60λ, so the 14 wires are spaced along this length as follows: the values of the genes corresponding to the spacings are totaled, then the boomlength is divided by this total. This result is multiplied by each spacing gene value to give the required spacing between each pair of wires. The last variable is the wire diameter, which is allowed to vary between 0.004λ and 0.012λ.

The criteria were VSWR and endfire gain. The score was given by:

$$\text{Score} = G - C_1 \times (\text{VSWR})$$

where G is the endfire gain and C_1 is 10 when the VSWR is greater than 3.0 and 0.50 when the VSWR is less than 3.0. (It should also be noted that (VSWR-1.0) is used instead of VSWR when it is less than 3.0 to further decrease the importance of this factor on the score.) The objective was to maximize the score.

These three antennas will show, on a preliminary level, the applicability of the clustering technique described in the next section.

2.0 The Clustering Method

GAs usually begin with a randomly generated population, scattered stochastically around the search space. As survival of the fittest is applied, the population quickly begins to avoid unfruitful areas. Then, the population begins to cluster around certain places in the search space. What is happening is that those regions are loci of good fitness, and individuals produced within them are viable—i.e., they will have sufficient fitness to survive. Those that are produced outside of these regions will probably not have enough fitness to survive once the population is firmly clustered around these points. This effect can also be regarded as speciation, for intraspecies individuals, likely to remain inside a cluster, will survive, while interspecies individuals, likely to fall outside of any cluster, will perish.

One the population is clustered, there will be little exploration of the search space. What will happen is a "battle" in which the clusters fight for individuals. The better-scoring clusters will generally receive more of the new children, and as the scores increase, the lesser clusters will lose individuals, finally dying off one by one until only one cluster is left.

Following is a graphical representation of this process, taken from an optimization of the two-wire Yagi antenna using a real-valued GA.

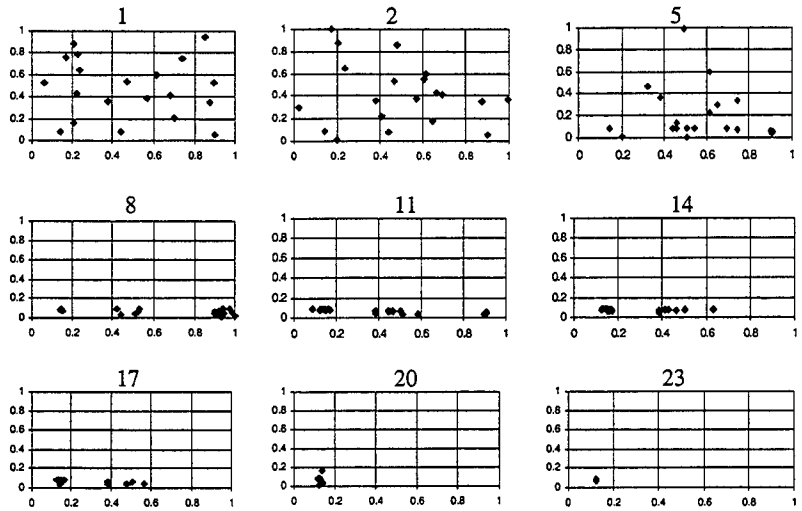

Figure 9. An example of clustering in the case of the 2-wire Yagi. From [6].

Generation 1 is randomly scattered throughout the space. As can be seen, the worst areas are avoided even beginning with generation 2, and by generation 8 the population is clustered around three points. From generation 8 through 23, nothing happens except gradual extinction of clusters until only the best remains. The GA requires just as many resources during this last process as it did when it was very effectively finding good regions in the search space.

It makes intuitive sense, then, that this battle is simply a waste of resources. Why not stop the GA when the population is clustered, and use a local optimizer on one or more of the clusters, since each cluster is probably a single peak in the search space?

The challenge in applying this idea is finding an automated technique that can detect when the population is properly clustered. Though there are many ways to determine this process, a simple approach was taken in this research, which involved using a threshold value for cluster radius, similar to [11].

To start the first cluster, the two closest individuals in the population, as determined by Euclidean distance, are clustered, if they are closer than the cluster threshold. The center point between them is calculated, then the nearest individual to this center point is added if its distance is less than the cluster threshold. The new center point of the cluster is calculated, the next-closest individual added, etc., until there are no other individuals within the cluster threshold distance from the cluster center.

The closest pair of individuals not already clustered is then checked to see if the distance between them is less than the cluster threshold. If it is, then a new cluster is formed in the manner of the first one. This process continues until there are no unclustered individuals closer to each other than the cluster threshold.

Once a specified percentage of parents is clustered, the GA is halted. As will be shown, this percentage makes a large difference on the effectiveness of this procedure, for if one halts the GA before a sufficient number of parents are clustered, the local optimization will not be very effective, for the best peak has not been sufficiently defined.

In addition, an elitist cluster routine was found to be the most effective. An elitist routine is one that specifies that regardless of the percentage of the parents that are clustered, the GA will not be halted until the best individual is clustered as well. A study comparing the elitist and non-elitist routines showed far better results with small additional computational expense for the elitist routine. This result is intuitive, for if the best individual is not in a region with a cluster, there is a good likelihood that the GA is not done exploring the space yet and there will still be some shifting in clusters before it is ready to be halted.

It was initially thought that the local optimizer might be most effective if it operated on the center of the cluster, as opposed to the best individual from the cluster. Study showed this was not the case; results were disappointing from the cluster center, but were very good from the best individual. For this reason, the score of the cluster is taken as the score of its best individual, and that individual is passed to the local optimizer when the GA is halted.

Before tuning the method, it was not known if one needed to optimize all clusters to be reasonably certain of getting the best answer, or if it was sufficient to optimize only the best cluster. We were surprised to learn that optimizing only the best individual, which is contained in the best cluster by default, is sufficient to produce excellent results. On rare occasions, the

second-best cluster actually was located on the best peak, but this happened so infrequently (less than 5% of the time) that the extra function calls necessary to optimize the second-best peak were deemed not worth the expense. However, this behavior needs to be explored for more problems, for it is conceivable that more complex problems in very spiky search spaces may show greater benefit when the less-fit clusters are optimized.

Though this process is tied to a specified cluster threshold, its effectiveness seems universal, and seems to be more effective with more difficult problems. The results of our experiments with this method will now be discussed.

3.0 Results

In this section, the effectiveness of the clustering routine is discussed for many different problems, including simple test functions, the two-wire Yagi, the loaded monopole, and the 14-wire Yagi. The routine seems to be effective on both simple and complex problems, as will be shown.

In order to compare the clustering method with a standard GA, a standard baseline GA needed to be created. This GA has the following convergence criteria, which are not particularly unusual: halting after the best individual has been static for 11 generations, or when the range of values present in the parents for each gene fall within 1% of the total gene range. After the GA is halted, a conjugate gradient local optimizer, the same as is used for the clustering method, is used to optimize the best individual.

3.1 Test functions

These functions were used to create and debug the clustering routine, though they could not be used to fine-tune the routine because they are so simple. However, they do show that the clustering routine is effective even for simple problems, and are included for completeness.

Three simple test cases were used. The first test case is De Jong's F5 [12], shown below. It has two dimensions, and a maximum value of 1.002.

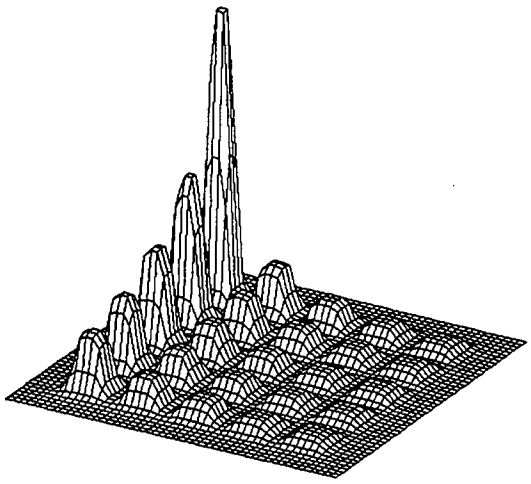

Figure 10. De Jong's F5 test function

The second test case is a low-modality sinusoidal function, given by the equation:

$$\text{Score} = \Sigma_{i=1 \text{ to } 6}(\sin(\pi x_i)-\cos(3\pi x_i))$$

One dimension is shown below:

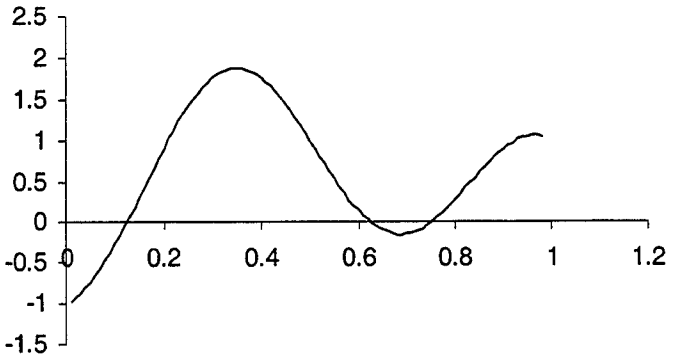

Figure 11. One dimension of sinusoidal test function #1

This function was tested in six dimensions, which has a maximum value of 11.272.

The third test case is a more challenging sinusoidal function, tested in 10 dimensions, has a maximum value of 20.0. Its equation is: Score = $\Sigma_{i=1 \text{ to } 10}(\sin(\pi x_i)-\cos(10\pi x_i))$

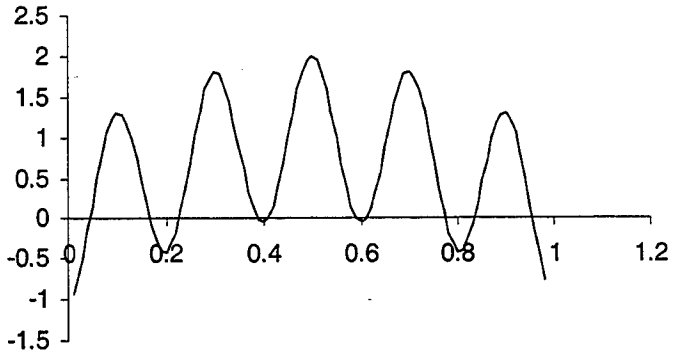

Figure 12. One dimension of sinusoidal test function #2

Each test case was tried over a range of population sizes (25, 50, 75, 100, 150, 200) and overlaps (0.25, 0.5, and 0.75). The results were averaged over all combinations of these two variables, to determine the overall effect of the method on results without bias toward a particular population or overlap value. The results of these experiments are contained in the table below.

	Average score			Average objective function calls		
	Baseline	Cluster method	% difference	Baseline	Cluster method	% difference
F5	0.789	0.724	-8.3%	693	459	-33.7%
Sin #1	10.9	11.0	0.3%	1236	669	-45.9%
Sin #2	18.9	17.9	-5.1%	1763	1358	-23.0%

Table 1. Results from test functions

For the F5 test function, the clustering method loses 8.3% in score while decreasing function calls by 33.7%, and both changes are statistically significant as shown by the student's t-test statistic.

The 2nd test case performed quite well. There was a statistically insignificant difference in the score between the clustering method and the baseline GA, while the decrease in function evaluations was 45.9%!

For the third case, the clustering technique took a loss of 5.1% on average score while providing only a 23.0% gain in efficiency. This is not particularly spectacular, though it is significant.

All three test cases showed varying degrees of improvement in runtime, between about 20% and 50%, and varying degrees of change (generally degradation) in optimization quality, between 0.3% and -10%. However, the real test of the method is in solving actual design problems, which will now be discussed.

3.2 The Two-wire Yagi

Two experiments were run with the two-wire Yagi: a parameter tuning experiment, and a confirmation of the clustering effect over a wide range of population sizes and overlaps.

3.2.1 Fine-tuning the clustering parameters

Though simple test cases showed improvement with this method, they were too simple to use in fine-tuning. The parameters for this method are the percentage of parents to be clustered before halting the GA and the cluster threshold (also called cluster size). Each was tuned preliminarily using the test functions above. However, the parameter values that worked for the test functions did not work at all well for the two-wire Yagi. Therefore, an experiment was run to determine the best values for these parameters for this more realistic engineering problem.

The data points shown in Table 4 are the average performance over three population sizes (25, 50 and 100) and two overlaps (0.25 and 0.5), which gives a broad indication of its effectiveness. The Cluster threshold (which is the maximum Euclidean distance between any two members in the cluster) was varied between 0.1 and 0.3, and the percentage of the parents that were required to be clustered varied from 70% and 90%. The resulting average scores and number of objective calls required to complete the optimization are shown below.

Cluster threshold	% clustered	Avg. score	Avg. objective function calls
0.1	70%	5.25	703
0.3	70%	5.55	523
0.1	90%	6.40	650
0.3	90%	5.29	592

Table 2. Cluster parameter experiment

The results show that the best scores resulted from a tight clustering threshold, and as large a percentage of the parents clustered as possible before halting the GA. Though these settings do not give the best time savings, the difference in scores make the extra simulations worthwhile. These settings make intuitive sense as well, for if the clusters are too large, the cluster may actually cover more than one local minimum, causing the local optimizer to fail. In addition, if some parents are not clustered, that means that some viable individuals are alone in their region of the search space, and they are probably on some sort of peak that should be investigated before halting the GA.

Further investigation showed that increasing the parent percentage clustered gave still better results, thus the parameter settings that were used for the rest of the experiments with clustering were 99% of parents clustered and 0.1 cluster threshold.

3.2.2 Confirming the effectiveness of the clustering method

Another full-factorial experiment shows the effectiveness of the clustering method on saving objective function calls while not significantly disrupting performance. The results are shown below.

As with the test cases, the baseline and clustering method were tried over a range of population sizes (25, 50, 75, 100, 150, 200) and overlaps (0.25, 0.5, and 0.75). The results were averaged over all combinations of these two variables, to determine the overall effect of the method on results without bias toward a particular population or overlap value. The results of these experiments are contained in the table below.

Average score			Average objective function calls		
Baseline	Cluster method	% difference	Baseline	Cluster method	% difference
6.241	6.395	2.5%	884	415	-53.0%

Table 3. Comparison of the baseline GA and the GA using the clustering method for the two-wire Yagi.

A student's t-test showed the difference in the baseline and clustering GA average scores were statistically insignificant, with a 44.5% probability it arose by chance. On the other hand, the difference in objective function calls is so significant that there is less than a 0.002% chance that it occurred by accident. The experiment also showed the best predictor of score performance was not clustering but population size. The data shows that the larger the population, the better the score, at least to the 200 individual population size. (Incidentally, previous research [6] has shown that too large a population can actually decrease performance.)

Of course, the major significance of these results is that the clustered GA requires less than 50% of the function calls that the baseline does, for essentially no change in score. This is a phenomenal result, but the next design case shows even greater improvement.

3.3 The Loaded Monopole

Using the tuned parameters of 99% of parents clustered and 0.1 cluster threshold size, the loaded monopole was optimized using the clustering method. A comparison of the two GAs follows, with population sizes and overlaps chosen for each at their optimal point as tuned by the two-wire Yagi experiment:

	Population	Overlap	Average Objectives	Average Score
Baseline	200	0.42	17736	18.1
Clustering	200	0.25	2078	67.3

Table 4. Baseline vs. Clustering GA performance for the loaded monopole

The baseline case was run 6 times, the clustering case 5. Both methods achieved very good designs, but there is an 88.3% savings in objective function calls using the clustering method! However, there is a statistically significant increase in the score for the clustered case. Recall that this objective function is to be minimized, with the ideal being zero. While this degradation may seem significant, the average difference of 49.1, distributed over the 1,188 angles in the objective function, equates to an additional 0.20 dB of variation per angle. This extra variation is insignificant to the design, especially in light of the expected fabrication tolerance and simulator accuracy.

However, this problem was fairly easy, so a more difficult problem is needed to show whether this method will be generally useful.

3.4 The 14-wire Yagi

Using the tuned parameters of 99% of parents clustered, the 14-wire Yagi was optimized using both methods. However, the cluster size made a significant difference in the resulting score of the Yagi antenna. Several runs were conducted with various cluster threshold values as shown below.

	Population	Overlap	Cluster threshold	Average objectives	Average score
Baseline	200	0.42	-	22299	16.29
Clustering	200	0.25	0.53	3549	14.94
	200	0.25	0.26	4930	15.51
	200	0.25	0.053	12898	16.22

Table 5. Baseline vs. Clustering GA performance for the 14-wire Yagi

Note that the largest two cluster threshold sizes used are larger than in the folded monopole, to account for the larger number of dimensions. However, the results show that increasing the cluster threshold caused significantly poorer scores.

In this case, a one-point difference in the score makes a big difference in the quality of the design, since Yagi antennas are desired to be as well-matched and as high-gain as possible. A drop of 1 point means a decrease of 1 dB of gain or a VSWR over 3.0. Thus, the difference in score between the baseline and the clustering method using a cluster size of 0.53 was unacceptable. The search space was too difficult to search with a local optimizer if the cluster had only converged to that size. However, by tightening up the size of the cluster, the clustering method was able to essentially match the baseline score, but in about 58% of the objective calls!

Incidentally, the gain of a typical Yagi with a score of 16.2 is 16.23 dB, with a VSWR of 1.06. A typical Yagi designed using conventional means has a gain of 15.9 and a VSWR of 1.23 [6].

Thus, there is a tremendous speed advantage to using this method for this and the previous time-intensive problems, and the price in design performance can be trivial if the proper settings are used.

Conclusion

In general, the clustering method shows significant, even remarkable, time savings over more typical methods of determining convergence. The time saved by using the clustering method is directly proportional to the decrease in the number of objective function calls for problems with any time-consuming simulations, as in wire antenna design. These savings can be as much as 90% without significant degradation to design performance.

However, the ideal settings for the method have been shown to be problem dependent, though the trend we have found is that the more the population is converged and the tighter the clusters are required to be, the less design performance degrades. Naturally, this performance is achieved at the expense of objective function calls. While good starting values seem to be 99% of the population clustered, and 0.1 cluster size (given a range of 0-1 for all genes), the best settings have to be determined on a case-by-case basis.

While the results presented here are very promising, there is much work that remains. First, an adaptive method of clustering that does not depend on an *a priori* setting of a cluster threshold is desired. Speciation techniques like mating restriction need to be tried with clustering to see if there is any advantage for encouraging early cluster formation beyond what the GA does normally. It would also be of interest to apply this method to a binary GA.

In addition, work must be done to refine the local optimizer, perhaps enhancing its ability to escape from small "traps," because it did not perform as well as expected, given that the cluster methods nearly always placed the local optimizer starting point fairly close to the optimum value. A "fully" converged GA often placed the local optimizer just a little closer to the true optimum—closer enough to produce a statistically significant difference in design performance in many cases.

In summary, then, the method of clustering described in this paper, though simple and relatively unsophisticated, shows tremendous promise at enhancing the efficiency of a GA. It showed time savings in every case it was applied, with the antenna design problems showing greater efficiency enhancement for less degradation in fitness than the test functions. This indicates that this method may be most effective for the problems where efficiency is most needed: large, time-consuming problems that are currently very difficult or even intractable using standard GA optimization.

References

[1] J.H. Holland, "Adaptation in Natural and Artificial Systems. University of Michigan Press, Ann Arbor (1975).
[2] David E. Goldberg, *Genetic Algorithms in Search, Optimization & Machine Learning*, Addison-Wesley (1989).
[3] Y. Rahmat-Samii and E. Michielssen, eds. *Electromagnetic System Design using Evolutionary Optimization: Genetic Algorithms*, Wiley, 1999.
[4] D.S. Linden. "Using a Real Chromosome in a Genetic Algorithm for Wire Antenna Optimization." Proceedings of the IEEE APS International Symposium, Montreal, Canada, 13-18 July 1997.
[5] A. Adewuya, " New Methods in Genetic Search with Real-valued Chromosomes," Master's Thesis, Mech. Engr. Dept., MIT, 1996
[6] D.S. Linden. "Automated Design and Optimization of Wire Antennas using Genetic Algorithms." Ph.D. Thesis, MIT, September 1997.
[7] D.S. Linden and E.E. Altshuler, "Automating Wire Antenna Design using Genetic Algorithms," Microwave Journal, Vol. 39, pp. 74-86, March 1996.
[8] E. E. Altshuler and D.S. Linden, "Design of a loaded monopole having hemispherical coverage using a genetic algorithm," IEEE Trans. Antennas Propagat., Vol. 45, pp. 1-4, Jan. 1997.
[9] G.J. Burke and A.J. Poffio, "Numerical Electromagnetics Code (NEC)-Method of moments, " Rep. UCID18834, Lawrence Livermore Lab. CA, Jan 1981.
[10] E.E. Altshuler, "A monopole antenna loaded with a modified folded dipole," IEEE Trans. Antennas Propagat. Vol. 41, pp. 871-876, July 1993.
[11] J.W. Duda and M.J. Jakiela. "Generation and Classification of Structural Topologies with Genetic Algorithm Speciation," Journal of Mechanical Design, Vol. 119, pp. 127-131, March 1997.
[12] De Jong, K.A. "An analysis of the behavior of a class of genetic adaptive systems." Doctoral Dissertation, University of Michigan, Dissertation Abstracts International 36(10), 5140B, University Microfilms No. 76-9381, 1975.

A Genetic Approach for the Efficient Numerical Analysis of Microwave Circuits

Luciano Tarricone

D.I.E.I., Via G. Duranti, 93, 06125, Perugia, Italy.

Abstract— **The development of efficient and effective algorithms for sparse matrix bandwidth minimization is of paramount importance for the enhancement of many numerical techniques for the analysis of microwave circuits. The task of bandwidth reduction is computationally hard. Several approaches have already been proposed, but the problem is still open.**

In this paper, a genetic solution is proposed. The genetic algorithm is described, as well as its main characteristics (choice of chromosomes, genetic operations, etc.). Results demonstrate that the advantages of the genetic approach vanish because of the huge computational effort required. This severe limitation is removed thanks to the natural amenability of genetic algorithms to a parallel implementation. Results in the paper prove that a parallel genetic approach is a state-of-the-art solution to the problem of bandwidth reduction of sparse matrices encountered in electromagnetic numerical methods.

I. Introduction

The use of numerical methods is nowadays the most typical way to approach the design of complex microwave circuits with a high degree of accuracy, with a low cost and a substantial reduction of times for trimming and tuning. The solution of a linear system of equations

$$Ax = B \tag{1}$$

is quite often the computational core of numerical methods [1]. In some cases, the system (1) is solved many times, with different right-hand-sides B and the same matrix A, and generally the matrix properties affecting the efficiency of the solution are

- its pattern
- its condition number

In many MW applications, both items have a predictable behaviour. For instance, some numerical approaches typically produce sparse matrices (such as in the case of Mode-matching [1], or Finite Element Methods [2]), with a distribution of non-zero elements which can be in some cases predicted. Other approaches, such as the discretization with the Method of Moments (MoM) of mixed-potential integral equations (MPIE) for planar circuits, generate impedance matrices which can be turned, with suitable thresholding actions over its entries, into sparse matrices with a typical blocked-banded pattern. The use of wavelet expansions, for instance in conjunction with a MoM discretization of the solving equations, can improve the condition number (when orthogonal wavelets are used) and increase the matrix sparsity.

Several efforts have been produced to suitably treat the matrix properties, so that efficient linear algebra can be performed inside electromagnetic (EM) codes: the use of appropriate solvers [3], [4], [5], or analytical/numerical approaches for reducing the filling-in of the moment matrix [6], or the coupled use of appropriate solvers with high-performance architectures [7], just to mention some recent works.

It has been demonstrated [8] that, in many cases, the most robust and efficient strategy is based on an appropriate numbering of the problem's unknowns (x in (1)), so that the system is reduced to a banded system with reduced bandwidth. This allows the use of a banded direct factorize-and-solve algorithm, with high efficiency (its complexity depends quadratically on the matrix bandwidth [9]).

As a matter of fact, the efficiency and effectiveness of algorithms for sparse matrix bandwidth reduction is crucial for the high-performance analysis of MW circuits. The identification of an optimum permutation matrix P so that

$$(PAP^T)(Px) = PB \tag{2}$$

is a banded system with minimum bandwidth is an NP-hard task [10], and amenable for a possible solution with a genetic algorithm.

In this paper, we propose a genetic method for the reduction of bandwidth of sparse matrices attained in different MW numerical methods. In Section II, we describe the problem and its general issues. In Section III we describe the proposed genetic solution. In Section IV we compare its results with other bandwidth reducers. In Section V we briefly discuss a parallel version of the genetic approach, and finally draw some conclusions.

II. The problem of bandwidth reduction: why using genetic algorithms

Referring to equation (1), the problem is the following: consider the bandwidth β of the A matrix,

$$\beta = max|i-j| \quad \forall i,j \mid a_{ij} \neq 0 \tag{3}$$

A sparse matrix of dimension N with symmetrical zero-non-zero-pattern can be represented by a graph, as in Fig. 1, once that each row/column is numbered. A vector $\Pi = \{\pi_1, \pi_2, ...\pi_N\}$ is a possible numbering, and

is represented by a permutation of the initial numbering $\{1, 2, ...N\}$. The solution of the problem is represented by an optimum Π_{opt} so that

$$\beta(\Pi_{opt}) = min(\beta(\Pi)) \quad \forall\Pi \tag{4}$$

In case of non symmetrical zero-non-zero pattern, this graph representation has some troubles, and is, as far as we know today, substantially useless.

The solutions to the bandwidth minimization problem proposed in the literature till now can be divided into two main classes:

- Solutions based on a graph representation
- Alternative solutions

The most important approach based on *graph representation* is the one proposed by Cuthill and McKee (CM) in 1969 [11]. They proposed some efficient heuristics to identify Π_{opt}, by introducing: 1) a partitioning of the graph into levels 2) new vertices at a maximum distance 3) heuristical rules for cutting some edges, and creating new ones (see Fig. 1). Several upgrades of the CM approach have been proposed. The one by Gibbs, Poole and Stockmeyer (GPS) [12] is extremely efficient, even though it has recently been overcome by the one by Esposito, Malucelli and Tarricone (EMT) [8], [13], which has been defined as the current state-of-the-art for the bandwidth minimization of matrices generated by EM codes [14].

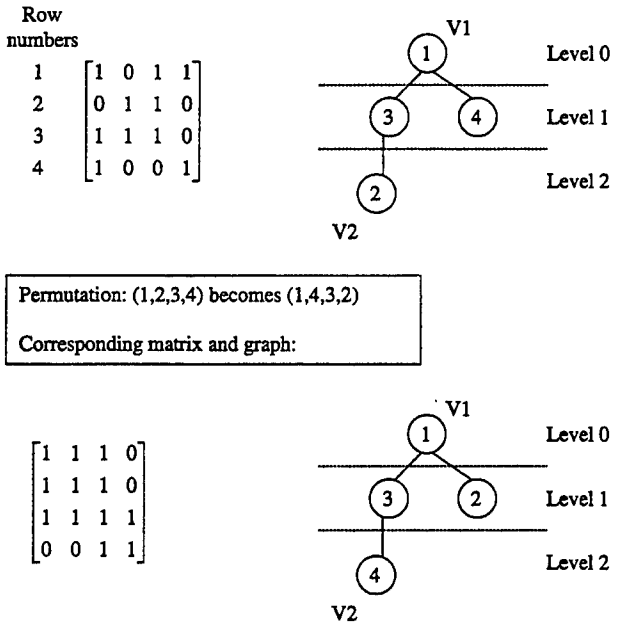

Fig. 1. A sparse matrix with symmetrical zero-non-zero pattern can be represented by a graph, once rows/columns have been numbered. A level partitioning can be identified on the graph, once two vertices V1 and V2 have been selected. A permutation or renumbering of rows/columns modifies the matrix pattern and the graph layout, with effects on the matrix bandwidth.

The *alternative approaches* proposed till now are based on combinatorial techniques based on global optimization. Examples are the use of simulated-annealing (SA) [15] and of Tabu-Search (TS) [16]. In both cases, heuristical laws are introduced, in conjunction with an appropriate use of data structures to take into account the evolution of the search, so that the risk of being trapped into local optima is reduced.

Despite the strong efforts performed till now, several problems are still open. For instance, CM and GPS have severe troubles with some pathological cases arising from FEM simulation of boxed microstrip lines, or MM analysis of rectangular waveguide circuits [1], [17]. Moreover, they cannot cope with the problem of non-symmetrical structures of matrices encountered, for instance, in some cases when wavelet expansions are used with the MoM [4]. The EMT approach has solved these problems, but its performance on non-symmetrical matrices can be enhanced. As for SA and TS approaches, they are quite appropriate to overcome the problem of non-symmetrical patterns, but their numerical weight is still too much to make their use appealing in routinely-used CAD tools.

On such bases, an experimentation of a genetic approach (GA) to the problem is quite interesting. In fact, especially for large matrices, the use of appropriate global search strategies, with the possibility of embedding complex heuristical laws, is essential for finding satisfactory solutions. Moreover, a GA is naturally amenable to represent non-symmetrical problems, with a consequent advantage with respect to graph approaches. It is also easier to implement than graph approaches. Finally, its expectable drawback, i.e. its numerical weight, can easily be circumvented by a migration to parallel platforms (GA is intrinsically amenable to a parallel design).

III. The Genetic Solution

Genetic algorithms are nowadays commonly used in the design and optimization of EM circuits [18]. We address to the pioneeristic works of Goldberg [19] and Holland [20] for the basic concepts, and describe here the main features of the GA proposed here.

A. Choice of chromosomes

As put forwards in (4), the problem unknown is a vector of natural numbers called Π_{opt}. Consequently, it is natural to define chromosomes as strings of natural numbers, of the same dimension of A matrix. This choice has a major drawback. In fact, during the usual operations over chromosomes, for instance when performing cross-overs, we risk the generation of non-feasible chromosomes, such as permutations of Π with repeated numbers. On the other side, cross-over, as quite well-known, is of fundamental importance for the efficiency and effectiveness of the GA. Therefore, in order to avoid the problems of repeated numbers after crossing-over, a set of data structures, and dedicated algorithms, have been designed. The data structures are: 1) the current permutation vector Π; 2) an auxiliary vector *Aux* initialized with a certain permutation without repeated

numbers; 3) a vector $New\Pi$ with the generated permutation. It must be stressed that $New\Pi$ can host permutations with repeated natural numbers. The dedicated algorithms allow the generation of permutations with repeated numbers, and their transformation into permutations without repeated numbers, so that a biunivocal correspondence is guaranteed between each $New\Pi$ instance and each feasible Π instance.

Before describing the algorithms, we introduce a function $foundpos(\Pi(1))$, which finds out the position inside Aux of the first entry $\Pi(1)$ of array Π. For instance, if we have $\Pi = \{3,1,5,4,2\}$, and $Aux = \{1,2,3,4,5\}$, $foundpos(\Pi(1)) = foundpos(3) = 3$. We also introduce a function $delete(arr(i))$, which deletes the entry i from array arr. For instance, if we have $Aux = \{1,2,3,4,5\}$, $delete(Aux(3))$ turns Aux into $\{1,2,4,5\}$ (its dimension has been reduced by one).

The algorithm for generating a modified permutation with repeated numbers is now described. The joint use of $New\Pi$ and Aux data structures guarantees a biunivocal correspondence between each instance of $New\Pi$ and one instance of Π (i.e. a permutation vector without repeated numbers):

for i=1,N
  $New\Pi(i)$ = foundpos(Π(1))-1
  delete(Aux($New\Pi(i)$+1))
  delete(Π(1))
end

The implementation of this algorithms results, for instance, in the following steps for a given current permutation and auxiliary permutation:

Π	Aux	$New\Pi$
31542	12345	2
1542	245	20
42	24	202
2	2	2021
-	-	20210

As apparent, the final $New\Pi$ vector has some repeated numbers. Its use, in conjunction with Aux, is sufficient to convert it into the corresponding Π. The conversion is performed by simply reverting the algorithm to generate the modified permutation.

B. Initial Population

The proposed implementation of the GA has been proved to be nearly unsensitive to the chosen starting population, provided that its cardinality is suitable with respect to the size of the problem (the matrix dimension N).

As already observed for different combinatorial heuristics [21], no deterministic laws have been determined to describe the convergence of the GA with respect to the population generation, as well as to its cardinality. In the current implementation, we generate a starting population by random extraction of permutation vectors from the starting choice $\Pi = \{1,2,....N\}$.

C. Cost function

The choice of a suitable cost function is of paramount importance for the convergence of a combinatorial optimization task. The bandwidth minimization can be performed with different choices of the cost function. One of the most important issues is the selection of a cost function so that as few different solutions Π as possible have equal cost, and risk to be considered as equivalent. For instance, the very trivial choice of a cost function

$$c(\Pi) = \beta(\Pi) \tag{5}$$

where the bandwidth corresponding to a certain permutation vector is the cost, is not satisfactory at all. An enhancement can be the following choice:

$$c(\Pi) = w_1\beta(\Pi) + w_2 N_\beta \tag{6}$$

where N_β is the number of rows/columns that have maximum bandwidth β, whilst w_1 and w_2 are tunable weights. Of course, in case of unsymmetrical patterns, the same function can be transformed into

$$c(\Pi) = (w_{1L}\beta_L(\Pi) + w_{2L}N_{\beta L}) + (w_{1U}\beta_U(\Pi) + w_{2U}N_{\beta U}) \tag{7}$$

where subscripts U and L correspond to "upper" and "lower" part of the matrix (with respect to the main diagonal). The three proposed choices are still not completely satisfactory: even in the case of (6) or (7) there are many different permutation vectors corresponding to the same value of $c(\Pi)$.

Some new ideas have been proposed in [15], and suggest the following solution to the problem of a suitable cost function:

$$c(\Pi) = \sum_{i,j} F(N, |i-j|) \tag{8}$$

where N is the matrix size, and F is the following function:

$$F(N,|i-j|) = \begin{cases} N & |i-j| = 0,1 \\ (N-|i-j|)\cdot(F(N,|i-j|-1) & elsewhere \end{cases} \tag{9}$$

The choice of (8) guarantees an adequate partitioning of the searching space, with a substantial reduction of the risk of equivalence among different permutations. This is the cost function implemented in the proposed GA.

D. Convergence Criterion

The sparse matrix bandwidth reduction is typically used in order to improve the solution time of linear systems by using banded solvers, which have a quadratic complexity with respect to the matrix bandwidth. Therefore, it is possible to evaluate the effectiveness of each iteration by comparing the time needed for a single iteration, with respect to the induced reduction of the solution time. This practical parameter, averaged over a certain number of iterations, is appropriate to evaluate when the bandwidth reduction should be stopped.

E. Genetic Operators

We use three operators: selection, crossover and mutation.

E.1 Selection

We adopt the most typical way of performing selection, i.e. on a cost-proportional basis. This means that N_{sel} elements of the population are randomly chosen, and the one with the lowest cost is selected.

E.2 Crossover

The basic idea is of generating hybrid chromosomes, by crossing together two selected chromosomes. This idea is here coupled with another empirical observation: for each matrix pattern, some rows/columns are more effective than others when performing the permutation. Therefore, when the optimum or quasi-optimum position is found for them, the corresponding information should be preserved in the permutation vector. The natural translation of this idea is the principle of building-blocks, further described.

Now we quickly describe *when* and *how* crossover is to be performed.

- When crossover is to be performed: this is decided following a probabilistic approach [22]. Two vectors from the old population are selected in accordance with the selection operator. One random number p_1 is generated. The two vectors are inserted into the new population if $p_1 \geq 1-p_c$. A second random number p_2 is generated, and crossover performed if $p_2 \geq p_c$. The value of p_c is a heuristically tunable parameter.
- How crossover is performed: two random numbers are generated to identify the beginning and the end of the crossing site. Two new chromosomes are attained by exchanging the crossing sites between the two vectors. For instance, if we indicate with n_1 and n_2 the two random numbers, and with Π_1 and Π_2 the two permutation vectors, the entries $\Pi_1(n_1, \cdots, n_2)$ are swapped with $\Pi_2(n_1, \cdots, n_2)$. In accordance with the principle of *preserving building blocks* [23], we know that a purely random choice of the crossing site is often unsatisfactory. Therefore, by using some statistical data about the role of each element of the permutation vector Π during the search, some positions inside the chromosome are prevented from destruction during crossover. The protected positions typically correspond to rows/columns of the matrix giving a low contribution to the value of the cost function (8). For instance, referring to the previous example, if a position within the range $(n_1, \cdots, n_2)$ is ranked as a building-block, no swapping is performed on it. Of course, when performing crossover, the data structures *Aux* and *New*Π must be suitably managed, so that the modified permutation can be turned into a permutation vector Π without repetitions. The algorithm mentioned in Section III.A is still valid, and must only be adjusted to cope with the problem of beginning and ending point of the crossing site.

E.3 Mutation

Three kinds of mutations are performed: swap, left and right shift. One tunable parameter p_m is chosen, and two random numbers pos_1 and pos_2 generated. A new random number is generated. If it is larger than p_m, genes pos_1 and pos_2 in the chromosome are swapped, and a left and right shift is performed over the partition of vector starting at pos_1 and ending at pos_2.

When mutation is performed, the principle of preserving building blocks is not respected. Moreover, a *distance-dependent* mutation is implemented [24]. In fact, it is well known that, especially when small populations of chromosomes are used, the use of a fixed value of p_m does not prevent from the premature convergence over local minima. Therefore, the value of p_m is dynamically adapted, in order to avoid being trapped into unsatisfactory solutions.

IV. Results on Serial Platforms

We propose two types of results. The former one refers to matrices encountered in the analysis of 1) rectangular waveguides inhomogeneously filled with dielectric (Fig. 2) or 2) boxed microstrip lines (Fig. 3). A revisited version of a public-domain FEM code, called EMAP1, based on a variational scalar formulation [25], is used.

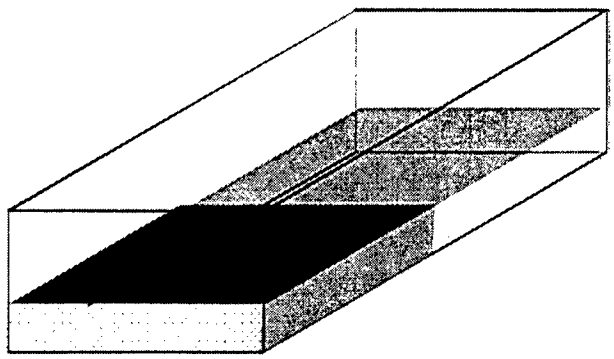

Fig. 2. A rectangular waveguide inhomogeneously filled with dielectric. Different dielectrics and geometries have been chosen. One of the examples is shown in the figure.

The latter refers to matrices generated during the analysis of microstrip circuits with an MPIE-MoM formulation [26]. In all the proposed cases, the performance of the GA is compared with a commercial CM approach available in MATLAB, a GPS and TS solution implemented by the author, and with the previously mentioned EMT solution described in [8], [13].

A. FEM Analysis

Table I proposes results for problems such as the one in Fig. 2. A standard WR90 is studied in the range 8-

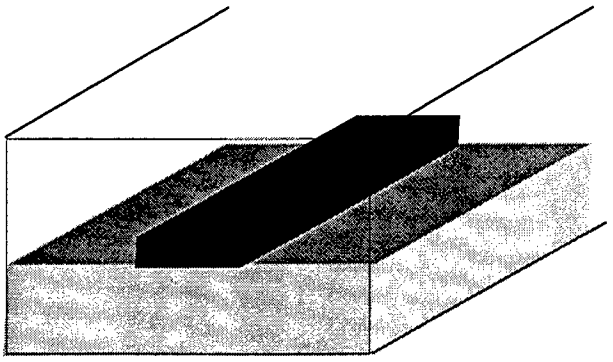

Fig. 3. A boxed microstrip line. Different cases with different dimensions and dielectric layers have been simulated.

12GHz, and the electric field distribution evaluated with different dielectric fillings.

N	In. β	GPS	CM	EMT	TS	GA
284	92	115	74	62	62	62
374	107	122	102	72	106	96
639	151	178	172	87	102	91
1231	251	247	242	199	233	212

Table I: Results for different matrices generated during a FEM analysis of inhomogeneously filled rectangular waveguides. Matrix size N, initial bandwidth β, and final bandwidth attained with different approaches are reported.

As apparent from Tab. I, GPS and CM have a critical behaviour with some pathological cases. The EMT approach is the more robust, even though the GA is quite effective as well. An essential issue is the time needed to achieve the solution. It is reported in Tab.II, on a Pentium 166MHz:

N	GPS	CM	EMT	TS	GA
284	0.218	0.22	0.215	6.9	7.2
374	0.74	0.87	0.560	19.1	18.9
639	2.4	3.2	1.44	498	480
1231	18.8	16	3.74	g.t. 10000	g.t. 10000

Table II: Times to find out the optimum Π for the cases in Tab. I.

Tab. II clearly demonstrates the real limitation of the GA: it is quite effective, but too computationally heavy. For instance, if we consider that the FEM generates banded matrices, we can compare the standard use of banded direct solver (BDS) without bandwidth reduction (i.e. what EMAP1 routinely does), with the case of a banded direct solver (BDS) used after bandwidth reduction. The time (in seconds) needed for a 100 frequency-point analysis is reported in Tab. III:

N	EMAP1	EMT+DBS	GA+DBS
374	264.8	186.1	242
639	798.4	395.2	961
1231	12270	1376	g.t. 30000

Table III: Times in seconds to analize at 100 frequency points some circuits with the FEM-code EMAP1, with respect to the use of bandwidth reduction in conjunction with a direct banded solver (DBS).

It is easily seen that when the problem dimension grows up the numerical complexity of the GA becomes a substantial limitation, whilst the EMT approach is quite advantageous. Similar results are attained in the case of circuits such as the one in Fig. 3. Table IV reports some results, with the same scheme of Tab. III:

N	EMAP1	EMT+DBS	GA+DBS
484	284.8	24.6	212.1
720	737.5	162.7	13211

Table IV: Times in seconds to analize at 100 frequency points some circuits with the FEM-code EMAP1, with respect to the use of bandwidth reduction in conjunction with a direct banded solver (DBS).

The matrices generated in the case of boxed microstrip lines have a smaller bandwidth with respect to the case of inhomogeneously waveguides, and this explains the reduced simulation times.

B. MPIE/MoM Analysis

We refer to a MPIE formulation using closed-form spatial-domain Green's functions, discretized with a Galerkin MoM with roof-top functions. As described in [26], the analysis of microstrip circuits with this approach originally generates dense impedance matrices; anyway, a thresholding action can be performed over the matrix, so that all entries smaller than a certain value are zeroed. This can imply a very small approximation error (around 1%) provided that a suitable threshold is identified. In the large majority of cases, a value of 10^{-6} with respect to the largest entry in the matrix is appropriate, and a matrix sparsity between 70 and 85 % is achieved.

Referring to the circuits of Fig. 4, we report results in Tab V, where we compare times for the analysis of the circuit by using an iterative sparse solver (ISS), with respect to the use of different bandwidth reduction approaches in conjunction with DBS. Both the ISS and the DBS come from the same public domain library (Lapack). A dispersion curve of 100 frequency point is evaluated for both circuits. The single-stub circuit operates in the range 7.5-12 GHz, the double stub between 8 and 18 GHz.

N	ISS	EMT+DBS	GA+DBS
280	113.4	23.6	57.1
448	312.5	84.1	412

Table V: Times in seconds to analize at 100 frequency points the two circuits in Fig. 4 with the MPIE/MoM with ISS, with respect to the use of MPIE/MoM with bandwidth reduction in conjunction with a DBS.

Also in this case, it is apparent that the performance of the GA is less attractive than the EMT's one, and, above all, it decreases when enlarging the size of the problem.

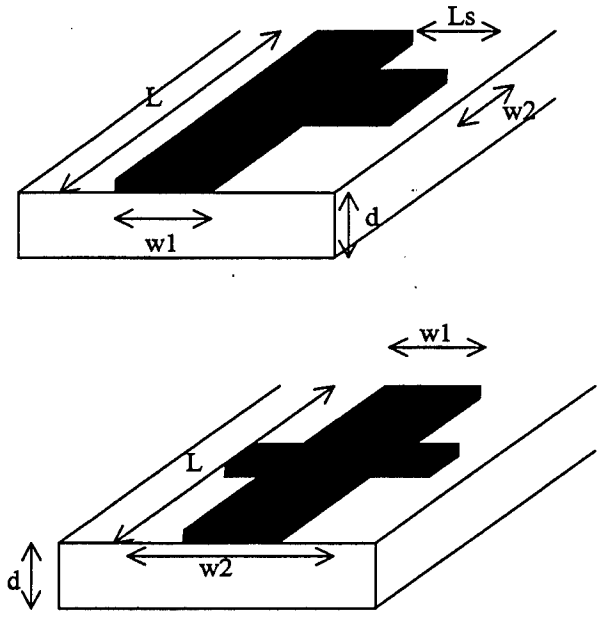

Fig. 4. The two circuits analized with the MPIE/MoM. For the single stub ε_r = 10.65, d=1.27mm, w1=w2=1.44mm, L=17.28mm, Ls=2.16mm. For the double stub ε_r = 9.9, d=10mm, w1=9.2mm, w2=23mm, L=110.6mm.

V. Parallel GA Solution

The recent progresses in parallel computing, and above all the development of low-cost and efficient parallel platforms, such as clusters of PCs, can change the perspective opened by the previous observations. As apparent in previous sections, the several advantages of the GA, i.e. its easy implementation, its amenability to cope with pathological cases, as well as to deal with non-symmetrical or unstructured patterns, are ineffectual, due to its large numerical complexity. Luckily, the nature of GA renders it intrinsically amenable to a parallel design. The large majority of tasks inside it, such as the generation of a farm of initial populations and the evolution of each population, can be performed in parallel on different processors. The percentage of potentially-parallel tasks, with respect to the overall serial work, ranges between 80 and 95 %, depending on the problem size (Π dimension) and the selection of some heuristical parameters, such as p_m and p_c.

Therefore, a parallel version of the GA, called PGA, has been implemented using Parallel Virtual Machine (PVM) programming interface, on an IBM SP2 with 8 nodes. The PGA performs a parallel generation of a farm of initial populations, and periodically collects the results of the evolutionary search from each population, so that cross-over and mutations are performed over chromosomes from different populations, with an increase of the level of hybridization. This can be described as a first *coarse* level of parallelism. A second *fine* level of parallelism is represented by the evaluation of the cost function, which is performed in parallel. This task is quite heavy, especially when large problems are attacked, and can be performed in parallel with a suitable block-decomposition of both the matrix and the permutation vector Π.

A. Results with PGA

In Tab. VI results of PGA for the matrices encountered in the FEM analysis are reported (see Tab. I). The achieved bandwidth, and the computing time when using 8 SP2 nodes, are reported.

N	In. β	Opt. β	Time (s)
284	92	54	1.4
374	107	66	2.5
639	151	74	54
1231	251	151	1123

Table VI: Results for PGA on matrices from FEM analysis of MW circuits. Matrix size N, initial bandwidth β, and final bandwidth are reported.

As shown in Tab. VI, computing times are reduced, and the effectiveness of bandwidth reduction is improved. The use of PGA results in the times reported in Tab. VII for a 100-frequency-point dispersion curve of circuits as in Fig. 2 (compare with Tab. III):

N	EMAP1	EMT+DBS	PGA+DBS
374	264.8	186.1	193.1
639	798.4	395.2	422.7
1231	12270	1376	1642

Table VII: Times in seconds to analize at 100 frequency points some circuits with the FEM-code EMAP1, with respect to the use of parallel bandwidth reduction in conjunction with a direct banded solver (DBS).

As demonstrated in Tab. VII, the performance of PGA turns the genetic approach into an effective method to reduce the time for the numerical analysis of MW circuits, thanks to the substantial decrease of bandwidth reduction time, as well as to the improvement in the effectiveness of the search. PGA's efficiency is similar to the state-of-the-art EMT's one. Speed-ups in the simulation times up to a factor 8 have been observed.

VI. Conclusions

A genetic solution (GA) to the problem of sparse matrix bandwidth minimization has been proposed. The main characteristics of the approach have been described, with respect to the choice of chromosomes, genetic operators, and other heuristical parameters. A suite of functions has been developed so that the crossover can be performed without risks of non-feasible chromosome generation. Results have proved that the GA, despite of its several attractive features (simplicity, flexibility, amenability to global optimization), is not efficient enough to be considered as an appropriate tool for CAD environments of MW circuits. Thanks to its natural parallelism, the approach has been migrated towards parallel platforms (PGA), with a substantial increase in its efficency and effectiveness, which are similar to those of state-of-the-art bandwidth reducers based on graph theory (EMT).

On the other side, the GA and PGA are rather simple to be implemented, whilst EMT is complex and deserves a deep knowledge of graph theory. Furthermore, it is reasonable to expect a substantial increase in the scalability and efficiency of clusters of PCs in the next future, thanks to the continuous evolution of switch and fast-ethernet technologies. As a matter of fact, with very affordable costs, parallel environments for the analysis of EM circuits can be predicted as the natural future infrastructure for MW CAD of large and complex circuits. In conclusions, the opening of such new perspectives turns the genetic approach into a candidate solution to improve the efficiency of numerical methods for EM circuits via sparse matrix bandwidth reduction.

References

[1] L. Tarricone, M. Dionigi, R. Sorrentino, "A strategy for the efficient fullwave description of complex waveguide networks", Int. Journal Microwave and MM-Wave Computer Aided Engineering, 6, 3, pp. 183–198, 1996.

[2] P.P. Silvester, R. L. Ferrari, Finite Elements for Electrical Engineers, Cambridge Univ. Press, Cambridge, 1990.

[3] K. Sabet, L. P. B. Katehi, "Analysis of Integrated Millimeter-Wave and Submillimeter-wave Waveguides using Orthonormal Wavelet Expansions", IEEE Trans. Microwave Th. Techn., 42, 12, pp. 2412-2422, Dec. 1994.

[4] K. Sabet, L. P. B. Katehi, "An Integral Formulation of Two- and Three-Dimensional Dielectric Structures Using Orthonormal Multiresolution Expansions", Int. Journal Num. Modelling, 11, pp. 3-19, 1998.

[5] K.F. Sabet, J. Cheng, L.P.B. Katehi, K. Sarabandi, J. F. Harvey, "Fast simulation of large-scale planar circuits using an object-oriented sparse solver", Proc. IEEE MTT-Symposium, 1999.

[6] K. Naishadham, T.W. Nuteson, R. Mittra, "Parametric Interpolation of the Moment Matrix in Surface Integral Equation Formulation", RF and MW Computer-Aided-Engineering, 9, 6, pp. 474–489, 1999.

[7] T. Cwik, D. S. Katz, J. Patterson, "Scalable Solutions to Integral-Equation and Finite-Element Simulations", IEEE Trans. on Antennas and Propagation, 45, 3, pp. 544-555, 1997.

[8] L. Tarricone, F. Malucelli, A. Esposito, "Efficient Solution of Linear Systems in MW Numerical Methods", to appear in Journal of Applied Comput. Electromagnetic Society, November 1999.

[9] Duff I. S., A. M. Erisman and J. K. Reid, Direct methods for sparse matrices, Oxford University Press, 1986.

[10] C. Papadimitriou, "The NP-completeness of the bandwidth minimization problem", Computing, 16, pp. 263-270, 1976.

[11] E. Cuthill, J. McKee,"Reducing the bandwidth of sparse symmetric matrices", Proc. ACM National Conference, Association for Computing Machinery, New York, pp. 157-172, 1969.

[12] Gibbs, N. E., W. G. Poole and P. K. Stockmeier, "An algorithm for reducing the bandwidth and profile of sparse matrix", SIAM Journal of Numerical Analysis, 13, 2, pp. 236-250, 1976.

[13] A. Esposito, S. Fiorenzo Catalano, F. Malucelli and L. Tarricone, "A new bandwidth matrix reduction algorithm", Operations Research Letters, 23/5, pp. 99-107, 1999.

[14] G. M. Del Corso, G. Manzini, "Finding exact solutions to the bandwidth minimization problem", Computing, 62, 3, pp. 189–203, 1999.

[15] Dueck, G. and J. Jeffs, "A heuristic bandwidth reduction algorithm", Journal of Combinatorial Mathematics and Combinatorial Computing, 18, pp. 97-108, 1995.

[16] A. Esposito, S. Fiorenzo Catalano, F. Malucelli and L. Tarricone, "Sparse Matrix Bandwidth Reduction: Algorithms, Applications And Real Industrial Cases In Electromagnetics", in "High Performance Algorithms for Structured Matrix problems", series "Advances in Computation: Theory and Practice", Nova Science, New York, 1999

[17] M. Dionigi, A. Esposito, R. Sorrentino and L. Tarricone, "A Tabu Search Approach for the Solution of Linear Systems in Electromagnetic Problems", Int. Journal of Numerical Modelling, 10, pp. 315-328, 1997.

[18] Y. Rahmat-Samii, E. Michielssen (Eds.), "Electromagnetic Optimization by Genetic Algorithms", Wiley, 1999.

[19] D. E. Goldberg, "Genetic Algorithms in Search, Optimization and Machine Learning", Addison-Wesley, 1989.

[20] J. Holland, "Adaptation in Natural and Artificial Systems", MIT Press, 1992.

[21] U. Faigle, W. Kern, "Some Convergence Results for probabilistic Tabu Search", ORSA Journal on Computing, pp. 32-37, 1992.

[22] M. Mitchell, "An Introduction to Genetic Algorithms", MIT Press, 1996.

[23] S. Forrest, M. Mitchell, "Relative Building Block Fitness and the Building-Block Hypothesis", in D. Whitley (Ed.), Foundations of Genetic Algorithms 2, Morgan Kaufmann, 1996.

[24] M. Sefrioui, J. Periaux, G.J. Ganascia, "Fast Convergence Thanks to Diversity", in L. Fogel (Ed.), Evolutionary Programming V, pp. 313-321, MIT Press, 1996.

[25] Hubing, T. H., M. V. Ali and G. K. Bat, "EMAP: A 3D finite element modeling code", Journal of Applied Comp. Electromagnetics Soc., 8(1), 1993.

[26] A. Caproni, F. Cervelli, M. Mongiardo, L. Tarricone, F. Malucelli, "Bandwidth Reduced Full-Wave Simulation of Planar Microstrip Circuits", Int. Journal of Appl. Comp. Electromagnetics Society, 13, 2, pp.197-204, 1998.

Optimum Population Size and Mutation Rate for a Simple Real Genetic Algorithm that Optimizes Array Factors

Randy L. Haupt
Utah State University
Electrical and Computer Engineering
4120 Old Main Hill
Logan, UT 84322-4120
haupt@ieee.org
435-797-2841

Sue Ellen Haupt
Utah State University
Mechanical and Aerospace Engineering
4130 Old Main Hill
Logan, UT 84322-4130
Suehaupt@helios.ece.usu.edu
435-797-2952

abstract *The population size and mutation rate of a genetic algorithm have great influence upon the speed of convergence. Most genetic algorithm enthusiasts use a large population size and low mutation rate due to the recommendations of several early studies. These studies were somewhat limited. This paper presents results that show a small population size and high mutation rate are actually better for many problems.*

I. Parameter Selection for a Simple Genetic Algorithm

Applications of a genetic algorithm (GA) to the optimization of electromagnetics problems started in the early 1990s [1], [2] and have exploded since then. The optimization of array patterns using a GA is particularly attractive for the synthesis of patterns that have desirable characteristics. Most of the work has followed traditional GA philosophy when choosing the population size and mutation rate of the GA: a relatively large population and a low mutation rate is used. The choice of population size and mutation rate can vary the run time of the GA by several orders of magnitude.

The first intensive study of GA parameters was done by De Jong [3] and is nicely summarized in Goldberg [4]. De Jong looked at both on-line and off-line performance of the GAs. On-line performance is an average of all costs up to the present generation. Off-line performance is the best cost found up to the present generation. He tested five algorithms of varying levels of complexity on five different cost functions while varying mutation rate, population size, crossover rate, and the generation. De Jong found that a small population size improved initial performance while large population size improved long-term performance. A higher mutation rate was good for off-line performance while low mutation rate was best for on-line performance. The highest mutation rate used was 0.1.

Grefenstette [5] used a meta GA to optimize the on-line and off-line performance of GAs based on varying six algorithm parameters: population size, crossover rate, mutation rate, scaling window, and whether or not elitism was used. A cost function evaluation for the meta GA consisted of a GA running until 5000 cost function evaluations were performed on one of the De Jong test functions and normalizing the result relative to that of a random search algorithm. Each GA in the population evaluated each of the De Jong test functions. The second step in this experiment took the 20 best GAs found by the meta GA and let them tackle each of the five test functions for five independent runs. The best GA for on-line performance had a population size of 30 and mutation rate of 0.01. The best off-line GA had a population size of 80 and mutation rate of 0.01. He concluded that good results could be obtained with a wide selection of GA parameters.

Schaffer, et. al. reported results on optimum parameter settings for a binary GA using a Gray code [6]. This approach added five more cost functions to the De Jong test function suite. They had discrete sets of parameter values (population size=10, 20, 30, 50, 100, and 200; mutation rate = 0.001, 0.002, 0.005, 0.01, 0.02, 0.05, and 0.10; crossover rate = 0.05 to 0.95 in increments of 0.10; and 1 or 2 crossover points) that had a total of 8400 possible combinations. Each of the 8400 combinations was run with each of the test functions. They averaged the results over 10 independent runs. The GA terminated after 10,000 function evaluations. The best on-line performance resulted for the following parameter settings: population size =20 to 30 (relatively small), crossover rate = 0.75 to 0.95, mutation rate = 0.005 to 0.01 (the highest rates tested), and two point crossover.

Thomas Back [7, 8, 9] has done more recent analyses of mutation rate. He showed that for the simple counting problem, the optimal mutation rate is $1/\ell$ where ℓ is the length of the chromosome [7]. He later showed that an even quicker convergence can be obtained by beginning with even larger mutation rates (on the order of ½) and letting it gradually adapt to the $1/\ell$ value [8]. In later

work [9], he compared this evolutionary GA approach with evolutionary strategies and showed that this adaptation is similar to the self-adaptation of parameters that characterizes evolutionary strategies approaches.

Gao [10] computed a theoretical upper bound on convergence rates in terms of population size, encoding length, and mutation probability in the context of Markhov Chain models for a canonical GA. His resulting theorem showed that the larger the probability of mutation and the smaller the population, the faster the GA should converge. However, he discounted these results as not viable for long-term performance.

Most of these previous studies were done with binary GAs. More engineers are discovering the benefits of using real parameter GAs, namely that a continuous spectrum of parameters can be represented. Our previous work with real GAs [11] devised a simple check to determine the best population size. The GA optimized several functions, and the results were averaged over 100 independent runs. The population size times the number of iterations (i.e., the total number of chromosomes evaluated) was kept constant. The "goodness" of the algorithm was judged by the minimum cost found. For both binary and continuous parameter GAs, a small population size allowed to evolve for many generations produced the best results. Similar sensitivity analyses with a wider range of mutation rates suggested that mutation rates in the range of 0.05 to 0.35 found the lowest minima.

A quick search of web sites on GAs also show conflicting evidence for the best parameters to use. Some sites [12, 13] suggest that GA performance may be improved for smaller population sizes and higher mutation rates. In addition, enough of our colleagues and students have found similar results for their GA problems that we decided further study is necessary.

These previous studies have shown that parameter settings are sensitive to the cost functions, options in the GA, bounds on the parameters, and performance indicators, which must be carefully considered. In addition, the optimum parameters seem to depend on whether the GA is just beginning its descent or whether it has advanced into the fine-tuning of the solution stage. Consequently, different studies result in different conclusions about the optimum parameter values depending on the problem and the parameters explored. Davis recognized this issue [14] and outlined a method of adapting the parameter settings during a run of a GA [15]. He does this by including operator performance in the cost. Operator performance is the cost reduction caused by the operator divided by the number of children created by the operator. Yet most GA practitioners still stick to large population sizes and very low mutation rates.

This paper extends the work in [11] from the optimization of contrived mathematical functions to the optimization of array factors. The goal is to help users of GAs select appropriate population sizes and mutation rates in order for their GAs to find the best answer as quickly as possible. Thus, emphasis is placed on off-line performance since we only care about the closeness of the final answer to the actual answer and not all the extraneous solutions included in the averaging of the on-line indicator. This paper reports the results of experiments to determine the optimum population size and mutation rate for a simple real GA on the types of problems that might be typical in electrical engineering. Since we want to minimize the run time of the GA, the criteria for judging the "goodness" of the results is the number of calls to the objective function required for solution. This is the metric that determines computer wall clock time to complete the solution. In addition, we choose to count function calls to the cost function as the criteria for how well the GA is performing. This choice is more in keeping with the usual engineering requirement to minimize run time. The parameters that produce the minimum number of function calls to produce an acceptable solution are deemed the "best." A solution is "acceptable" when a predetermined value close to the minimum is found. This definition is consistent with finding the deepest well, then diving to the bottom with a fast local optimizer. Determining the optimum population size and mutation rate must take into account the random components of the GA. Therefore, we average over a large number of runs of our GA before choosing the best parameters.

The GA used here is termed a real GA because the variables to be optimized are continuous and are not converted to binary values. Figure 1 shows a flow chart of a simple real GA. In each block of the flow chart, choices must be made on how to perform the GA operations in that block. The GA in this paper uses a roulette wheel proportional weighting selection and the single point crossover using the method described in [11]. Elitism is used. These are common choices used in practice and are constants for this particular study.

The results of this investigation show that, for the problems solved here, small population size and relatively large mutation rate are far superior to the large population sizes and low mutation rates that are used by most of the papers presented in the electromagnetics community and by the GA community at large. Such results suggest that future research

consider carefully what parameters are appropriate to the particular problem.

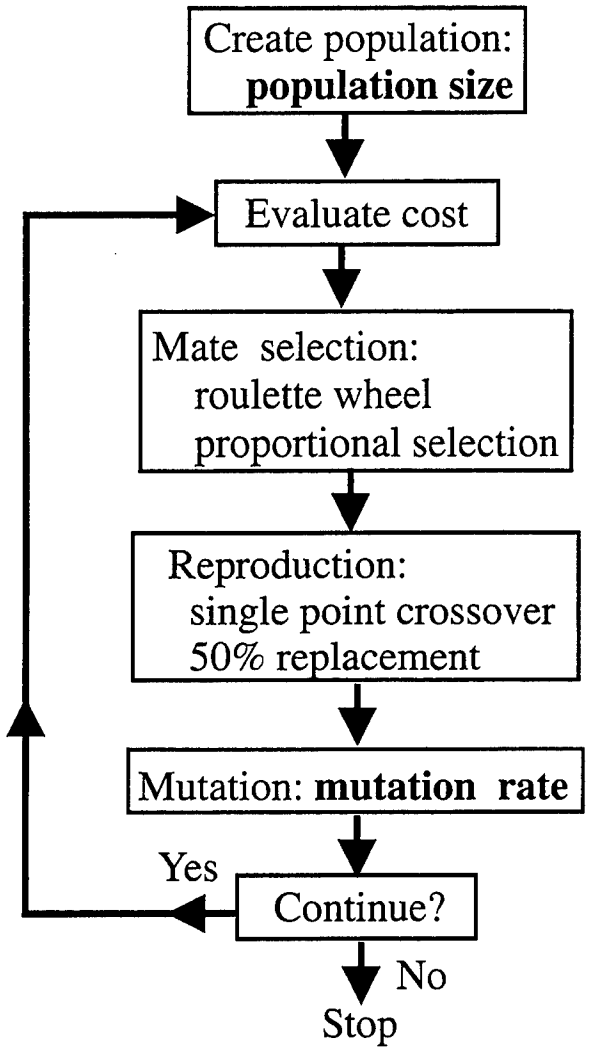

Figure 1. Flow chart of the real GA. Finding the optimum mutation rate and population size would cause the GA to find an acceptable solution faster.

II. A Simple Undulating Function

The first example is a highly undulating function with many local minima. This function is

$$f(x,y) = x\sin(x) + 1.1\sin(y) \text{ for } 0 \le x, y \le 10 \quad (1)$$

Figure 2 shows a graph of this function. The global minimum over the specified range is -18.5547 at (x,y) = (9.0390,8.6682).

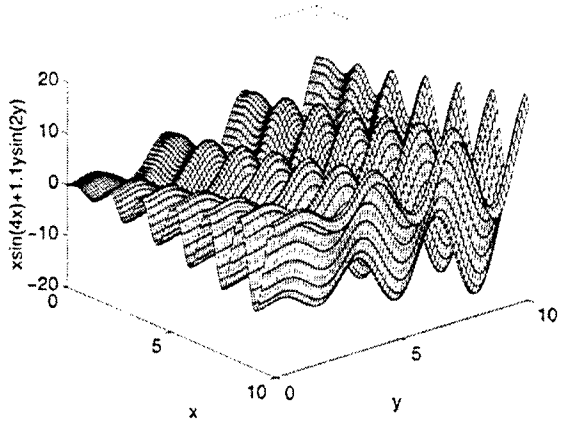

Figure 2. Plot of the first function minimized by the GA.

Doing single runs of a GA for different sets of population sizes and mutation rates doesn't yield sufficient information due to the statistical nature of the GA. To dampen the effects of the random processes, results are averaged over many runs for each set of parameters. Thus, the GA is run for one set of parameters until the solution is found. After performing T independent runs, the results for the T trials are averaged.

We posed the problem to minimize the function with the fewest number of function evaluations. Many engineering and scientific applications require the evaluation of very complex fitness functions. These function evaluations drive the time needed for the GA to converge. Therefore, our criteria for how "good" a GA run performs are a count of the number of calls to the cost function. A function evaluation is necessary for each new offspring (mutated or not) plus each mutated member of the old population. If a new offspring is selected to be mutated 3 times, then only one function evaluation is done. Otherwise, a high mutation rate would force a large number of unnecessary function evaluations.

One problem with a GA is determining when the "correct" answer is found. We addressed this issue in two ways for the function in (1). The first method used –18.5 as stopping criteria. Figure 3 shows the number of function calls vs. the number of GA runs averaged for a stopping point of –18.5. Oscillations occur until the GA is averaged about 150 times. For these criteria, we would not consider the average to be stable until about 150 runs have been averaged.

The second method of defining the "correct" solution was less rigorous but probably more realistic. The

second lowest minimum for is -16.9847 and occurs at (x,y) = (7.4697,8.6681). Thus, if we obtain a value less than this local minimum, we are assured that we have found the valley of the global minimum. From there, we could use the solution as a first guess for a local optimizer that would quickly converge on the actual minimum point. Since this two-step process is often applied in practice, we stop the function when the cost is less than –17. Figure 4 shows the number of function calls vs. the number of GA runs averaged for a stopping point of –17. These results indicate that averaging as few as 40 or 50 runs would give a reasonably consistent average. Note that using –17 as the stopping point resulted in about ¼ of the runs needed for averaging than using –18.5 as the stopping point.

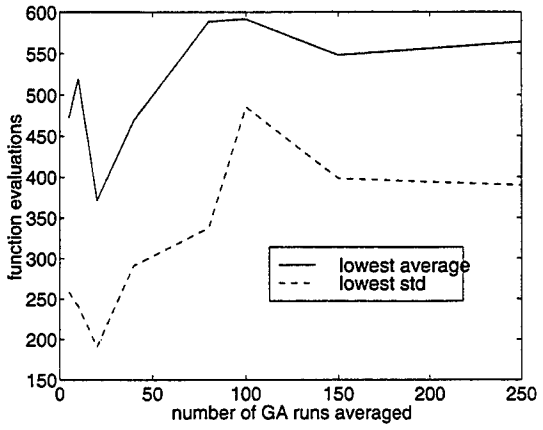

Figure 3. These plots show both the average and the standard deviation of the number of function evaluations when the GA was stopped for a fitness that was less than –18.5.

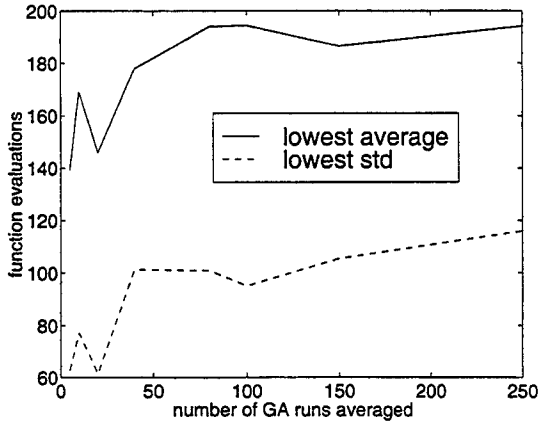

Figure 4. These plots show both the average and the standard deviation of the number of function evaluations when the GA was stopped for a fitness that was less than –17.

Now that we have determined the number of runs needed to average the GA to find the optimum parameter set, the GA with stopping criteria of –17 is averaged over 40 runs with mutation rates and population sizes of:

mutation rate: .01 to .49 in increments of .02
population size: 4, 12, 20, 28, 36, 44, 52, 60

We analyze the number of cost function evaluations required to converge for three different cost functions. Figure 5 shows the number of function calls required to find a point lower than –17. Very low mutation rates result in a huge number of function calls. Small population sizes seem to generally require fewer function calls than larger ones. The results indicate that a GA with a small population size (<16) and a mutation rate between .15 and .5 works best.

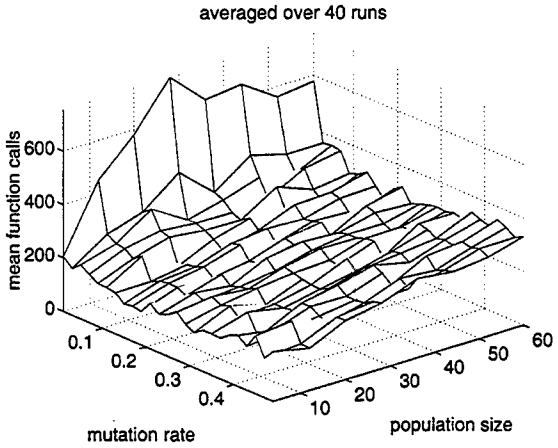

Figure 5. The mean number of function calls are plotted vs. the mutation rate and population size when the GA is averaged over 40 runs.

III. Optimizing Side Lobe Tapers – Example 1

It is well known that a low sidelobe taper can be analytically found using a variety of methods including the Dolph-Chebychev and Binomial distributions. The point here is to just use a test case for the GA where we know the best solution – a binomial array. In fact, local optimizers provide excellent solutions for this problem as well. The authors are not advocating that an antenna designer should use a GA to find an amplitude taper for an array. There are many other much better techniques.

Problem Formulation

The goal of the optimization is to find the weighting for a linear array that produces the minimum maximum sidelobe level. The objective function is given by

$$f = \max \textit{ sidelobe of} \left\{ \sum_{n=1}^{N} a_n e^{jp_n} e^{j(n-.5)kdu} \right\} \qquad (2)$$

where
N = number of array elements
a = vector of amplitude weights
p = vector of phase weights
k = 2π/wavelength
d = element spacing
u = angle variable

In the cases presented, only a or p are optimized but not both in the same GA run. Thus, the number of parameters to be optimized is the length of the a or p vector. The array factor is calculated from broadside to endfire, and a search is performed to find all the peaks. The highest peak (outside the main beam) is returned as the cost of the function call. Most of the electromagnetics community use elitism and off-line performance for the various applications reported. These assumptions are used but not tested here.

The GA was run 500 times to find the minimum maximum sidelobe level for a 29 element array. Figure 6 shows three independent plots of the average number of function calls to reduce the sidelobe level below –25 dB vs. the number of GA runs included in the average. The lines become very close when the number of runs exceeds 250. That's a lot of averaging. Figure 7 shows the previous plot enlarged in the region of 1 to 25 averages. This region clearly shows that averaging the runs is critical to making valid interpretations of the data. When averaging is used, the number of function calls varies within a range of 500 for the three trials. At ten runs in the average, the number of function calls varies by 90 and at 20 the variation is down to 76. Averaging more than 100 runs adds a high level of confidence in any conclusions made concerning the optimum population size and mutation rate.

Results

The GA is first used to find the optimum amplitude taper for an 18 element uniformly spaced array (d = 0.5 wavelengths). The taper is symmetric about the center of the array and the two center elements have an amplitude of one. Whenever the minimum maximum sidelobe level falls below 25 dB below the peak of the main beam or the number of function calls exceeds 50,000, the algorithm stops. The GA was run 20 independent times and the results were averaged for the following population sizes and mutation rates:

Population size = 4, 8, 12, ..., 64

Mutation rate=.01, .02, .03,..., .4

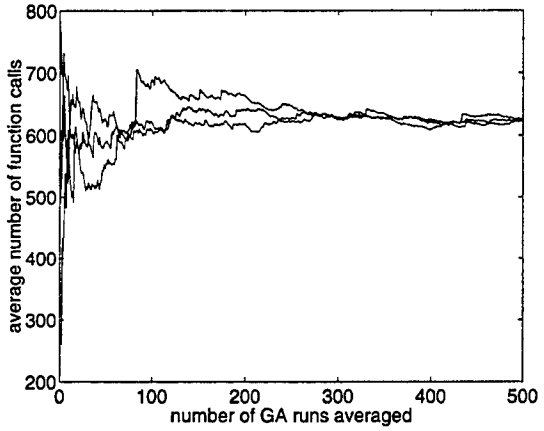

Figure 6. Plot of the average number of function calls used by a GA to find the minimum maximum sidelobe amplitude taper of an 18 element linear array. The GA was run for up to 500 averages on three independent occasions.

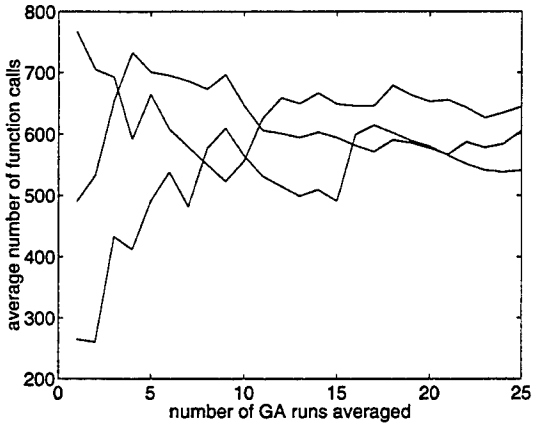

Figure 7. This plot magnifies the left region of the graph in Figure 6.

Figure 8 displays a plot of the average number of function calls vs. population size and mutation rate when the results were averaged over 20 independent runs. This graph is very low when the mutation rate is less than 20%, except for a subregion where the population size and mutation rate are small. Figure 9 shows another result where 20 independent runs were averaged and the population size varied from 4 to 128 and the mutation rate was between 1 and 19%. This plot shows the minimum number of function calls gradually increases as population size increases. GAs take a long time to converge when the population size is small and the mutation rate is small because population diversity comes at a slower rate.

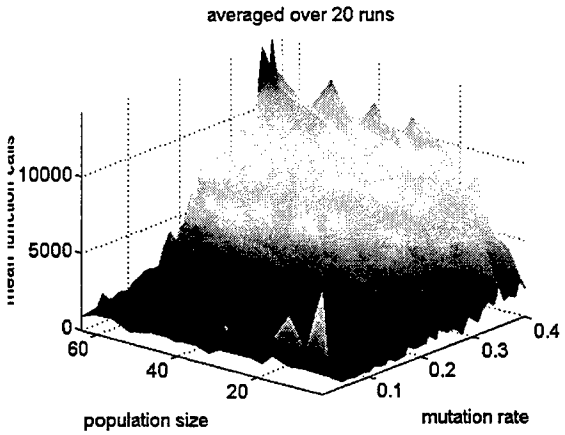

Figure 8. The GA performed best (used the lowest number of function calls) when the population size was small and the mutation rate around 10%.

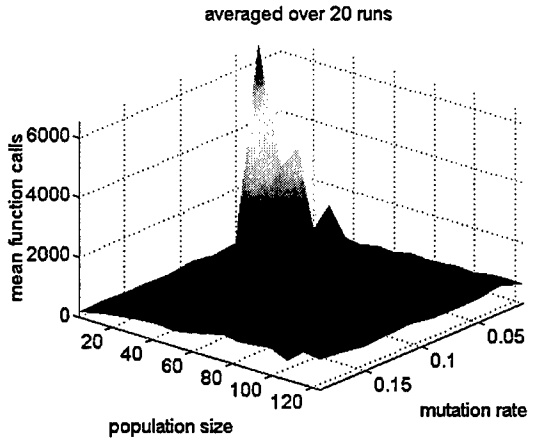

Figure 9. The lower mutation was run again and the range of population sizes was increased.

A strong region of performance in Figure 8 occurs between a population size of 4 to 16 and a mutation rate of 0.1 to 0.2. Figure 10 shows this region when the GA is averaged over 50 runs. The plot shows a population size of 8 or less and a mutation rate of 13% or less produce excellent results. Still afraid of abandoning conventional wisdom, the region between a population size of 4 and 128 and a mutation rate of 0.0 to 0.05 is examined, averaging the GA over 50 runs. Results, shown in Figure 11, are best for the smallest population sizes and mutation rate of 5%. Again, the region of low population size and low mutation rate yields slow convergence. Avoiding that range, it's quite apparent that the average number of function calls increases as the population size increases. Mutation rate doesn't seem to play much of a factor above a population size of 30. The next best mean number of calls was for a population size of 8 and mutation rate of 15% then mutation rate of 20%. These results are consistent with those in Figure 8. The poor performance of the large population sizes and a population size of 4 with mutation rate of 20% was predicted in Figure 10.

In order to become more confident with the results presented in the previous figures, the GA was averaged over 500 runs for several different mutation rates and population sizes as shown in Table 1. Results (in number of function calls) from running a GA 200 times to find the optimum amplitude taper for an 18 element array that minimizes the maximum sidelobe level. A single GA run stopped when the sidelobe level went below –25dB or the number of function calls exceeded 50,000. The minimum and maximum number of function calls over the 200 runs as well as the mean, and standard deviation of the number of function calls are shown here. A population size of 4 with a mutation rate of 15% produced the best average results.

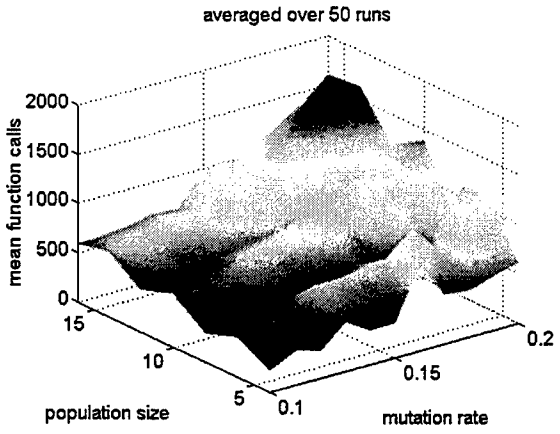

Figure 10. This graph shows that a small population size and mutation rate of 0.1 causes a GA to find an answer in the fewest number of function evaluations.

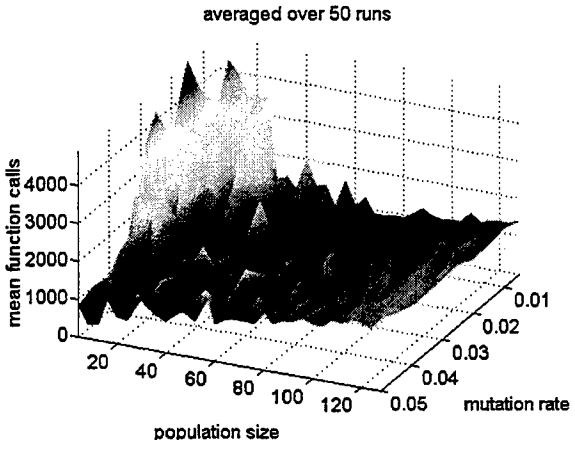

Figure 11. Small population sizes and low mutation rates cause the GA to perform poorly. Note that, aside from very small population sizes, the mean number of function calls increases with population size independent of mutation rate.

Table 1. Results (in number of function calls) from running a GA 200 times to find the optimum amplitude taper for an 18 element array that minimizes the maximum sidelobe level. A single GA run stopped when the sidelobe level went below –25dB or the number of function calls exceeded 50,000. The minimum and maximum number of function calls over the 200 runs as well as the mean, and standard deviation of the number of function calls for the 200 runs are shown here.

Run	Mutation rate	Population size	minimum	maximum	mean	standard deviation
1	0.15	4	26	3114	398	455
2	0.20	4	110	50002	7479	12798
3	0.15	8	60	2457	461	332
4	0.20	8	49	2624	654	466
5	0.01	64	300	50031	1158	3498
6	0.02	64	277	11818	1028	911
7	0.01	128	393	2535	1410	365
8	0.02	128	1215	50071	10208	16077

IV. Optimizing Side Lobe Tapers – Example 2

The next example finds a low sidelobe taper for a linear array. Table 2 shows the results (in number of function calls) from running a GA 100 times to find the optimum phase taper that minimizes the maximum sidelobe level of a 40 element array. A single GA run stopped when the sidelobe level went below –14dB or the number of function calls exceeded 50,000. The minimum and maximum number of function calls over the 100 runs as well as the mean, and standard deviation of the number of function calls for the 100 runs are shown here. Once again the number of function calls is smallest for the smaller population sizes coupled with relatively large mutation rates.

It should be noted that even for the best parameters used in these tables, not all runs converged as evidenced by the maximum entries greater than 50,000. This fact has two implications. The first is that the mean number of function calls in the table would actually be higher if a limit were not in place. The second implication is that one should always be prepared to do multiple runs when using a GA since convergence is not assured.

V. Optimizing Side Lobe Tapers – Example 3

In this example, a GA is run for 100,000 function evaluations in order to find the optimum amplitude taper for a 20 element array that minimizes the maximum sidelobe level. Table 3 shows the results in dB. The minimum and maximum result as well as the mean and standard deviation of the best sidelobe level for the 100 runs are shown here. The population size of 4 and 8 with 15% mutation rate outperformed the GA's with population sizes of 64 and 128 with a mutation rate of 2%.

Table 2. Results (in number of function calls) from running a GA 100 times to find the optimum phase taper that minimizes the maximum sidelobe level of a 40 element array. A single GA run stopped when the sidelobe level went below –14dB or the number of function calls exceeded 50,000. The minimum and maximum number of function calls over the 100 runs as well as the mean, and standard deviation of the number of function calls for the 100 runs are shown here.

Run	Mutation rate	Population size	minimum	maximum	mean	standard deviation
1	0.15	4	134	50002	2973	5856
2	0.20	4	163	50000	5232	9744
3	0.15	8	168	8223	1827	1510
4	0.20	8	124	21307	3220	3604
5	0.01	64	614	50024	7914	15040
6	0.02	64	546	50036	6624	13130
7	0.01	128	955	50043	4791	9708
8	0.02	128	933	50033	3942	7636

Table 3. Results (in dB) from running a GA for 100,000 function evaluations in order to find the optimum amplitude taper for a 20 element array that minimizes the maximum sidelobe level. The minimum and maximum result as well as the mean, and standard deviation of the best sidelobe level for the 100 runs are shown here.

Run	Mutation rate	Population size	minimum	maximum	mean	standard deviation
1	0.15	4	-57.5	-28.4	-36.1	4.6
3	0.15	8	-46.0	-29.5	-36.5	3.3
6	0.02	64	-42.5	-27.1	-32.5	3.3
8	0.02	128	-41.2	-28.0	-32.5	2.5

VI. Conclusions

The results of the numerical experiments presented in this paper suggest that the best mutation rate for GAs used on these problems lies between 5 and 20% while the population size should be less than 16. These results disagree with some of the previous studies cited and common usage. The primary reasons for these results are that off-line performance was used and that a broader range of population size and mutation rate was included. In addition, the criteria judged here is the number of function evaluations, which is a good indicator of the amount of computer time required to solve the problem.

A way to interpret these results is in the context of analyzing the trade-offs between exploration versus exploitation. Traditionally, large populations have been used to thoroughly explore complicated cost surfaces. Crossover is then the operator of choice to exploit promising regions of phase space by combining information from promising solutions. The role of mutation is somewhat nebulous. As stated by Back [8], mutation is typically considered as a secondary operator of little importance. Like us, he found that larger values than typically used are best for the early stages of a GA run. In one sense, greater exploration is achieved if the mutation rate is great enough to take the gene into a different region of solution space. Yet a mutation in the less critical genes may result in further exploiting the current region. Perhaps the larger mutation rates combined with the lower population sizes act to cover both properties without the large number of function evaluations required for large population sizes. Iterative approaches where mutation rate varies over the course of a run such as done by Back [8, 9] and Davis [15] are likely optimal, but require a more complex approach and algorithm. Note that when real parameters, small population sizes, large mutation rates, and an adaptive mutation rate are used, the algorithm begins to lurk more in the realms of what has been traditionally referred to as evolutionary strategies. We feel that names are a mute point and choose to do what we find works best for a problem. In particular, we prefer the engineering approach of switching to a different optimization algorithm once the global well is found, since at that point the more traditional optimization algorithms become more efficient.

When the population sizes are as small as found here, tournament selection offers no advantage to roulette wheel selection, so an evaluation of the trade-off between these selection operators was not done. Selecting a small population size takes a very small amount of computer time. When doing the calculations for Table 3, the GA runs with large population size took at least 10% longer to run than the GAs with small population sizes for a fixed number of function calls. This difference can be attributed to the weighting and ranking in the selection operator.

These results are not totally alone. They are confirmed by our own prior results in [11] as well as those of Back [7, 8, 9] and predicted by the theory of Gao [10]. Also De Jong [3] found that a small population size and high mutation rate worked best during the initial generations and off-line performance. This is consistent with the results here since the algorithm is stopped when a prescribed minimum in the valley of the true minimum is found. If the GA were then used to pass results to a local optimizer, the GA need only work on the problem a short time.

Although these conclusions strictly apply to only the problems presented, in practice we have found many other problems where similar principles applied. No attempt has been made to thoroughly investigate all possible combinations of parameters. We chose to concentrate on population size and mutation rate after our own experience with optimizing GA performance. We make no claims that this is a definitive analysis: our purpose is merely to suggest that future GA practitioners consider a wider range of possible combinations of population size and mutation rate.

Bibliography

[1] E. Michielssen, et. al., "Design of lightweight, broad-band microwave absorbers using genetic algorithms," IEEE MTT Transactions, Vol. 41, No. 6/7, Jun/Jul 93, pp. 1024-1031.

[2] R.L. Haupt, "Thinned arrays using genetic algorithms," IEEE AP-S Transactions, Vol. 42, No. 7, Jul 94, pp. 993-999.

[3] K. A. De Jong, "Analysis of the Behavior of a Class of Genetic Adaptive Systems," Ph.D. Dissertation, The University of Michigan, Ann Arbor, MI, 1975.

[4] D. E. Goldberg, *Genetic Algorithms in Search, Optimization, and Machine Learning*, Reading, MA: Addison-Wesley, 1989.

[5] J. J. Grefenstette, "Optimization of control parameters for genetic algorithms," IEEE Trans. on Systems, Man, and Cybernetics 16, January/February 1986, p. 128.

[6] J. D. Schaffer, et. al., "A study of control parameters affecting online performance of genetic algorithms for function optimization," in *Proceedings of the Third International Conference on Genetic Algorithms*, ed. J. D. Schaffer, Los Altos, CA: Morgan Kaufmann, June 4-7, 1989, pp. 51-60.

[7] T. Back, "Optimal mutation rates in genetic search," in *Proceedings of the 5th International Conference on Genetic Algorithms*, ed. S. Forrest, Morgan Kaufmann, 1993, pp. 2-9.

[8] T. Back and M. Schutz, "Intelligent mutation rate control in canonical genetic algorithms," in *Foundations of Intelligent Systems 9th International Symposium*, ed. Z.W. Ras and M. Michalewicz, Springer Verlag, Berlin, 1996, pp. 158-167.

[9] T. Back, "Evolution strategies: An alternative evolutionary algorithm," in *Artificial Evolution*, ed. J.M. Alliot, et al., Springer Verlag, Berlin, 1996, pp. 3-20.

[10] Y. Gao, "An upper bound on the convergence rates of canonical genetic algorithms," *Complexity International*, Vol. 5, 1998.

[11] R.L. Haupt and S.E. Haupt, *Practical Genetic Algorithms*, New York: John Wiley & Sons, 1998.

[12] http://www.revolver.demon.co.uk/ga/

[13]http://www.irg.lbl.gov/COMPS/numerical/NUMgas.html

[14] L. Davis, "Adapting operator probabilities in genetic algorithms," *in Proceedings of the Third International Conference on Genetic Algorithms*, ed. J. D. Schaffer, Los Altos, CA: Morgan Kaufmann, 1989, pp. 61-67.

[15] L. Davis, ``Parameterizing a genetic algorithm," in *Handbook of Genetic Algorithms*, ed. L. Davis, New York: Van Nostrand Reinhold, 1991.

A Novel Preconditioning Technique and Comparison of Three Formulations for Hybrid FEM/MoM Methods

Yun Ji, Hao Wang, and Todd H. Hubing
University of Missouri-Rolla

Abstract – **Hybrid FEM/MoM methods combine the finite element method (FEM) and the method of moments (MoM) to model inhomogeneous unbounded problems. These two methods are coupled by enforcing field continuity on the boundary that separates the FEM and MoM regions. There are three ways of formulating hybrid FEM/MoM methods: outward-looking formulations, inward-looking formulations and combined formulations. In this paper, the three formulations are compared in terms of computer-resource requirements and stability for four sample problem geometries. A novel preconditioning technique is developed for the outward-looking formulation. This technique greatly improves the convergence rate of iterative solvers for the types of problems investigated in this study.**

Index Terms: **FEM, MoM, EMC, sparse matrix, permutation, preconditioning, iterative solvers.**

I. INTRODUCTION

Hybrid FEM/MoM methods, which are also referred to as FE-BI, FE-MM, or FEM/BEM in the literature, combine the finite element method (FEM) and the method of moments (MoM) to model inhomogeneous unbounded problems. FEM is used to analyze the details of the structure and MoM is employed to terminate the FEM meshes and to provide an exact radiation boundary condition (RBC). These two methods are coupled by enforcing tangential-field continuity on the boundary separating the FEM and MoM regions. Hybrid FEM/MoM techniques were introduced in the early seventies by Silvester and Hsieh [1], and McDonald and Wexler [2] as attempts to apply FEM to model unbounded radiation problems. FEM/MoM was not widely used until the late eighties due to its large computational requirements. Yuan [3], and Jin and Volakis [4], [5] were among the first to apply FEM/MoM to 3D electromagnetic problems using vector basis functions. Angélini *et al.* [6], and Antilla and Alexopoulos [7] later applied FEM/MoM to 3D scattering in anisotropic media.

FEM/MoM has been used to analyze electromagnetic compatibility (EMC) problems since the mid-nineties. Ali *et al.* [8] employed FEM/MoM to analyze scattering and radiation from structures with attached wires. Shen and Kost [9] used FEM/MoM to analyze EMC problems in power cable systems. FEM/MoM has also been utilized to model thin shielding sheets and microstrip lines [10], [11]. Electronic devices with printed circuit boards (PCBs) are usually composed of many detailed structures: dielectrics, traces, cables, holes and vias. MoM is not well suited to model this kind of complex geometry efficiently. With a hybrid FEM/MoM technique, the details of a printed circuit board can be modeled using FEM and an exact radiation boundary can be provided using MoM to terminate the FEM meshes. When the structure has long cables, a FEM/MoM method is particularly efficient because the cables can be modeled by MoM without meshing the empty space around the cable.

There are three formulations for hybrid FEM/MoM methods [12]-[14]. The first formulation constructs an RBC using MoM and incorporates the RBC into the FEM equations. The second formulation derives an RBC from FEM and incorporates the RBC into the MoM equations. The third formulation combines the FEM and MoM matrix equations to form a large matrix equation and solves for all unknowns simultaneously. The first and second formulations are referred as *outward-looking* and *inward-looking*, respectively, in [13], [14]. The last formulation is referred to as the *combined formulation* in this paper.

This paper compares the three formulations for hybrid FEM/MoM methods and presents a novel preconditioning technique that can be applied to outward-looking formulations. Section II describes the matrix equations generated by FEM/MoM. Section III introduces four sample problems used to compare the three formulations. In Section IV, preconditioning and permutation techniques are presented. Section V presents the outward-looking formulation and the new preconditioning technique. The inward-looking formulation is described in Section VI. Section VII presents the combined formulation. Section VIII compares the three formulations in terms of computer resource requirements. Finally, conclusions are drawn in Section IX.

II. MATRIX EQUATIONS GENERATED BY FEM/MoM

Full-wave hybrid FEM/MoM methods are well suited for solving problems that combine small complex structures and large radiating conductors. The original problem must be divided into an exterior equivalent problem and an interior equivalent problem. MoM is used to model the exterior equivalent problem and FEM is employed to analyze the interior equivalent problem. The two equivalent problems are related by enforcing the continuity of tangential fields on the boundary separating the FEM and MoM regions [14]-[16].

The electric-field integral-equation (EFIE) is generally used to describe the exterior equivalent problem [17],

$$\mathbf{E}^{inc}(\mathbf{r}) = \frac{1}{2}\mathbf{E}(\mathbf{r}) + \int_S \left\{ \begin{array}{l} \mathbf{M}(\mathbf{r}') \times \nabla' G_0(\mathbf{r},\mathbf{r}') + j k_0 \eta_0 \mathbf{J}(\mathbf{r}') G_0(\mathbf{r},\mathbf{r}') \\ - j \frac{\eta_0}{k_0} \nabla' \bullet \mathbf{J}(\mathbf{r}') \nabla' G_0(\mathbf{r},\mathbf{r}') \end{array} \right\} dS' \quad (1)$$

where k_0 and η_0 are the wavenumber and the intrinsic wave impedance in free-space, and S is the surface enclosing the exterior equivalent problem. The integral term with a bar in Equation (1) denotes a principal-value integral. The singularity at $\mathbf{r}=\mathbf{r}'$ is excluded. The three-dimensional homogeneous Green's function is given by,

$$G_0(\mathbf{r},\mathbf{r}') = \frac{e^{-jk_0|\mathbf{r}-\mathbf{r}'|}}{4\pi|\mathbf{r}-\mathbf{r}'|} . \quad (2)$$

If S is a closed surface, the EFIE is not immune to false interior resonances [15], [17], [18]. If the interior resonances cause serious problems, the combined field formulation may be employed [12], [18].

Triangular basis functions (RWG functions) [19] may be employed to approximate surface fields. A Galerkin procedure can be used to test Equation (1). The resulting MoM matrix equation follows [8],

$$\begin{bmatrix} C_{hh} & C_{hc} \\ C_{ch} & C_{cc} \end{bmatrix} \begin{bmatrix} J_h \\ J_c \end{bmatrix} = \begin{bmatrix} D_{hd} & 0 \\ D_{cd} & 0 \end{bmatrix} \begin{bmatrix} E_d \\ 0 \end{bmatrix} - \begin{bmatrix} F_h \\ F_c \end{bmatrix} \quad (3)$$

where $\{J_h\}$ and $\{J_c\}$ are sets of unknowns for the electric current densities on the dielectric surface and perfect-electric-conductor (PEC) surface, respectively; $\{E_d\}$ is a set of unknowns for the electric field on the dielectric surface; C_{hh}, C_{hc}, C_{ch}, C_{cc}, D_{hd} and D_{cd} are dense coefficient matrices; F_h and F_c are source terms. The matrix formed by C_{hh}, C_{hc}, C_{ch} and C_{cc} in Equation (3) is called the MoM matrix or matrix $\boldsymbol{C}$ in this paper.

The interior equivalent problem is modeled using FEM. The goal is to solve the weak form of the vector wave equation as follows [14], [20]. (This equation can also be derived using a variational approach [16], [21].)

$$\int_{V_1} \left[\left(\frac{\nabla \times \mathbf{E}(\mathbf{r})}{j\omega\mu_0\mu_r} \right) \bullet (\nabla \times \mathbf{w}(\mathbf{r})) + j\omega\epsilon_0\epsilon_r \mathbf{E}(\mathbf{r}) \bullet \mathbf{w}(\mathbf{r}) \right] dV$$

$$= \int_{S_1} (\hat{\mathbf{n}} \times \mathbf{H}(\mathbf{r})) \bullet \mathbf{w}(\mathbf{r})\, dS - \int_{V_1} \mathbf{J}^{int}(\mathbf{r}) \bullet \mathbf{w}(\mathbf{r})\, dV \quad (4)$$

where S_1 is the surface enclosing the interior equivalent problem, $\mathbf{w}(\mathbf{r})$ is the weighting function, and $\mathbf{J}^{int}$ is an impressed source. Vector tetrahedral elements [22] can be used to approximate the E field. A Galerkin procedure can be used to test Equation (4). The resulting FEM matrix equation follows [8],

$$\begin{bmatrix} A_{ii} & A_{id} \\ A_{di} & A_{dd} \end{bmatrix} \begin{bmatrix} E_i \\ E_d \end{bmatrix} = \begin{bmatrix} 0 & 0 \\ 0 & B_{dh} \end{bmatrix} \begin{bmatrix} 0 \\ J_h \end{bmatrix} + \begin{bmatrix} g_i \\ g_d \end{bmatrix} \quad (5)$$

where $\{E_i\}$ and $\{E_d\}$ are sets of unknowns for the electric field within the FEM volume and on the dielectric surface, respectively; $\{J_h\}$ is a set of unknowns for the electric current density on the dielectric surface; A_{ii}, A_{id}, A_{di}, A_{dd} and B_{dh} are sparse coefficient matrices; g_i and g_d are source terms. The matrix formed by A_{ii}, A_{id}, A_{di}, and A_{dd} in Equation (5) is called the FEM matrix or matrix $\boldsymbol{A}$ in this paper. Both the FEM and the MoM matrices are symmetric. Note that neither the FEM matrix equation nor the MoM matrix equation can be solved independently. They are coupled through the J_h and E_d terms.

One objective of this study is to determine which formulation works best for various problems. A coupling index, ρ, is defined in this paper as follows,

$$\rho = \frac{\text{Number of FEM unknowns}}{\text{Number of MoM unknowns}} . \quad (6)$$

The value of ρ is determined by the problem geometry and how it is meshed. As shown in later sections, the coupling index ρ can be used as a rough measure to determine which formulation is preferred for a given problem.

III. SAMPLE PROBLEMS

Four sample problems are presented to compare the outward-looking, inward-looking and combined formulations and to validate the preconditioning techniques discussed in later sections. Three of the problems include PCB structures, which are key elements of devices that are frequently modeled by EMC and signal integrity (SI) engineers. Each of these three problems has a thin rectangular shape and presents a unique challenge. The remaining problem has a spherical shape and provides a contrast to the PCB-like structures.

A. Problem 1: A PCB Power Bus Structure

The first problem is to model the input impedance of a PCB power bus structure. As shown in Figure 1, the board dimensions are 5 cm × 5 cm × 1.1 mm. The top and bottom planes are PECs. The dielectric between the PEC layers has a relative dielectric constant of 4.5. A source is placed in the middle of the board between the planes. The MoM boundary is chosen to coincide with the physical boundary of the board. The E fields tangential to the top and bottom planes are zero, thus no E-field unknowns are assigned on the two planes and the number of FEM unknowns is small. Table 1 summarizes the discretization of this problem and the other problems presented in this section.

B. Problem 2: Scattering from a Dielectric Sphere

The second problem is to model the scattering fields from a dielectric sphere. As illustrated in Figure 2, the radius of the sphere is 0.15λ. The relative dielectric constant of the sphere material is 4.5. The incident wave travels along the z-axis. The polarization of the E field is along the x-axis. The goal is to model the far fields. The discretization of this problem is summarized in Table 1.

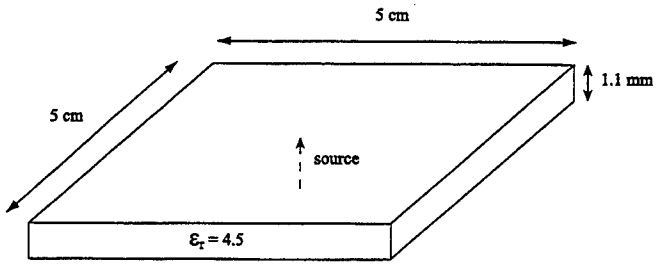

Figure 1. A PCB power bus structure.

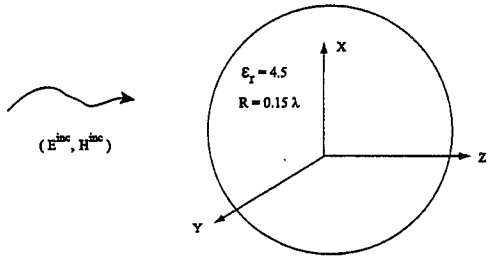

Figure 2. Scattering from a dielectric sphere.

C. Problem 3: A Gapped Power Bus Structure

The third problem is to model a gapped power bus structure. As shown in Figure 3, the board dimensions are 152.4 mm × 101.6 mm × 2.39 mm. The board has a solid PEC plane on the bottom and a gapped PEC plane on the top. The dielectric between the top and bottom planes has a relative permittivity of 4.5. The gap is 5.1 mm wide and located in the center of the top plane. The discretization of this problem is summarized in Table 1. This board is much larger than the board in Problem 1. A fine mesh is used in the vicinity of the gap. To reduce the number of MoM elements, the MoM boundary is placed 9.56 mm above the gap, resulting in a large number of FEM unknowns.

D. Problem 4: A Microstrip Line

The fourth problem is to model the behavior of a microstrip line. The board dimensions are 5 cm × 5 cm × 1.1 mm as shown in Figure 4. The bottom is a solid PEC plane. The trace placed on the top plane is 3 cm long and 0.5 mm wide. The dielectric has a relative permittivity of 4.5. The goal of this problem is to determine the input impedance of the microstrip line at one end when the other end is terminated by a resistor. The discretization of this problem is summarized in Table 1. To reduce the number of boundary elements, the MoM boundary is placed 3.3 mm above the microstrip line. A fine FEM mesh is required near the vicinity of the microstrip line as shown in Figure 5. As a result, this problem has a large coupling index.

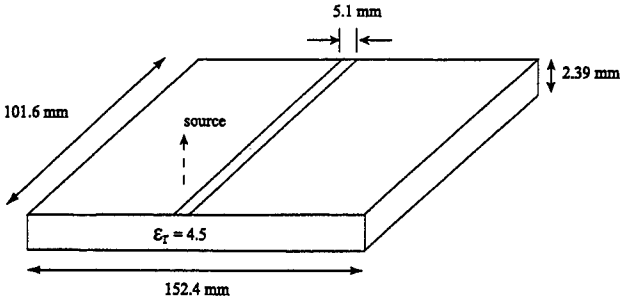

Figure 3. Configuration of a gapped power bus structure.

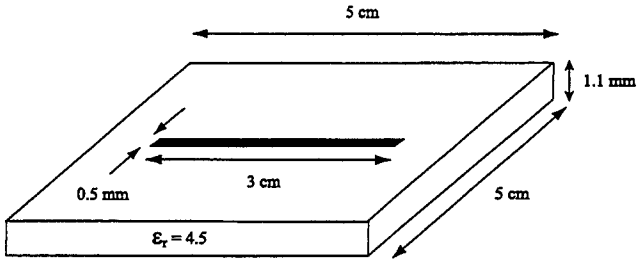

Figure 4. A microstrip line configuration.

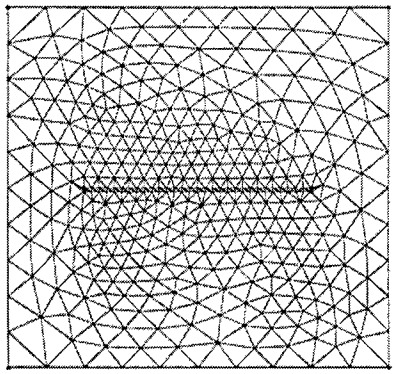

Figure 5. The FEM mesh in the plane of the trace.

Table 1. Summary of the discretization of the four sample problems

	# of FEM unknowns		# of MoM unknowns		Total # of unknowns	Coupling index ρ
	E_i	E_d	J_h	J_c		
Problem 1	402	80	80	575	1,137	0.74
Problem 2	699	612	612	0	1,923	2.14
Problem 3	4,521	1,223	1,223	454	7,421	3.43
Problem 4	2,277	360	360	136	3,133	5.32

IV. TECHNIQUES FOR SOLVING SPARSE MATRIX EQUATIONS

A. Preconditioning

Iterative solvers are widely used to solve large sparse matrix equations of the form,

$$Mx = b \tag{7}$$

where M is a square matrix and b and x are column vectors. b is the source vector and x is the unknown vector. Equation (7) is also called a *linear system.*

To have a non-trivial solution, the matrix M must be non-singular ($\det(M)\neq 0$). The convergence rate of iterative solvers depends mainly on the condition number of the matrix M, which is defined as [14],

$$K(M) = \sqrt{\frac{\lambda_{\max}}{\lambda_{\min}}} \tag{8}$$

where $\lambda_{\min}$ and $\lambda_{\max}$ are the smallest and largest eigenvalues of the matrix $M^H M$, where M^H is the transpose conjugate of M. The condition number provides a measure of the spectral properties of a matrix. The identity matrix has a condition number of 1.0. A singular matrix has a condition number of infinity. A matrix with a large condition number is nearly singular, and is called *ill-conditioned.* An ill-conditioned linear system is very sensitive to small changes in the matrix. Iterative solvers may not converge smoothly, or may even diverge when applied to ill-conditioned systems.

The coefficient matrices generated by FEM and MoM usually have very large condition numbers. It may be difficult to apply iterative solvers to the original FEM and MoM matrix equations. However, a linear system can be transformed into another linear system so that the new system has the same solution as the original one, but has better spectral properties. For instance, both sides of Equation (7) can be multiplied by a square matrix P^{-1},

$$P^{-1}Mx = P^{-1}b \tag{9}$$

where P has the following properties,

(A) $K(P^{-1}M) << K(M)$

(B) $\det(P^{-1}M) \neq 0$

(C) It is inexpensive to solve $Px = b$.

Such a matrix P is called a *preconditioner*. This technique is called *preconditioning*. Condition (A) assures favorable spectral properties for the new linear system. Condition (B) guarantees that the new system, Equation (9), has the same non-trivial solution as Equation (7). Condition (C) is essential to ensure the efficiency of preconditioned iterative solvers. In preconditioned iterative algorithms, it is not necessary to solve P^{-1} explicitly. Instead, a linear system of the form $Px = b$ is solved at each step.

If the preconditioner P is chosen to be M, $P^{-1}M$ becomes an identity matrix. However, finding M^{-1} is generally more difficult than solving Equation (7). It is more practical to find a preconditioner P that is an approximation of M, and satisfies all three conditions. There is a trade-off between the cost of constructing and applying the preconditioner, and the gain in the convergence rate [23].

LU factorization and incomplete LU (ILU) factorization are commonly used to construct preconditioners. LU factorization decomposes a matrix M into a lower triangular matrix L and an upper triangular matrix U, which satisfy,

$$M = LU. \tag{10}$$

ILU factorization ([23], [24]), decomposes matrix M into a lower triangular matrix L and an upper triangular matrix U so that the residue matrix $R = M\text{-}LU$ is subject to certain constraints, such as levels of fill-in, or drop tolerance.

B. Permutation

Because the FEM matrix, A, is sparse, LU factorization may generate a lot of *fill-in elements*, which refer to matrix entries that are zero in the matrix A but are non-zero in the L and U matrices [24]. *Permutation* is a technique that can be used to reduce the number of fill-ins in LU factorization by reordering the matrix. Generally, a symmetric permutation on matrix M is defined as follows [24],

$$M_P = P\,M\,P^T \tag{11}$$

where M_P is the new matrix after permutation and P is the permutation matrix. P is a unitary matrix [24], which satisfies,

$$P^{-1} = P^T. \tag{12}$$

Figure 6 illustrates the sparsity pattern of the original FEM matrix in Problem 1. The number of unknowns in the FEM matrix is 482. A fully populated matrix has 482×482 = 232,324 entries. Figure 6 shows only 3,772 non-zero entries. The percentage of non-zero elements is 1.6%, indicating that the FEM matrix is highly sparse. Figure 7 illustrates the sparsity patterns of the L and U matrices after applying LU factorization to the FEM matrix in Problem 1. The data in Figure 7 was generated using MATLAB® [25]. The L matrix obtained by MATLAB is a "psychologically lower triangular matrix" (i.e. a product of lower triangular and permutation matrices) [26]. This explains why the L matrix is not a strictly lower triangular matrix. The total number of non-zero entries in L and U is 34,640 + 35,379 = 70,019. The total number of fill-ins is 70,019-3772 = 66,247.

The *reverse Cuthill-McKee algorithm* can be used to minimize the bandwidth of a matrix [16], [27]. Bandwidth reduction techniques are useful because they save both storage and operation counts in LU factorization. Figure 8 shows the sparsity pattern of the FEM matrix in Figure 6 after performing a symmetric reverse Cuthill-McKee permutation. Figure 9 illustrates the sparsity patterns of the

L and U matrices after the permutation. The number of fill-ins is 10,457+12,457 – 3,772 = 19,142. Compared with Figure 7, the number of fill-ins has been reduced by 71%.

The *minimum degree permutation* is a complicated and powerful technique that has many advantages over other permutation techniques [16], [26]. One widely used implementation was proposed by George and Liu [28]. This technique reduces fill-ins during Gaussian elimination based on graph theory [16], [29]. In this study, the authors used the symmetric minimum degree permutation provided by MATLAB®. Figure 10 shows the sparsity pattern of the FEM matrix in Figure 6 after performing the symmetric minimum degree permutation. Figure 11 illustrates the sparsity patterns of the L and U matrices after performing the symmetric minimum degree permutation. The number of fill-ins is 7,901+9,628 – 3,772 = 13,757. Compared with Figure 7, the number of fill-ins has been reduced by 79%.

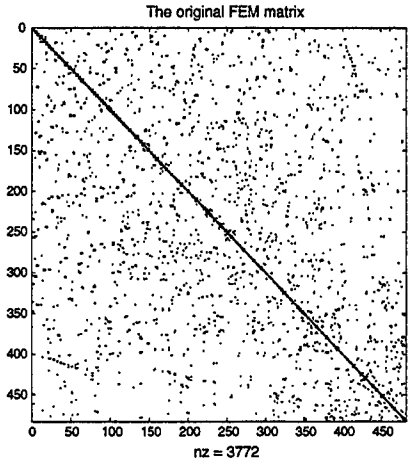

Figure 6. Sparsity pattern of Problem 1 FEM matrix ("nz" is # of non-zero entries).

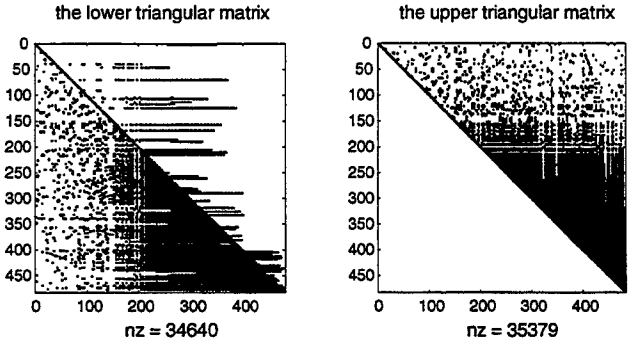

Figure 7. Sparsity pattern of the Problem 1 L and U matrices after LU factorization

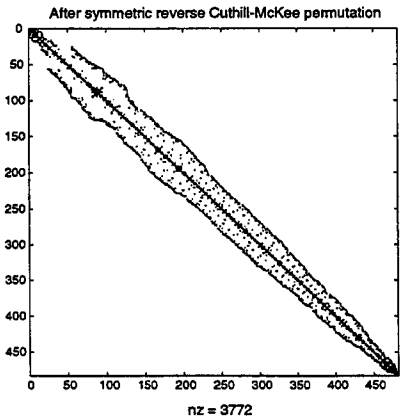

Figure 8. Sparsity pattern of the Problem 1 FEM matrix after symmetric reverse Cuthill-McKee permutation.

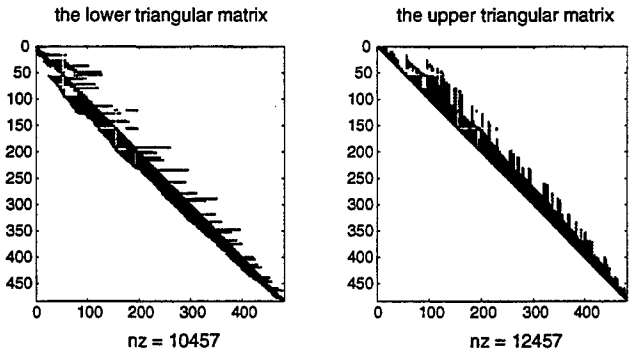

Figure 9. Sparsity pattern of the Problem 1 L and U matrices after symmetric reverse Cuthill-McKee permutation.

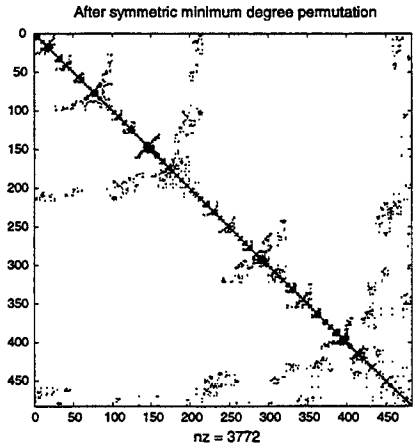

Figure 10. Sparsity pattern of the Problem 1 FEM matrix after symmetric minimum degree permutation.

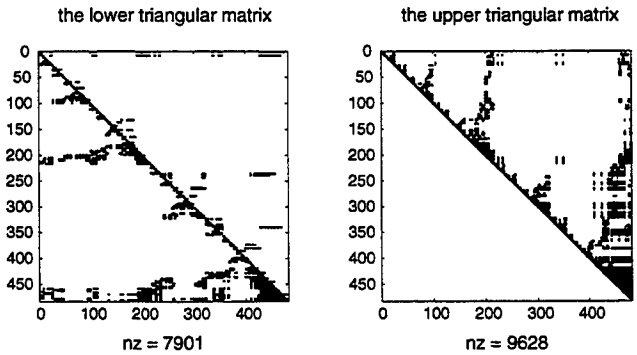

Figure 11. Sparsity pattern of the Problem 1 L and U matrices after symmetric minimum degree permutation.

V. THE OUTWARD-LOOKING FORMULATION AND A NOVEL PRECONDITIONING TECHNIQUE

The outward-looking formulation uses the coefficients of the electric field expansion in the interior equivalent problem, E_i and E_d in Equation (5), as the primary unknowns in the final matrix equation. This formulation has been employed by Paulsen *et al.* [31], Jin and Volakis [32], and Ramahi and Mittra [33].

From Equation (3), the following equations can be derived,

$$C_{ch}J_h + C_{cc}J_c = D_{cd}E_d - F_c$$

$$\Rightarrow \quad J_c = C_{cc}^{-1}(D_{cd}E_d - C_{ch}J_h - F_c) \tag{13}$$

$$C_{hh}J_h + C_{hc}J_c = D_{hd}E_d - F_h \quad . \tag{14}$$

Substituting Equation (13) into Equation (14) gives,

$$\left(C_{hh} - C_{hc}C_{cc}^{-1}C_{ch}\right)J_{hh}$$

$$= (D_{hd} - C_{hc}C_{cc}^{-1}D_{cd})E_d + C_{hc}C_{cc}^{-1}F_c - F \; . \tag{15}$$

To save computation time and memory, the following intermediate terms are introduced,

$$N_{hc} \equiv C_{hc}C_{cc}^{-1} \tag{16}$$

$$C'_{hh} \equiv \left(C_{hh} - N_{hc}C_{ch}\right)^{-1} \tag{17}$$

$$D'_{hd} \equiv D_{hd} - N_{hc}D_{cd} \tag{18}$$

$$K_h \equiv N_{hc}F_c - F_h \, . \tag{19}$$

Equation (15) can now be written as,

$$J_h = C'_{hh}(D'_{hd}E_d + K_h) \, . \tag{20}$$

Substituting Equation (20) into Equation (5) gives,

$$\left([A] + \begin{bmatrix} 0 & 0 \\ 0 & -B_{dh}C'_{hh}D'_{hd} \end{bmatrix} \right) \begin{bmatrix} E_i \\ E_d \end{bmatrix}$$

$$= \begin{bmatrix} g_i \\ g_d \end{bmatrix} + \begin{bmatrix} 0 \\ B_{dh}C'_{hh}K_h \end{bmatrix} \tag{21}$$

where the matrix A is the FEM matrix. Matrix A_c, A', and vector b are defined as follows,

$$A_c \equiv \begin{bmatrix} 0 & 0 \\ 0 & -B_{dh}C'_{hh}D'_{hd} \end{bmatrix} \tag{22}$$

$$A' \equiv A + A_c \tag{23}$$

$$b \equiv \begin{bmatrix} g_i \\ g_d \end{bmatrix} + \begin{bmatrix} 0 \\ B_{dh}C'_{hh}K_h \end{bmatrix} \tag{24}$$

$$x \equiv \begin{bmatrix} E_i \\ E_d \end{bmatrix} \; . \tag{25}$$

Equation (21) now becomes,

$$A'x = b \, . \tag{26}$$

Equation (26) is a fully determined system and is the final matrix equation to solve. Note that the order of this linear system is the same as the order of the original FEM matrix. The Bi-Conjugate Gradient Stabilized (BiCGSTAB) method [23], [24], can be used to solve Equation (26). Although BiCGSTAB requires less memory than direct solvers such as the Gaussian elimination method, it may have difficulty converging, or may even diverge. Preconditioning techniques can be utilized to improve the efficiency and accuracy of BiCGSTAB. LU factorization can be employed to construct preconditioners.

As shown in Figure 12, most of the non-zero elements are located in the bottom-right corner of matrix A'. Table 2 summarizes the number of non-zero entries in A, A', and their LU factorizations. It is inefficient to perform LU factorization on A' because the computer resources required for factorization may exceed those required for an iterative solution.

In Equation (23), the entries in the matrix A_c have much smaller values than those in the matrix A for each of the sample problems. It seems reasonable to construct preconditioners from the matrix A instead of the matrix A'. Furthermore, the matrix A is sparse and symmetric, so the symmetric minimum degree permutation can be applied to reduce fill-ins in the LU factorization,

$$A_P = P\,A\,P^T \tag{27}$$

where P is the permutation matrix and A_P is the new matrix after permutation. Next, an LU factorization can be applied to A_P to obtain a lower triangular matrix L and an upper triangular matrix U,

$$A_P = LU. \tag{28}$$

Multiplying both sides of Equation (26) by P and combining with Equation (12) gives,

$$PA'P^T Px = Pb \, . \tag{29}$$

The following new terms are defined,

$$A'' \equiv PA'P^T \tag{30}$$

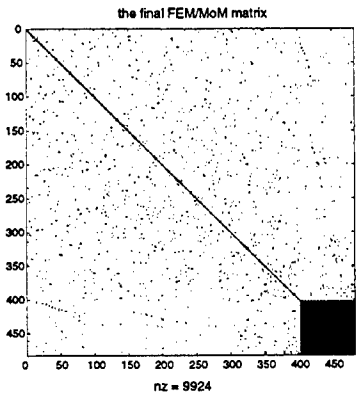

Figure 12. Sparsity pattern of Problem 1 A' in Equation (26).

$$y \equiv Px \quad \text{and} \quad b'' \equiv Pb \ . \tag{31}$$

Equation (29) becomes,

$$A''y = b'' \ . \tag{32}$$

Permutation does not change the condition number of a matrix,

$$K(A'') = K(A') \ . \tag{33}$$

Next, the preconditioners L and U can be applied to Equation (32),

$$(LU)^{-1}A''y = (LU)^{-1}b'' \ . \tag{34}$$

Iterative solvers can be used to solve Equation (34). Note that it is not necessary to explicitly compute $(LU)^{-1}$ when using iterative solvers [23], [24]. After y is obtained, x can be calculated from Equation (31),

$$x = P^{-1}y = P^{T}y \ . \tag{35}$$

The technique discussed above was implemented using MATLAB®. Table 3 shows the condition number of A' in Equation (26) and $(LU)^{-1}A''$ in Equation (34) for all four sample problems. This preconditioning technique greatly reduced the condition number of the matrix A' and therefore improved the efficiency of the iterative solver.

Table 4 shows the solution times for each of the four problems using the un-preconditioned BiCGSTAB solver and the preconditioned BiCGSTAB solver. Only a small amount of time was spent constructing preconditioners. The preconditioning technique reduced the number of iterations by a factor ranging from 202 to 879, and achieved 15.9- to 149.6-fold improvements in the Equation (26) solution time. Table 5 examines the time spent on each step of the solution process for the four sample problems using the un-preconditioned solver and the preconditioned solver. For the first problem, there is not much difference between the un-preconditioned and the preconditioned solvers, because the time spent computing the matrix entries and on the coupling process is the dominant factor. For Problems 2, 3, and 4, the preconditioned solver yields 2.21-, 7.83- and 6.36- fold improvements, respectively. The bottom-right part of A' is dense as shown in Figure 12 and is scattered after A' is permuted as illustrated in Figure 13. This is not preferred because the locality of data in matrix A_c is destroyed and this has a negative effect on the efficiency of the iterative solver. BiCGSTAB only needs to compute the inner product between the matrix A' and the searching vector q. Because

$$A'q = Aq + A_c q \ , \tag{36}$$

it is not necessary to compute the matrix A' explicitly. The FEM matrix can be stored using the ITPACK format [16], and the bottom-right part of A_c can be stored in a two-dimensional array. Permutation is performed on the matrix A, vector q and $A_c q$ but the matrix A_c is not permuted. This storage scheme makes it unnecessary to keep track of the row and column information for every entry in A_c. Therefore, it uses much less computer memory than computing A' explicitly and storing A' as a sparse matrix.

Table 2. Non-zero elements in A, A′, and their LU factorizations

	nz(A)*	nz(A′)	$\frac{\text{nz}(A)}{\text{nz}(A')}$ (%)	nz(L)+nz(U) $A = LU$ **	nz(L′)+nz(U′) $A' = L'U'$ ***
Problem 1	3,772	9,924	38%	17,175	33,488
Problem 2	17,745	389,229	4.6%	192,865	1,000,728
Problem 3	65,558	1,555,144	4.2%	983,322	2,962,187
Problem 4	36,135	163,829	22%	468,849	798, 028

* nz(A) refers to the number of non-zero elements in matrix A.
** After symmetric minimum degree permutation.
*** After symmetric Cuthill-McKee permutation.

Table 3. Outward-looking formulation condition numbers before and after preconditioning

	$K(A')$	$K((LU)^{-1}A'')$
Problem. 1	8.32×10^{6}	1.07
Problem. 2	4.27×10^{3}	18.7
Problem. 3	4.27×10^{7}	N/A*
Problem. 4	5.56×10^{7}	813

* Data not available due to excessive memory requirement.

Table 4. Solution times for Equation (26) using the un-preconditioned and preconditioned BiCGSTAB solvers (The drop tolerance for the BiCGSTAB solver is 1.0×10^{-3}.)

	LU Factorization (sec)	Iteration			Total (sec)	Improvement (fold)
		Number	Converged (Yes/No)	Time (sec)		
Problem 1 (orig.*)	N/A	202	Yes	2.03	2.03	
Problem 1 (new**)	0.03	1	Yes	0.09	0.12	15.9
Problem 2 (orig.*)	N/A	715	Yes	206.10	206.10	
Problem 2 (new**)	1.63	2	Yes	1.92	3.55	58.1
Problem 3 (orig.*)	N/A	5,096	Yes	6,037.90	6,037.9	
Problem 3 (new**)	12.06	9	Yes	28.03	40.09	149.6
Problem 4 (orig.*)	N/A	2,637	No	386.77	386.77	
Problem 4 (new**)	5.19	3	Yes	2.91	8.10	46.7

* "orig." refers to the un-preconditioned BiCGSTAB solver.

** "new" refers to the preconditioned BiCGSTAB solver.

Table 5. Time required to solve the four problems

	Compute matrix entries (sec)	Coupling Equations (13) - (21) (sec)	Original		Preconditioned		Improvement (%)
			Solving Eq. (17) (sec)	Total (sec)	Solving Eq. (29) (sec)	Total (sec)	
Problem 1	46.00	20.76	2.03	68.79	0.12	66.88	3%
Problem 2	48.00	40.23	206.10	294.22	3.55	91.78	221%
Problem 3	287.20	438.60	6,037.90	6,763.7	40.10	765.90	783%
Problem 4	40.12	11.33	386.77	438.22	8.10	59.55	636%

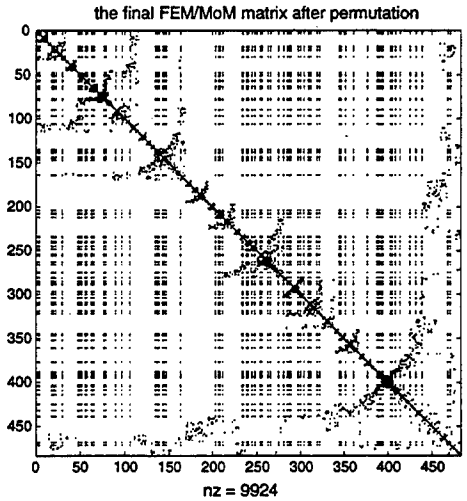

Figure 13. Sparsity pattern of Problem 1 A'' in Equation (32) after minimum degree permutation.

VI. THE INWARD-LOOKING FORMULATION

The inward-looking formulation chooses the coefficients of the equivalent surface current expansion in the exterior equivalent problem (J_h and J_c in Equation (3)) as the primary unknowns in the final matrix equation. This formulation has been implemented by Jin and Liepa [34], Yuan *et al.* [35], and Cangellaris and Lee [36].

From Equation (5), the following derivation can be made,

$$A_{ii}E_i + A_{id}E_d = g_i \Rightarrow E_i = A_{ii}^{-1}(g_i - A_{id}E_d) \quad (37)$$

$$A_{di}E_i + A_{dd}E_d = B_{dh}J_h + g_d \Rightarrow$$

$$(A_{dd} - A_{di}A_{ii}^{-1}A_{id})E_d = B_{dh}J_h + (g_d - A_{di}A_{ii}^{-1}g_i). \quad (38)$$

To save computation time and memory, the following intermediate terms are introduced,

$$M_{dd} \equiv (A_{dd} - A_{di}A_{ii}^{-1}A_{id})^{-1} \quad (39)$$

$$N_{dh} \equiv M_{dd}B_{dh} \quad (40)$$

$$K_d \equiv M_{dd}(g_d - A_{di}A_{ii}^{-1}g_i). \quad (41)$$

Equation (38) can be rewritten as,

$$E_d = N_{dh}J_h + K_d. \quad (42)$$

Substituting Equation (38) into Equation (3) gives the final matrix equation,

$$\begin{bmatrix} C_{hh} - D_{hd}N_{dh} & C_{hc} \\ C_{ch} - D_{cd}N_{dh} & C_{cc} \end{bmatrix} \begin{bmatrix} J_h \\ J_c \end{bmatrix} = \begin{bmatrix} D_{hd}K_d - F_h \\ D_{cd}K_d - F_c \end{bmatrix}. \quad (43)$$

Note that the order of this equation is the same as that of the MoM matrix. The inward-looking formulation inverts one sparse matrix A_{ii}, and one dense matrix $(A_{dd} - A_{di}A_{ii}^{-1}A_{id})$. Because the matrix in Equation (43) is dense, the Gaussian elimination method is used to solve the final matrix equation.

The outward-looking formulation is better suited to problems with a large number of FEM unknowns and fewer MoM unknowns. The inward-looking formulation is

preferred for problems with a higher percentage of MoM unknowns. Of the four problems presented here, only Problem 1 has more MoM unknowns than FEM unknowns. As shown in Table 6, the inward-looking formulation is faster than the outward-looking formulation at solving Problem 1. However, the inward-looking formulation is not the best choice for the other three problems.

VII. THE COMBINED FORMULATION

The outward-looking and inward-looking formulations are computationally expensive because they invert two matrices. An alternative is to combine Equation (3) and Equation (5) to form the final matrix as follows,

$$\begin{bmatrix} A_{ii} & A_{id} & 0 & 0 \\ A_{di} & A_{dd} & -B_{dh} & 0 \\ 0 & -D_{hd} & C_{hh} & C_{hc} \\ 0 & -D_{cd} & C_{ch} & C_{cc} \end{bmatrix} \begin{bmatrix} E_i \\ E_d \\ J_h \\ J_c \end{bmatrix} = \begin{bmatrix} g_i \\ g_d \\ -F_h \\ -F_c \end{bmatrix} \quad (44)$$

and solve for all unknowns simultaneously [14]. This is referred to as the *combined formulation* in this paper. It has become more popular recently and has been employed by Sheng *et al.* [18], Janković *et al.* [37], and Shen *et al.* [38].

The combined formulation does not require any matrix inversions. However, it generates a larger matrix equation. The order of the final matrix is equal to the sum of the orders of the FEM and MoM matrices. As shown in Table 7, the matrix in the combined formulation has a much larger condition number than the final matrix in the outward-looking formulation. Due to these large condition numbers, it can be very difficult to generate preconditioners using LU factorization or other preconditioning techniques. Consequently, iterative methods may not work well, especially when the MoM part is large. Table 8 lists the normalized residue of the solutions to Equation (44) for the four sample problems using the Bi-Conjugate Gradient (BiCG), BiCGSTAB and Generalized Minimal Residual (GMRES) methods [23]. None of them reaches the designated drop tolerance of 1.0×10^{-3}. Problem 2, which has a different geometry (a sphere) from the other three PCB problems, has a much smaller condition number and two of the iterative solvers converge to acceptable residues. This may explain why the authors in [18], [37] did not report convergence problems for the combined formulation. Shen *et al.* [38] showed that the ILU factorization with different fill-in levels worked very well for their applications. However, the problems presented in [38] have a large number of FEM unknowns (>16,000) and very few MoM unknowns (<200). The four sample problems presented in this paper have a higher percentage of MoM unknowns because the MoM boundary is applied closer to the object being modeled. For the four sample problems presented here, the ILU factorization technique fails to converge.

The Gaussian elimination method can also be used to solve Equation (44). However, a large number of fill-ins are generated during Gaussian elimination. To reduce the number of fill-ins, $\{E_i\}$ in Equation (44) can be permuted. However, permuting $\{E_d, J_d, J_c\}$ in Equation (44) destroys the data locality of the matrix C and D and therefore is not preferred.

VIII. COMPARING THE THREE FORMULATIONS

Table 9 lists the time required using each of the three formulations to solve the sample problems. The outward-looking formulation inverts two dense matrices and performs a lot of matrix multiplication. However, this formulation is excellent when the coupling index ρ is large, mainly because the preconditioning technique presented in Section III greatly reduces the time spent solving the final matrix equation. The inward-looking formulation excels when the coupling index ρ is small. It performs poorly when ρ is large because the inverse of the sparse FEM matrix is dense and the coupling process is time-consuming. The combined formulation was not optimum for any of the sample problems although it worked reasonably well for solving Problem 1 and Problem 2.

Table 10 lists the computer memory requirements for each of the three formulations. The outward-looking formulation required the least amount of memory. One reason for this was that BiCGSTAB was used to solve the final equation and the FEM matrix was stored as a sparse matrix. Another reason was that the symmetric minimum degree permutation significantly reduced the number of fill-ins when constructing preconditioners. For the inward-looking formulation, the inverse of the FEM matrix and the matrix in Equation (43) were dense, so this formulation required more memory than the outward-looking formulation. The inward-looking formulation required less or more memory than the combined formulation, depending on the value of ρ. The combined formulation required much more memory than the outward-looking formulation because the Gaussian elimination method was used to solve the matrix equation. The exact amount of time and memory required to solve a problem depends on many factors such as the mesh quality, the order of $\{E_i, E_d, J_h, J_c\}$, and the convergence rate of iterative solvers. The coupling index ρ can be used as a rough measure to determine which formulation is preferred. Based on the four sample problems and the authors' experience, the outward-looking formulation is preferred when $\rho>2.0$; the inward-looking formulation is preferred when $\rho<1.5$. The combined formulation is not preferred due to its large memory requirement (when using a Gaussian elimination solver), and its poor convergence rate (when using an iterative solver). The combined formulation is acceptable when the problem is not memory-constrained.

Depending on the type of problems being solved, the three formulations may exhibit instability problems. As

pointed out by Pearson *et al.* [13] and Peterson *et al.* [14], the inward-looking formulation is susceptible to uniqueness difficulties. As shown in Equation (37), A_{ii}^{-1} must be computed. A_{ii} is essentially the FEM matrix for a closed cavity that might be resonant, which means A_{ii}^{-1} does not exist or is nearly singular at resonant frequencies. However, typical EMC problems that model the high-frequency loss present in the problem geometries are not likely to exhibit this instability.

Table 6. Comparison between the outward-looking and inward-looking formulations

	Compute matrix entries (sec)	Outward-looking (preconditioned BiCGSTAB)			Inward-looking (Gaussian elimination)		
		Coupling Equations (13) - (21) (sec)	Solving Equation (32) (sec)	Total (sec)	Coupling Equations (37) - (43) (sec)	Solving Equation (43) (sec)	Total (sec)
Problem 1	46.00	20.76	0.12	66.88	1.63	11.19	58.82
Problem 2	48.00	40.23	3.55	91.78	46.83	8.80	103.60
Problem 4	40.12	11.33	8.10	59.55	174.92	4.89	219.90

* Problem 3 is not listed in this table because the inward-looking formulation requires excessive computer memory.

Table 7. The condition number for the outward-looking and combined formulations without preconditioning

	K (LHS*) (Outward-looking)	K (LHS**) (Combined)
Problem 1	8.32×10^{6}	4.38×10^{10}
Problem 2	2.87×10^{3}	2.71×10^{7}
Problem 3	4.27×10^{7}	3.81×10^{11}
Problem 4	5.56×10^{7}	1.78×10^{11}

* LHS refers to the matrix on the left-hand side of Equation (26).
** LHS refers to the matrix on the left-hand side of Equation (44).

Table 8. Solutions to Equation (44) using iterative solvers without preconditioning
(The drop tolerance was 1.0×10^{-3}; the maximum iteration number was set to be the size of the matrix equation.)

	Normalized least residue			
	Problem 1	Problem 2	Problem 3	Problem 4
BiCG	0.66	0.89	0.60	0.50
BiCGSTAB	0.34	0.0058	0.19	0.41
GMRES(5) *	0.31	0.0049	0.19	0.39

* GMRES restarted after every five search-directions.

Table 9. Time required by the three formulations

	ρ	Outward-looking* (sec)	Inward-looking (sec)	Combined (sec)
Problem 1	0.74	66.88	58.82	59.81
Problem 2	2.12	91.78	103.60	92.66
Problem 3	3.43	765.90	N/A**	N/A**
Problem 4	5.32	59.55	219.90	76.59

* The drop tolerance for the BiCGSTAB solver is 1.0×10^{-3}.
** The results are not available due to excessive memory requirements.

Table 10. Computer memory requirements of the three formulations

	ρ	Outward-looking (MBytes)	Inward-looking (MBytes)	Combined (MBytes)
Problem 1	0.74	7	17	34
Problem 2	2.12	23	42	70
Problem 3	3.43	107	N/A*	N/A*
Problem 4	5.32	11	126	36

* Data not available due to excessive memory requirements

The outward-looking and the combined formulations do not have the uniqueness problem associated with A_{ii}^{-1}. However, all three formulations may have uniqueness difficulties at interior resonant frequencies caused by the EFIE [15], [17], [18]. The exterior equivalent problem can be constructed in a manner (e.g. using a combined field formulation [6], [18]), to avoid the problem of interior resonance.

IX. CONCLUSIONS

This paper presents three formulations for the hybrid FEM/MoM method. The outward-looking formulation constructs an RBC using MoM and then substitutes the RBC into the FEM equations. Iterative solvers can be used to solve the final matrix equation efficiently. The authors have found that it is much faster and less memory intensive, to construct preconditioners based on LU factorization of the FEM matrix rather than the final matrix. The symmetric minimum degree permutation can reduce the number of fill-ins resulting in further memory reduction. The preconditioning technique presented greatly reduced the number of iterations required by the solver for the sample problems presented here. The outward-looking formulation is preferred when the coupling index ρ is larger than 2.0.

The inward-looking formulation derives an RBC using the FEM, then substitutes the RBC into the MoM equations. The Gaussian elimination method is generally used to solve the final matrix equation. The inward-looking formulation is preferred when the coupling index ρ is smaller than 1.5.

The combined formulation generates a large matrix equation directly without inverting any matrices, and solves for all unknowns simultaneously. For the types of problems studied here, it was difficult to apply iterative solvers to the resulting matrix equations due to their large condition numbers.

The choice of hybrid FEM/MoM formulation depends on the problem geometry and the way it is meshed. However, for the printed circuit board geometries investigated in this paper, the outward-looking formulation appears to be the most effective and most efficient approach.

REFERENCES

[1] P. Silvester and M. S. Hsieh, "Finite element solution of 2-dimensional exterior field problems," *Proc. Inst. Elect. Eng.*, vol. 43, pp. 1743-1747, Dec. 1971.

[2] B. H. McDonald and A. Wexler, "Finite element solution of unbounded field problems," *IEEE Trans. Microwave Theory Tech.*, vol. 20, pp. 841-847, Dec. 1972.

[3] X. Yuan, "Three dimensional electromagnetic scattering from inhomogeneous objects by the hybrid moment and finite element method," *IEEE Trans. Microwave Theory Tech.*, vol. 38, pp. 1053-1058, Aug. 1990.

[4] J.-M. Jin and J. L. Volakis, "Electromagnetic scattering by and transmission through a three-dimensional slot in a thick conducting plane," *IEEE Trans. Antennas Propagat.*, vol. 39, pp. 543-550, Apr. 1991.

[5] J.-M. Jin and J. L. Volakis, "A hybrid finite element method for scattering and radiation by microstrip patch antenna and arrays residing in a cavity," *IEEE Trans, Antennas Propagat.*, vol. 29, pp. 1598-1604, Nov. 1991.

[6] J. Angélini, C. Soize, and P. Soudais, "Hybrid numerical method for harmonic 3D Maxwell equations: Scattering by a mixed conducting and inhomogeneous anisotropic dielectric medium," *IEEE Trans. Antennas Propagat.*, vol. 41, pp. 66-76, Jan. 1993.

[7] G. E. Antilla and N. G. Alexopoulos, "Scattering from complex three-dimensional geometries by a curvilinear hybrid finite element-integral equation approach," *J. Opt. Soc. Amer. A*, vol. 11, no. 4, pp. 1445-1457, Apr. 1994.

[8] M. W. Ali, T. H. Hubing, and J. L. Drewniak, "A hybrid FEM/MOM technique for electromagnetic scattering and radiation from dielectric objects with attached wires," *IEEE Trans. Electromagnetic Compatibility*, vol. 39, pp. 304-314, Nov. 1997.

[9] J. Shen and A. Kost, "FE-BE method for EMC problems in power cable systems," *IEEE Trans. Magn.*, vol. 32, pp. 1493-1496, May 1996.

[10] A. Kost and H. Igarashi, "Different numerical methods for electromagnetic field computation with thin shielding sheets," *Proceedings of the IEEE 1997 International Symposium on Electromagnetic Compatibility*, pp. 248-253, Austin, Texas, Aug. 1997.

[11] Y. Ji, M. Ali, and T. H. Hubing, "EMC applications of the EMAP5 hybrid FEM/MoM code", *Proceedings of the IEEE 1998 International Symposium on Electromagnetic Compatibility*, vol. 1, pp. 177-181, Denver, Colorado, Aug. 1998.

[12] B.-S. Yang, A. W. Glisson, and P. M. Goggans, "Interior resonance problems associated with hybrid integral equation/partial differential equation methods," *Proceedings of the 1992 International IEEE Antennas and Propagation Society Symposium*, pp. 781-784, Chicago, Illinois, Jul. 1992.

[13] L. W. Pearson, A. F. Peterson, L. J. Bahrmasel, and R. A. Whitaker, "Inward-looking and outward-looking formulations for scattering from penetrable objects," *IEEE Trans, Antennas Propagat.*, vol. 40, pp. 714-720, Jun. 1992.

[14] A. F. Peterson, S. L. Ray, and R. Mittra, *Computational Methods for Electromagnetics*, New York: IEEE Press and Oxford University Press, 1997.

[15] J. L. Volakis, T. Özdemir, and J. Gong, "Hybrid finite-element methodologies for antennas and scattering", *IEEE Trans, Antennas Propagat.*, vol. 45, pp. 493-507, Mar. 1997.

[16] J. L. Volakis, A. Chatterjee, and L. C. Kempel, *Finite Element Method for Electromagnetics*, New York: IEEE Press and Oxford University Press, 1998.

[17] J. J. H. Wang, *Generalized Moment of Methods in Electromagnetics*, New York: John Wiley & Sons, 1990.

[18] X.-Q. Sheng, J.-M. Jin, J. Song, C.-C. Lu, and W.C. Chew, "On the formulation of hybrid finite-element and boundary-integral methods for 3-D scattering," *IEEE Trans, Antennas Propagat.*, vol. 46, pp. 303-311, Mar. 1998.

[19] S. M. Rao, D. R. Wilton, and A. W. Glisson, "Electromagnetic scattering by surfaces of arbitrary shape," *IEEE Trans. on Antennas and Propagat.*, vol. 30, pp. 409-418, May 1982.

[20] P. P. Silvester and R. L. Ferrari, *Finite Elements for Electrical Engineers*, Cambridge University Press, 1996.

[21] J.-M. Jin, *The Finite Element Method in Electromagnetics*, New York: John Wiley & Sons Inc, 1993.

[22] M. L. Barton and Z. J. Cendes, "New vector finite elements for three-dimensional magnetic field computation," *Journal of Applied Physics*, vol. 61, pp. 3919-3921, Apr. 1987.

[23] R. Barrett, M. Berry, T. F. Chan, F. Demmel, J. M. Donato, J. Dongarra, V. Eijkhout, R. Pozo, C. Romine, and H. Van der Vorst, *Templates for the Solution of Linear Systems: Building Blocks for Iterative Methods*, Philadelphia: SIAM, 1994.

[24] Y. Saad, *Iterative Methods for Sparse Linear Systems*, Boston: PWS Publishing Company, 1996.

[25] MATLAB is a product of Mathworks, Inc, U.S.A..

[26] MATLAB manuals, Mathworks, Inc, U.S.A..

[27] E. Cuthill and J. McKee, "Reducing the bandwidth of sparse symmetric matrices," *Proceedings of the 24th National Conference of the ACM*, New Jersey: Brandon Systems Press, 1969.

[28] A. George and J. W. H. Liu, *Computer Solution of Large Sparse Positive Definite Systems*, New Jersey: Prentice-Hall, 1981.

[29] S. Pissanetzky, *Sparse Matrix Techniques*, New York: Academic Press, 1984.

[30] J. R. Gilber, C. Moler, and R. Schreiber, "Sparse matrices in MATLAB: Design and implementation," *SIAM J. Matrix Anal. Appl.*, vol. 13, pp. 333-356, Jan. 1992.

[31] K. D. Paulsen, D. R. Lynch, and J. W. Strohbehn, "Three-dimensional finite, boundary, and hybrid element solutions of the Maxwell equations for lossy dielectric media," *IEEE Trans. Microwave Theory Tech.*, vol. 36, pp. 682-693, Apr. 1988.

[32] J.-M. Jin and J. L. Volakis, "A finite element-boundary integral formulation for scattering by three-dimensional cavity-backed apertures," *IEEE Trans, Antennas Propagat.*, vol. 39, pp. 97-104, Jan. 1991.

[33] O. M. Ramahi and R. Mittra, "Finite element solution for a class of unbounded geometries," *IEEE Trans, Antennas Propagat.*, vol. 39, pp. 244-250, Feb. 1991.

[34] J.-M. Jin and V. V. Liepa, "A note on hybrid finite element method for solving scattering problems," *IEEE Trans, Antennas Propagat.*, vol. 36, pp. 1486-1490, Oct. 1988.

[35] X. Yuan, D. R. Lynch, and J .W. Strohbehn, "Coupling of finite element and moment methods for electromagnetic scattering from inhomogeneous objects," *IEEE Trans, Antennas Propagat.*, vol. 38, pp. 386-393, Mar. 1990.

[36] A. C. Cangellaris and R. Lee, "Finite element analysis of electromagnetic scattering from inhomogeneous cylinders at oblique incidence," *IEEE Trans, Antennas Propagat.*, vol. 39, pp. 645-650, May 1990.

[37] D. Janković, M. LaBelle, D. C. Chang, J. M. Dunn, and R. C. Booton, "A hybrid method for the solution of scattering from inhomogeneous dielectric cylinders of arbitrary shape," *IEEE Trans, Antennas Propagat.*, vol. 42, pp. 1215-1222, Sept. 1994.

[38] J. Shen, T. Hybler, and A. Kost, "Preconditioned iterative solvers for complex and unsymmetric systems of equations resulting from the hybrid FE-BE method," *IEEE Trans. Magn.*, vol. 33, pp. 1764-1767, Mar. 1997.

A NEW EXCITATION MODEL FOR PROBE-FED PRINTED ANTENNAS ON FINITE SIZE GROUND PLANES

F. Tiezzi, A. Alvarez-Melcón and Juan R. Mosig
Laboratoire d'Electromagnétisme et d'Acoustique (LEMA)
Ecole Polytechnique Fédérale de Lausanne (EPFL)
CH-1015 Lausanne, Switzerland
Ferdinando.Tiezzi@epfl.ch, Alejandro.Alvarez@upct.es, Juan.Mosig@epfl.ch.

ABSTRACT *– This paper presents a new excitation model for probe-fed printed antennas on both infinite and finite size ground planes. The model has been developed within the general frame of the mixed potential integral equation (MPIE) and the method of moments (MoM). The technique is based on a delta-gap voltage model, and a special procedure is implemented inside the integral equation to effectively impose a voltage reference plane into a floating metallic plate which is acting as a ground plane. The present technique allows the accurate calculation of the input impedance of printed antennas, and the effects of finite size ground planes can be easily accounted for in the calculations. In addition, an efficient technique is presented for the evaluation of the radiation patterns of printed antennas, taking also into account the presence of finite size ground planes. Comparisons with measured results show that the new derived excitation method is indeed accurate, and can be used for the prediction of the backside radiation and side lobe levels of real life finite ground plane printed antennas.*

Keywords.— Integral equation, excitation models, finite ground plane, backside radiation, printed antennas.

1 INTRODUCTION

During the last decades, printed circuits and antennas have played an important role in many branches of electrical engineering and the field of application is spreading to new technologies and to even higher frequencies. The need for miniaturisation is increasing in many applications e.g., telecommunications and space missions. Obviously, these compact geometries are not adequate for the use of models assuming infinite ground planes.

The need to take into account for finite ground plane dimensions in microstrip antennas modelling arises especially in applications where patches are used as free standing structures and front-to-back ratio must be maximized in order to avoid interference problems [Bokhari *et al.* 1992], or to locate a potential main beam deformation caused by the diffraction from the ground plane edges. Moreover, the need to model the excitation on two floating metallic patches can become inevitable in applications like dual band stacked printed antennas where a first patch acts as ground plane for a second radiating element [Zürcher *et al.* 1999].

To solve this problem a new excitation model and de-embedding technique for the computation of the input impedance of probe-fed printed antennas on finite size ground planes using a Mixed Potential Integral Equation technique (MPIE) [Mosig and Gardiol 1988, Hall and Mosig 1996] has been developed. This approach accounts for the effect of the ground plane dimensions on the input impedance, the mutual coupling, and the radiation characteristics of a single antenna element or a finite array.

As a first step to attain this goal, a new attachment mode for probe-fed printed antennas on infinite ground plane has been developed. The most widely used excitation model for probe-fed antennas is the impressed-current model [Pozar 1982, Hall and Mosig 1989]. This model assumes that a constant impressed current is exciting the antenna and it use the derived distribution of currents on metallic surfaces to compute the voltage at the probe location. This method may lead to accurate results but needs the computation of a surface integral over all the metallic surfaces present in the structure to obtain the input impedance. Contrary to the previous one, the model presented here, as described in Sec. 3, uses a delta gap

voltage excitation model (to the authors' knowledge used until now only for microstrip line fed antennas [Davidovitz and Lo 1989, Harokopus and Katehi 1991, Eleftheriades and Mosig 1996]). This model assumes an impressed voltage between the antenna and the ground plane and, once the surface currents have been computed, only a normalisation by the excitation voltage is needed to obtain the input admittance. Another remarkable difference between the two models is the type of special basis functions used in the attachment mode. Considering the case of triangular meshing (the extension to rectangular cells is straightforward), in the impressed current model one (or more) entire basis function with opposite sign of the current on its two halves is used to model the horizontal spreading of the vertical current coming from the coaxial probe. In the present model, one to three half basis functions are introduced for the attachment mode depnding on the location of the feed. This implies that the present excitation model can be used for any probe location inside the patch, including its edge and also for microstrip line fed antennas [Tiezzi *et al.* 1999] without exception.

These excitation models as well as the subsequent technique for computing impedances are implicitly based on the assumption of an infinite ground plane, which according to image theory automatically produces a zero voltage at ground plane level. In Sec. 4 the attachment mode is modified in order to take into account the finiteness of the ground plane. Here, instead of using Green's functions including the ground plane effect through image theory, a specific numerical treatment is applied to the ground plane. To the authors' knowledge, the first approach using an MPIE formulation for the study of finite size ground planes can be found in [Bokhari *et al.* 1992]. This work, however, only represents an approximation of the real finite structure, since the currents induced on the antenna are computed using an infinite ground plane model. Once the induced currents are computed, the finite size nature of the ground plane is taken into account, at a later stage, during the calculation of the scattering problem associated with the computed currents. Hence the results presented in [Bokhari *et al.* 1992] are only accurate, if the ground plane is sufficiently large: it would therefore be desirable to develop a rigorous method, which remains valid even for very small ground planes. The method presented in this paper is a full wave method based on the MPIE technique, and the only approximation introduced is that we use the Green's functions multilayered media formulated in the traditional form of Sommerfeld integrals [Mosig and Gardiol 1988, Mosig 1989]. Therefore the currents induced in the structure are computed taking into account since the beginning the finite size of the ground plane but the second-order effect of dielectric truncation is neglected. This approximation has been introduced to maximize the numerical efficiency and its accuracy is confirmed by our results. In addition to being more rigorous, another advantage of this approach is that the effects on the input impedance of the finite size ground planes can accurately be evaluated and moreover scattering from ground plane edges can be taken into account. Thus full range (including backside scattering) radiation patterns can also be predicted.

2 BACKGROUND AND STATEMENT OF THE PROBLEM

The new excitation model presented in this paper has been developed in the frame of the analysis of multilayered printed circuits and antennas following the MPIE formulation [Mosig and Gardiol 1988]. The generic structure under analysis is presented in Fig. 1. As shown, it is composed by one or more conducting patches embedded on a stratified medium. Either a perfect conductor ground plane or a free space layer extending to $z = -\infty$ can be placed at the bottom of the structure. Each dielectric layer, which may be lossy, is assumed to be homogeneous, isotropic and transversally infinite. The conducting patches are assumed to have finite transverse size, arbitrary shape, negligible thickness and an infinite conductivity, although finite conductivity can easily be taken into account using Leontovich boundary conditions [Mosig and Gardiol 1985].

Under these assumptions the boundary condition for the electric field on the surface of the conducting strips is written as

$$\hat{e}_z \times (\vec{E}^e + \vec{E}^s) = 0 \tag{1}$$

where $\vec{E}^e$ and $\vec{E}^s$ are respectively the excitation and the scattered electric field.

The scattered field is expressed in terms of the vector and scalar potential $\vec{A}$ and V as

$$\vec{E}^s = -j\omega\vec{A} - \nabla V \qquad \vec{H} = \frac{1}{\mu}\nabla \times \vec{A} \tag{2}$$

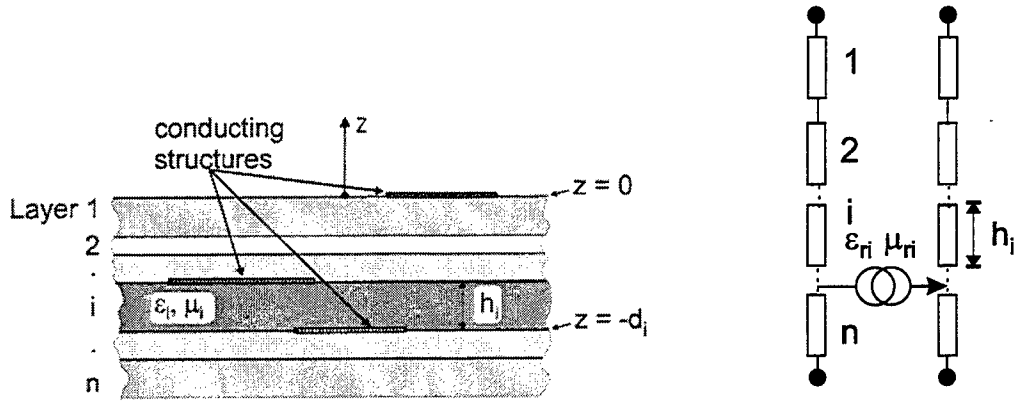

(a) Multilayered medium. **(b)** Equivalent network.

Figure 1: Generic multilayered structure containing an arbitrary number of finite metallizations.

with the potentials related by the Lorentz gauge [Mosig 1989]

$$j\omega\mu\epsilon V + \nabla \bullet \vec{A} = 0 \tag{3}$$

The vector and scalar potentials $\vec{A}, V$ can in turn be expressed in terms of superposition integrals of the corresponding Green's functions $\overline{\overline{G}}_A, G_V$ weighted by the unknown distribution of surface current and electric charge $\vec{J}_s, \rho_s$ as

$$\begin{aligned} \vec{A} &= \int_S \overline{\overline{G}}_A(r|r') \bullet \vec{J}_s(r')\, dS' \\ V &= \int_S G_V(r|r')\, \rho_s(r')\, dS' \end{aligned} \tag{4}$$

and finally, using the continuity equation to express the electric charge in terms of current, the boundary condition in equation (1) becomes

$$\begin{aligned} \hat{e}_z \times \vec{E}^e &= \hat{e}_z \times \left(j\omega \int_S \overline{\overline{G}}_A(r|r') \bullet \vec{J}_s(r')\, dS' \right. \\ &+ \left. \frac{1}{j\omega} \nabla \int_S G_V(r|r')\, \nabla \bullet \vec{J}_s(r')\, dS' \right) \end{aligned} \tag{5}$$

which is the basic integral equation to be solved to find the unknown distribution of surface currents.

The multilayered media Green's functions appearing in equation (5) are derived, in the spectral domain, from the equivalent transmission line circuit shown in Fig. 1(b), as described in [Mosig and Gardiol 1988, Michalski and Mosig 1997]. Furthermore, these Green's functions are calculated in the spatial domain using special numerical methods for the evaluation of the Sommerfeld integral, as extensively described in [Mosig 1989, Alvarez-Melcon and Mosig 1996].

The previous integral equation (5) is solved by the Method of Moments. The conducting patches are segmented into triangular cells and triangular rooftops [Rao *et al.* 1982] are used as basis and test functions, applying a Galerkin method. If coaxial excitation is used, modified basis functions are introduced at the coaxial pin location in order to model the spread on the patch of the current flowing on the vertical pin.

3 A NEW ATTACHMENT MODE

A special set of basis functions, called the attachment mode, is used to ensure the continuity of the current between the coaxial probe and the antenna. In the present approach the attachment mode is derived directly from the delta-gap voltage excitation model used on microstrip lines [Eleftheriades and Mosig 1996]. As shown in fig. 2 an efficient excitation model is obtained for the microstrip case applying a voltage source of magnitude V_m between an infinitesimally small gap of length $\delta \rightarrow 0$ across the feeding line and the ground plane. The flow of induced currents through the edge of the microstrip line is modeled introducing one or more half subsectional basis functions (half rooftop in the present case) as shown in Figs. 2a, 2c, and 2d [Eleftheriades and Mosig 1996].

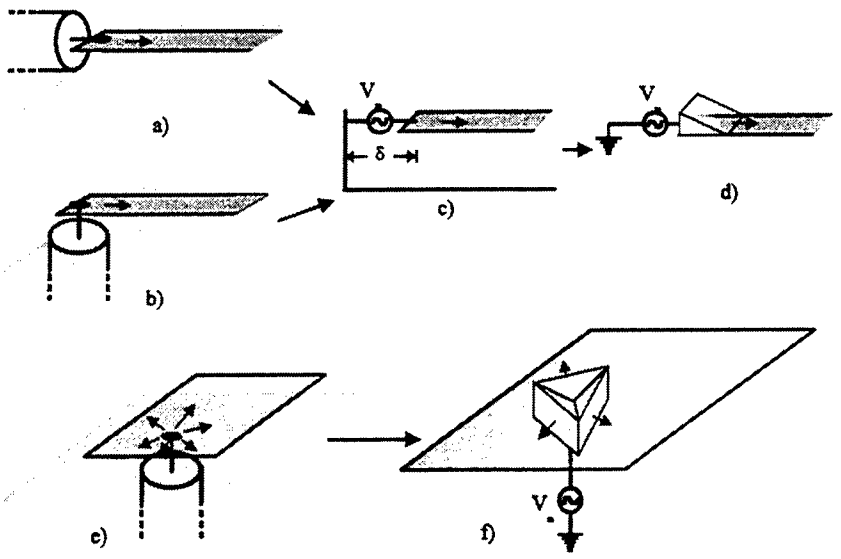

Figure 2: A delta-gap voltage source exciting printed circuits. a) Colinear transition between a coaxial probe and a microstrip line. b) perpendicular transition between a coaxial probe and a microstrip line. c) Delta-Gap voltage model applyed to a coaxial probe-fed microstrip line. d) Associated MoM description of the excitation model. e) Coaxial probe-fed patch antenna. f) Associated MoM description of the of the excitation of a probe-fed patch antenna

It is well known that at least for electrically thin dielectrics, no difference in the measurement can be noticed when the microstrip line is fed by a vertical coaxial probe (Fig. 2b), so it can be affirmed that the previous delta-gap excitation model is still valid in this case. The next step is to apply the same method to a point located inside the patch (see Fig. 2e) having in mind that current can spread in any direction. This behaviour can be obtained introducing 3 (or less if the feed is close to the edge) new half rooftops, one for each edge of the triangle containing the feeding point, which are superimposed to the halves of the standard rooftops already attached to the triangle (see Fig. 2f). It must be stressed that at this point six half rooftops (one couple for each side) are present in the triangle, but only three of them are involved in the attachment mode and they are attached to three virtual vertical half rooftops, while the other three are connected to the halves located in the adjacent triangles to form standard "planar" basis function. It is also important to point out that to reach a good model of the physical excitation, the area of the triangle with the attachment mode must be reasonably small, the lower limit being imposed by the section of the internal conductor of the coaxial cable.

The application of the Method of Moments (MoM) to solve the integral equation (5) leads to a system of linear equations that can be shortly expressed as

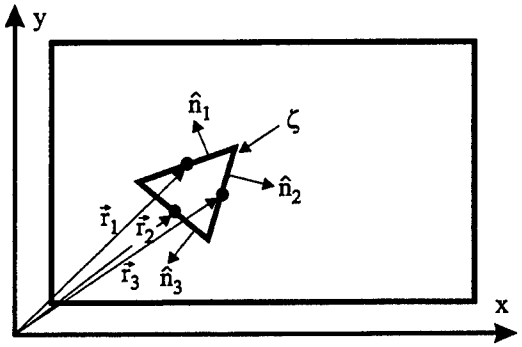

Figure 3: Basic geometry of a probe-fed printed antenna used in the formulation of the excitation model.

$$e_i = \sum_{k=1}^{N_f} \alpha_k \, P_{i,k} \, , \qquad i = 1, 2, \cdots, N_f \tag{6}$$

where $P_{i,k}$ is the i,k-th term of the moments matrix, α_k is the k-th term of the unknown electric current density vector, N_f is the total number of basis functions and e_i is the i-th term of the excitations vector. The latter is defined as

$$e_i = \int_S \vec{E}^e \bullet \vec{f}_i(\vec{r}) \, ds \tag{7}$$

where $\vec{E}^e$ represents the impressed electric field, and $f_i(\vec{r})$ is the subsectional testing functions of the MoM. The un-

knowns electric currents can now be expanded as

$$\vec{J}_s = \sum_{k=1}^{N_f} \alpha_k \, \vec{f}_k(\vec{r}') \tag{8}$$

where N_f is the total number of basis functions, and α_k are the unknown coefficients in the expansion.

With reference to the port geometry shown in Fig. 3, we apply the delta-gap model only to the three "half" basis functions of the attachment mode, which allows us to write the excitation field created by the voltage source as

$$\vec{E}^e = V_m \sum_{p=1}^{3} \delta(\vec{r} - \vec{r}_p) \, \hat{n}_p \tag{9}$$

where $\vec{r}_p$, $p = 1, 2, 3$, denotes the position vector of the three edge associated to the port. Substituting equation (9) in equation (7) we obtain

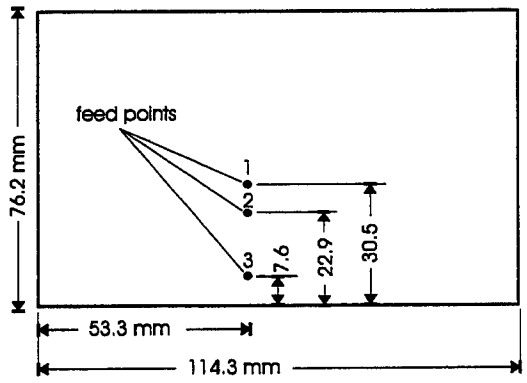

Figure 4: Probe-fed patch antenna on an infinite ground plane. Substrate: REXOLITE 2200, $h = 1.59$ mm, $\varepsilon_r = 2.62$, $tan\delta \approx 0.002$.

$$e_i = V_m \int_S \left[\sum_{p=1}^{3} \delta(\vec{r} - \vec{r}_p) \, \hat{n}_p \bullet \vec{f}_i(\vec{r}) \right] ds \tag{10}$$

Using the integration properties of the Dirac delta function and defining $\vec{f}_i^{\hat{n}_p}(\vec{r}) = \hat{n}_p \bullet \vec{f}_i(\vec{r})$ as the component of the basis function perpendicular to p-th triangle's edge, equation (10) reduces to

$$e_i = V_m \oint_\zeta \left[\sum_{p=1}^{3} f_i^{\hat{n}_p}(\vec{r}_p) \right] dl \tag{11}$$

where ζ is the perimeter of the triangle with the attachment mode (see Fig. 3). Defining now

$$\gamma_i = \oint_\zeta \left[\sum_{p=1}^{3} f_i^{\hat{n}_p}(\vec{r}_p) \right] dl \tag{12}$$

which is an integral with an easily obtained analytical solution, we can introduce (11) in (6) and obtain the following system of linear equations

$$V_m \, \gamma_i = \sum_{k=1}^{N_f} \alpha_k \, P_{i,k} \, , \qquad i = 1, 2, \cdots, N_f \tag{13}$$

The solution of this system of linear equations gives the

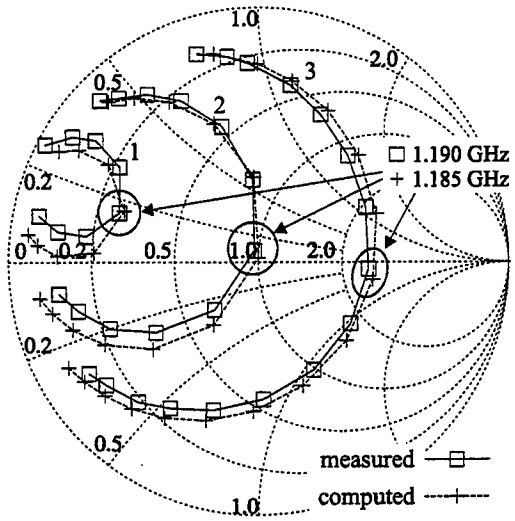

Figure 5: Comparison of measured and computed results of the input impedance of the antenna in Fig. 4. □ measure, + theory. (increment 5 MHz clockwise, measurement reproduced from [James and Hall 1989])

values of the unknown coefficients α_k. These can then be used to compute the current I_m flowing through the port as follows

$$\begin{aligned} I_m &= \oint_\zeta \left[\sum_{p=1}^{3} \vec{J}_s(\vec{r}_p) \bullet (\hat{n}_p) \right] dl \\ &= \sum_{k=1}^{N_f} \alpha_k \oint_\zeta \left[\sum_{p=1}^{3} f_k^{\hat{n}_p}(\vec{r}_p) \right] dl \\ &= \sum_{k=1}^{N_f} \alpha_k \, \gamma_k \end{aligned} \tag{14}$$

From equation (14) the input impedance of the circuit is directly obtained by dividing both the terms of the equation by the exciting voltage V_m, and then by inverting the resulting input admittance, namely:

$$Z_{in} = \frac{1}{Y_{in}} \qquad Y_{in} = \frac{I_m}{V_m} = \sum_{k=1}^{N_f} \frac{\alpha_k \, \gamma_i}{V_m} \tag{15}$$

To verify the validity of the derived model we have analysed the basic probe-fed printed patch antenna presented in [James and Hall 1989]. For simplicity the geometry of the antenna is reported in Fig. 4. The input impedance of the antenna has been measured for the fundamental (TM_{10}) mode and for three different placements of the feed (see Fig. 4). The comparison between the measurement and the computed results, presented in fig. 5, show the accuracy achieved with the present model.

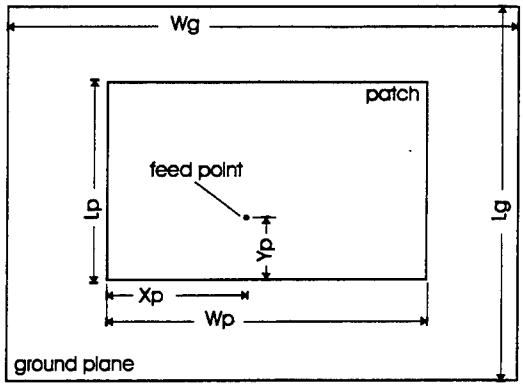

Figure 6: Probe-fed patch antenna on an finite size ground plane.

4 ANALYSIS OF PROBE-FED PATCH ANTENNAS ON FINITE SIZE GROUND PLANES

In this section we describe how the excitation model presented in the previous section must be modified in order to take into account the finiteness of the ground plane. The study is presented for a simple printed patch antenna, but the extension to more complicated structure is straightforward. An important difference between the analysis presented in the present paper and traditional analysis like the one performed in the previous section (see also [Bunger and Arndt 1997]), is that in the present case the Green's functions derived do not take into account infinite ground planes, and therefore, all metallizations are considered to be finite. The main difficulty in doing this is that the condition of null potential at the ground plane is not automatically imposed by the Green's functions. As a consequence, now the finite ground plane must be introduced inside the integral equation to enforce the proper boundary conditions on it, and the currents induced on this reference ground plane must also be computed. Also, a new excitation model and de-embedding technique must be derived to be able to extract the actual input impedance of the antenna when such floating grounds are considered as references. This is mainly due to the fact that the ground plane is no longer acting as an automatic reference plane for the generator, so that the reference condition of the finite ground plane must be introduced explicitly in the model.

The advantages of such finite ground plane models are clear. First, the effects of a finite size ground plane on the input impedance of antennas can be accurately taken into account. Secondly, the diffraction of the radiated field on the edges of finite size ground planes can also be studied. This will give an idea of the back-radiation of microstrip antennas, including the side-lobe levels which might be expected in their radiation patterns. Both elements are of key importance in the design of antennas, and up to now they could only be evaluated through measurements, or with lengthy numerical calculations using techniques such as the finite elements or the finite differences [Ciampolini *et al.* 1996].

Let us now consider the basic microstrip antenna with finite size ground plane represented in Fig. 6. Opposite to the case of an infinite ground plane, where the excitation is injected only through the patch while the ground plane is included in the Green's functions, the model must be modified in the finite ground case so that the finite ground plane is connected to the generator and surface currents must be free to flow through this connection. This is obtained by using a "mirror" attachment model in the ground plane with the sign of the currents reversed. Also, the potential of the ground plane is set to zero by means of a numerical treatment acting on the MPIE formulation. Fig. 7 presents the basic idea of the extended attachment mode. If we take again the case of a transition from a coaxial cable to a microstrip line, but where the size of the microstrip's ground plane is now finite (Fig. 7a), the equivalent excitation model can be represented with a voltage generator connected to the microstrip line as in the previous case, but with the grounded terminal now connected to the physical ground plane (Fig. 7b). As depicted in the figure, the currents flowing through the two terminals of the generator must be the same. Therefore the same "spreading" behavior of the current must be imposed in both the microstrip patch and the ground plane. This behaviour can be obtained in the MoM implementation by introducing one half basis function on the ground

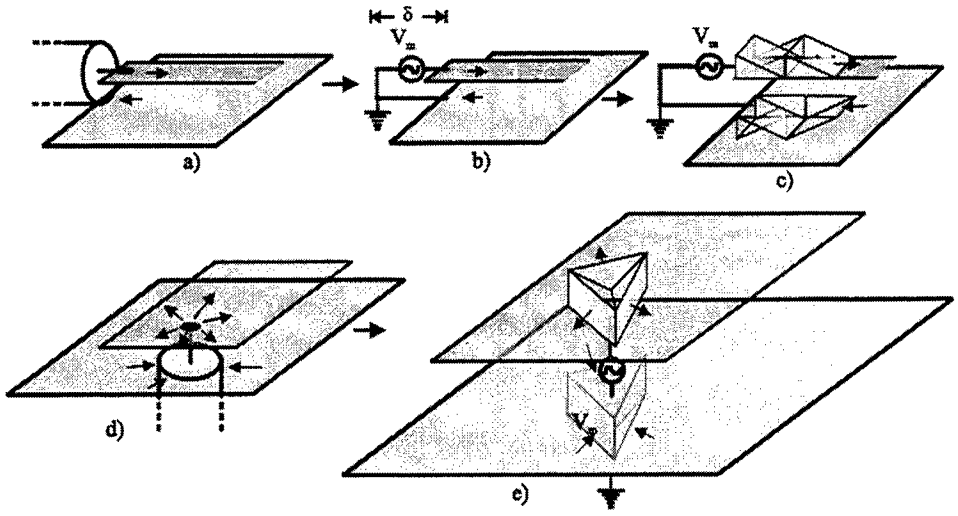

Figure 7: Attachment mode for patch antennas on finite ground planes. a) Colinear transition between a coaxial probe and a microstrip line. b) Delta-Gap voltage model applyed to a coaxial probe-fed microstrip line. c) Associated MoM description of the excitation model. d) Coaxial probe-fed patch antenna. e) Associated MoM description of the of the excitation of a probe-fed patch antenna

plane for each of these present in the microstrip and linking the two halves together to form an entire basis function (see Fig. 7c), i.e. only one unknown term for each couple is present in the MoM matrix [Tiezzi *et al.* 1999]. This implies that the free edges of the two half basis function must have the same length. Applying now the same scheme to the probe-fed patch antenna represented in Fig. 7d, starting from the attachment mode sketched in Fig. 2e, we obtain the new attachment mode composed by three (or less) half basis functions on the patch and the same number of half basis functions with opposite sign on the ground plane.

To demonstrate the effectiveness of the derived model, the antenna in Fig. 4 has been simulated with a ground plane of width $W_g = 214\ mm$ and length $L_g = 214\ mm$ for again three position of the coaxial excitation. The agreement between theory and measurement (Fig. 8)is rather good. Indeed our model can work for any size of ground plane from the completely unbalanced antenna (infinite ground plane) to a perfectly balanced antenna (ground plane having the patch's size). The latter case has been tested for an antenna on a RT/DUROID 5870 substrate with thickness $h = 1.57$ mm and relative dielectric constant $\varepsilon_r = 2.33$. With respect to Fig. 6 the dimensions of the antenna are $W_p = W_g = 120.1$ mm, $L_p = L_g = 79.5$ mm, $X_p = 60$ mm, $Y_p = 29$ mm. The results are presented in Fig. 9. The agreement between measured and computed results is ex-

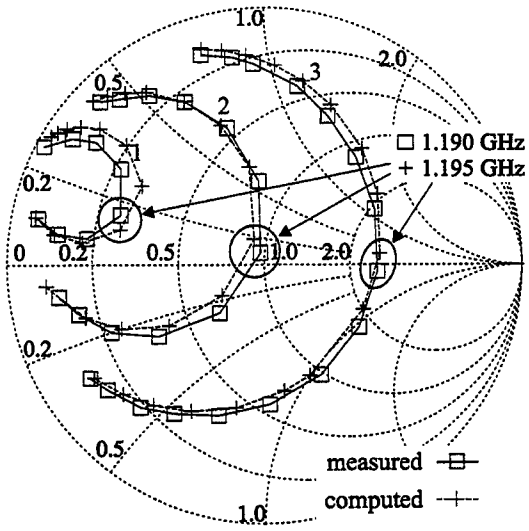

Figure 8: Measured versus simulated results for the patch antenna shown in Fig. 4, when the new excitation model is used: $W_g = 214$ mm, $L_g = 214$ mm. (increment 5 MHz clockwise, measurement reproduced from [James and Hall 1989])

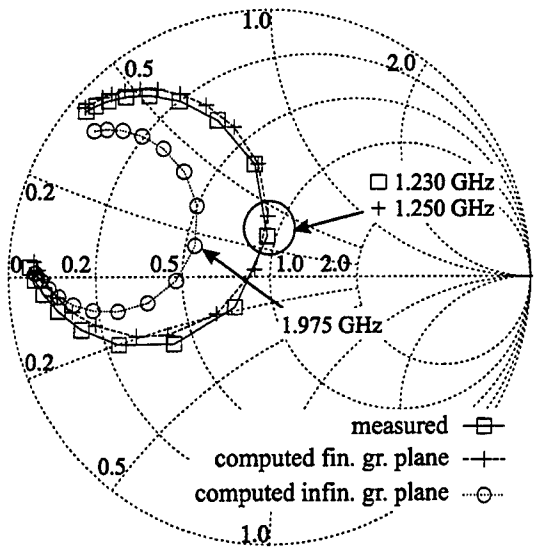

Figure 9: Measured versus simulated results for a perfectly balanced patch antenna: $W_p = W_g = 120.1$ mm, $L_p = L_g = 79.5$ mm, $L_p = L_g = 80$ mm, $X_p = 60$ mm, $Y_p = 29$ mm. Substrate: RT/DUROID 5870, $h = 1.57$ mm, $\varepsilon_r = 2.33$, $tan\delta = 0.0012$. (increment 2.5 MHz clockwise)

cellent. As a matter of comparison, the result obtained using the infinite ground plane model has also been included and it show that in this extreme case the infinite ground plane approximation is definitely too rough.

4.1 RADIATION PATTERNS

Another interesting aspect of the excitation model derived in this paper is the prediction of the back radiation and the side lobe levels of microstrip printed antennas. In the present work the far field radiated by the structure has been computed with the aid of asymptotic expressions for the multilayered media Green's functions, valid for large values of source-observer distances. These asymptotic expressions are based on the use of the saddle point method, which allows the analytical evaluation of a Fourier integral by just considering the contribution of the function at the saddle point [Mosig and Gardiol 1982]. It is important to have in mind that in a multilayered medium, horizontal currents can in general produce both horizontal and longitudinal (along z) components of the electromagnetic fields. This comes from the fact that the dyad associated with the magnetic vector potential is not a diagonal dyad, but it rather contains off diagonal elements. For instance, if the so called Sommerfeld choice is selected, then the whole magnetic vector potential dyad can be written, for only horizontal currents, as [Mosig and Gardiol 1985, Mosig 1989]

$$\begin{aligned}\overline{\overline{G}}_A &= \left(\hat{e}_x\, G_A^{xx} + \hat{e}_z\, G_A^{zx}\right)\hat{e}_x \\ &\quad + \left(\hat{e}_y\, G_A^{yy} + \hat{e}_z\, G_A^{zy}\right)\hat{e}_y \end{aligned} \qquad (16)$$

where, as already said, the spectral domain Green's functions appearing in equation (16) are derived from voltages and currents computed in the equivalent transmission line network of Fig. 1(b), as described in [Mosig and Gardiol 1988, Michalski and Mosig 1997]. For the Green's functions of interest in (16) one obtains [Michalski and Mosig 1997]

$$\begin{aligned}\tilde{G}_A^{xx} &= \tilde{G}_A^{yy} = \frac{V_j^{TE}}{j\,\omega}, \\ \tilde{G}_A^{zx} &= -\frac{\mu}{k_\rho^2} j\, k_x \left(I_j^{TM} - I_j^{TE}\right), \\ \tilde{G}_A^{zy} &= -\frac{\mu}{k_\rho^2} j\, k_y \left(I_j^{TM} - I_j^{TE}\right), \end{aligned} \qquad (17)$$

where TE, TM denotes transverse electric and transverse magnetic (with respect to the z-axis) waves, and the transverse wavenumbers are given by [Mosig and Gardiol 1982]: $k_\rho = k_0 \sin\theta$, $k_x = -k_0 \sin\theta\, \cos\varphi$, $k_y = -k_0 \sin\theta\, \sin\varphi$.

The main difficulty is then reduced to the calculation of these Green's functions in the spatial domain. For this purpose the inverse Fourier integral is evaluated with the saddle point technique, and, as shown in [Mosig and Gardiol 1982], one finally obtains in the spatial domain the following simple relation

$$G_A^{st} = j\, k_0\, \cos(\theta)\, \tilde{G}_A^{st}\, \frac{\exp(-j\, k_0\, R)}{R} \qquad (18)$$

where $s, t = x, y, z$, and R is the source-observer distance. It is important to remark that for the derivation of equation (18) the spectral domain Green's functions are assumed to have a free space dependence of the type: $\exp(-j\,\beta\, z)$. The main implication of this is that the voltages and currents in equation (17) must be computed at the first air-dielectric interface for: $0 < \theta < \pi/2$, and they must be computed at the last air-dielectric interface for: $\pi/2 < \theta < \pi$. Having all these computational details in mind, an accurate evaluation of the radiation patterns of microstrip antennas printed on finite size ground planes has been carried out. Figs. 10, 11 and 12. present the measured and computed results

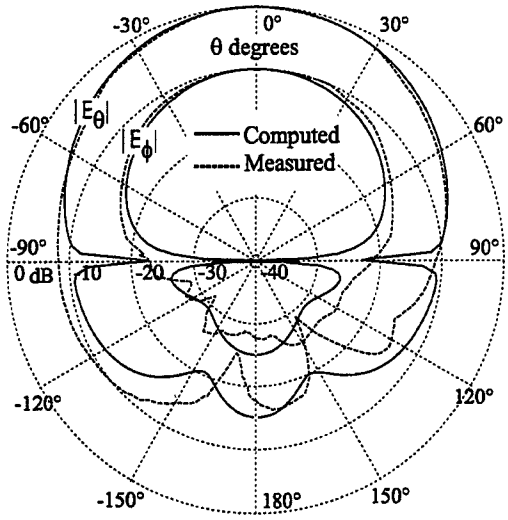

(a) E-plane.

Figure 10: Radiation patterns of the printed patch antenna shown in Fig. 4. Ground plane size: $W_g = 60$ mm, $L_g = 60$ mm. Frequency is 5.020 GHz. (measurement reproduced from [Bokhari *et al.* 1992])

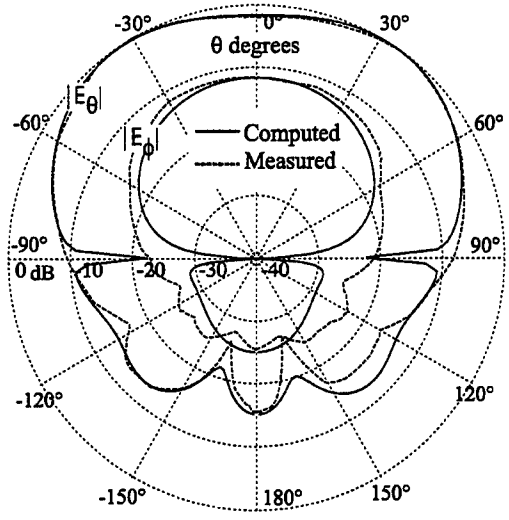

(a) E-plane.

Figure 11: Radiation patterns of the printed patch antenna shown in Fig. 4. Ground plane size: $W_g = 90$ mm, $L_g = 90$ mm. Frequency is 5.020 GHz. (measurement reproduced from [Bokhari *et al.* 1992])

for the E and H-plane radiation patterns of the antenna shown in Fig. 4 with ground plane size: $W_g = 60\ mm$, $L_g = 60\ mm$, $W_g = 90\ mm$ $L_g = 90\ mm$ and $W_g = 180\ mm$ $L_g = 180\ mm$ (respectively $\lambda_0 \times \lambda_0$, $1.5\lambda_0 \times 1.5\lambda_0$ and $3\lambda_0 \times 3\lambda_0$ at 5.02 GHz). The results presented indicate that the agreement is good, and in particular the predicted level of back radiation is approximately the measured one. It is important to mention that a model using an infinite ground plane gives no information concerning the level of back radiation of the antenna, which is assumed to be zero. On the contrary, with the new excitation model derived in this paper, an accurate estimation of the back radiation level can be obtained. It must be also pointed out that the present model still uses layered Green's functions and doesn't include neither the radiation of the probe itself nor the effect of the dielectric layer finiteness.

These two aspects of the problem could also be included in the model by means of respectively, vertical conduction and polarisation currents and work towards this goal is in progress. However the results of figures 10-12 shows clearly that the only noticeable improvement would be the filling of the deep nulls at $\pm 90°$ and that except for this minor correction, our model in its current status follows closely the measured values, while still retaining a reasonable simplicity which would be lost if the aforementioned effects are included.

5 CONCLUSION

A new excitation model for coaxially fed printed microstrip antennas, developed in the frame of the mixed potential integral equation (MPIE) and the method of moments (MoM), has been presented. Moreover, a modified version of this model allows the analysis of these antennas on finite size ground planes. This model has been successfully applied to the prediction of input impedances for patches above ground planes whose size ranges from the patch size to infinity. With this approach, scattering from ground plane edges can be taken into account and full range (including backside scattering) radiation patterns can also be predicted. The paper has first presented the theoretical basis of the new derived excitation method, including the numerical details needed for a correct far field computation. Theoretical results have been compared with measurements, for both the input impedance and the radiation patterns. Comparisons have revealed that the accuracy achieved with the new ex-

citation method is very satisfactory, and in particular the backside radiation and side lobe levels of real life printed antennas can accurately be predicted.

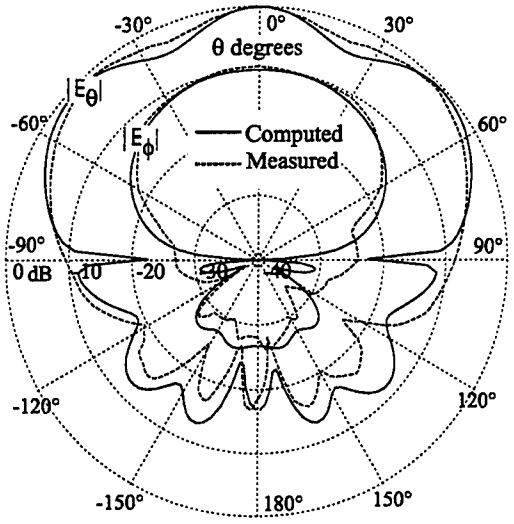

(a) E-plane.

Figure 12: Radiation patterns of the printed patch antenna shown in Fig. 4. Ground plane size: $W_g = 180$ mm, $L_g = 180$ mm. Frequency is 5.020 GHz. (measurement reproduced from [Bokhari *et al.* 1992])

References

[Alvarez-Melcon and Mosig 1996] A. Alvarez-Melcon and Juan R. Mosig, "Green's Functions in Layered Media: Imaginary Axis and Asymptotic Behavior", *AP-S International Symposium on Antennas*, (Baltimore, Maryland, USA), pp. 416-419, IEEE AP-S, 21-26 July 1996.

[Balanis 1982] Constantine A. Balanis, *Antenna Theory Analysis and Design*, New York: John Wiley & Sons 1982.

[Bokhari *et al.* 1992] S. A. Bokhari and J. R. Mosig and F. E. Gardiol, "Radiation Pattern Computation of Microstrip Antennas on Finite Size Ground Planes", *IEE Proceedings*, vol. 139, Pt. H, No. 3, pp. 278-286, June 1992.

[Zürcher *et al.* 1999] J-F. Zürcher, Quin Xu, J.R. Mosig and A.K. Skrivervik, "Dual-frequency, dual-polarisation four-port printed planar antennas", *Microwave and Optical Technology Letters*, vol. 23, No. 2, pp. 75-78, Oct. 20, 1999.

[Bunger and Arndt 1997] Rainer Bunger and Fritz Arndt, "Efficient MPIE Approach for the Analysis of Three-Dimensional Microstrip Structures in Layered Media", *IEEE Trans. Microwave Theory Tech.*, vol. MTT-45, No. 8, pp. 1141-1153, Aug. 1997.

[Ciampolini *et al.* 1996] P. Ciampolini, P. Mezzanotte, L. Roselli and R. Sorrentino, "Accurate and Efficient Circuit Simulation with Lumped-Elements FDTD Technique", *IEEE Trans. Microwave Theory Tech.*, vol. MTT-44, No. 12, pp. 2207-2215, Dec. 1996.

[Davidovitz and Lo 1989] M. Davidovitz and Y. T. Lo, "Rigorous Analysis of a Circular Patch Antenna Excited by a Microstrip Transmission Line", *IEEE Trans. Microwave Theory Tech.*, vol. MTT-37, No. 8, pp. 949-958, Aug. 1989.

[Eleftheriades and Mosig 1996] G. V. Eleftheriades and J. R. Mosig, "On the Network Characterization of Planar Passive Circuits Using the Method of Moments", *IEEE Trans. Microwave Theory Tech.*, vol. MTT-44, No. 4, pp. 438-445, Mar. 1996.

[Hall and Mosig 1989] R. C.Hall and J. R. Mosig, "The Analysis of Coaxially fed Microstrip Antennas with Electrically Thick Substrates", *Electromagnetics*, vol. 9, pp. 367-384, 1989.

[Hall and Mosig 1996] R. C.Hall and J. R. Mosig, "The Analysis of Arbitrarily Shaped Aperture-Coupled Patch Antennas Via a Mixed-Potential Integral Equation", *IEEE Trans. Antennas Propagat.*, vol. AP-44, No. 5, pp. 608-614, May 1996.

[Harokopus and Katehi 1991] W. P. Harokopus and L. B. Katehi, "Electromagnetic Coupling and Radiation Loss Considerations in Microstrip (M)MIC Design", *IEEE Trans. Microwave Theory Tech.*, vol. MTT-39, No. 3, pp. 413-421, Mar. 1991.

[James and Hall 1989] J. R. James and P. S. Hall, *Handbook of Microstrip Antennas*. London, UK, Peter Peregrinus Ltd., 1989

[Michalski and Mosig 1997] Krzysztof A. Michalski and Juan R. Mosig, "Multilayered Media Green's Functions in Integral Equation Formulations", *IEEE Trans. Antennas Propagat.*, vol. AP-45, No. 3, pp. 508-519, Mar. 1997.

[Mosig 1989] Juan R. Mosig, *Integral Equation Techniques*, ch. 3 in: Numerical Techniques for Microwave and Millimeter-Waves Passive Structures, pp. 133-213. New York, USA: T. Itoh, ed. John Wiley and Sons, 1989.

[Mosig and Gardiol 1982] Juan R. Mosig and Fred E. Gardiol, *A Dynamical Radiation Model for Microstrip Structures*, ch. 3 in: Advances in Electronics and Electron Physics, vol. 59, pp. 139-237. New York, USA: Peter W. Hawkes, Academic Press, 1982.

[Mosig and Gardiol 1985] Juan R. Mosig and Fred E. Gardiol, "General Integral Equation Formulation for Microstrip Antennas and Scatterers", *IEE Proceedings*, vol. 132, Pt. H, No. 7, pp. 424-432, Dec. 1985.

[Mosig and Gardiol 1988] Juan R. Mosig and Fred E. Gardiol, "Integral Equation Techniques for the Analysis of Microstrip Discontinuities", *ALTA FREQUENZA*, vol. LVII, pp. 171-181, June 1988.

[Pozar 1982] David M. Pozar, "Radiation Pattern Computation of Microstrip Antennas on Finite Size Ground Planes", *IEEE Trans. Antennas Propagat.*, vol. 30, No. 6, pp. 1191-1196, Nov. 1982.

[Rao *et al.* 1982] S. M. Rao, D. R. Wilton and A. W. Glisson, "Electromagnetic Scattering by Surface of Arbitrary Shape", *IEEE Trans. Antennas Propagat.*, vol. AP-30, No. 3, pp. 409-418, May 1982.

[Tiezzi *et al.* 1999] F. Tiezzi, A. Alvarez-Melcon and J. R. Mosig, "A new Excitation Model for Microstrip Antennas on Finite Size Ground Planes", *AP-2000 Millennium Conference on Antennas and Propagation Proceedings*, to be published, Davos, Switzerland, Apr. 2000.

2000 INSTITUTIONAL MEMBERS

ADVANSIS, INC.
20370 Town Center
Cupertinb, CA 95014

ALGON MOBILE COMM.
Nasvagen 17
Akersberga, SWEDEN S-18425

ANDREW CORPORATION
10500 W. 153rd Street
Orland Park, IL 60462

AUSTRALIAN DEFENCE LIB.
Northcott Drive
Campbell, A.C.T. AUSTRALIA 2600

BAE SYSTEMS
Gunnelswood Road
Stevenage, HERTS, UK SG1 2DB

BOEING CO, RENTON TECH LIB
PO Box 3707
Seattle, WA 98124-2207

BOEING NORTH AMERICAN SVCS
1745 Jefferson Davis Hwy
Arlington, VA 22202

BPLUS
100 University Court, PO B 1428
Blackwood, NJ 08012

BRITISH AEROSPACE
Newport Road
Isle of Wight, PO 318 PF UK

BRITISH AEROSPACE
FPC 267 PO Box 5
Filton, BRISTOL, BS12 7QW UK

CENTER HP COMPUTING
PO Box 830657
Birmingham, AL 35283-0657

CHALMERS UNIV of TECHNOLOGY
Dept of Microwave Technology
Gothenburg, SWEDEN S 41296

CHIHUAHUA UNIVERSITY
P.O. Box 830657
Birmingham, AL 35283-0657

CST GMBH
Lauteschlagerstrasse 38
Darmstadt, GERMANY D-64289

CULHAM SCIENCE LAB
UK Atomic Energy Authority
Abingdon, OXFORD, OX14 3DB UK

DARTMOUTH COLLEGE
Feldberg Library
6193 Murdough Ctr.
Hanover, NH 03755-3560

DEFENCE TECH & PROCUREMNT
NEMP LAB
SPIEZ, SWITZERLAND CH 3700

DEFENSE RESEARCH ESTAB. LIB.
3701 Carling Avenue
Ottowa, ON, K1A 0Z4 CANADA

DEUTSCHE TELEKOM AG
PO Box 10-00-03
Darmstadt, D-64 276 GERMANY

EASTWOOD BOOKS
3250 Wilshire Blvd
Los Angeles, CA 90010

ELECTRICAL COMM LIBRARY
1-1 Hikarinooka
Kanagawa, Ken, 239-0847 JAPAN

ERA TECHNOLOGY
Cleve Road
Leatherhead, SU, UK KT22 7SA

ERICSSON SAAB
Gelbgjutaregat
Linkoping, SWEDEN SE 58188

FACOLTA INGEGNERIA
Library, Via G Duranti 89
Perugia, ITALY 06125

FANFIELD LTD
Braxted Park
Witham, Essex, CM8 3XB UK

FUNDACAO CPqD, BIBLIOTECA
Rod. Campinas M
Campinas, SP, BRAZIL 13083-970

GEC MARCONI RES. CTR. LIB.
W. Hanningfield Road, Gt. Baddow
Chelmsford, ESSEX, CM2 8HN UK

HARRIS CORP
1680 University Avenue
Rochester, NY 14610-9983

HKUST, UNIVERSITY LIBRARY
Clear Water Bay Road
Kowloon, HONG KONG

HUNTING ENGINEERING LTD.
Reddings Wood, Ampthill
Bedford, MK45 2HD UK

IABG MBH
Einsteinstrasse
Ottobrunn, GERMANY D-85521

IIT RESEARCH INSTITUTE
185 Admiral Cochrane Drive
Annapolis, MD 21401-7396

IMAGINEERING LTD.
1090 Don Mills Road
Toronto, M3C 3R6, CANADA

IPS RADIO & SPACE SVC/LIBRARY
PO Box 5606
W. Chatswood, 2057 AUSTRALIA

KATHREIN-WERKE
PO Box 100 444
Rosenheim, D-83004 GERMANY

LINDA HALL LIBRARY
5109 Cherry Street
Kansas City, MO 64110-2498

MISSISSIPPI STATE UNIV LIBRARY
PO Box 9570
Mississippi State, MS 39762

MIT LINCOLN LAB LIBRARY
244 Wood Street
Lexington, MA 02173-0073

MITRE CORPORATION LIBRARY
202 Burlington Road
Bedford, MA 01730-1407

MYERS ENGINEERING INTL.
PO Box 15908, 5425 NW 24th St.
Margate, FL 33063

NATIONAL AEROSPACE LAB, NLR
Anthony Fokkerweg 2
Emmeloord, 8300 NETHERLANDS

NATL GROUND INTELLIGENCE
220 7th St. N.E.
Charlottesville, VA 22902-5307

NATL RADIOLOGICAL PROT. BD.
Chilton, Didcot, OXON,
OX11 0RG UK

NAVAL RESEARCH LABORATORY
C. Office
Washington, DC 20375

NEMP –LABOR SPIEZ LABS
Nemp Laboratory
Spiez, CH 3700 SWITZERLAND

NGIC
220 7th Street, NE
Charlottesville, VA 22902-5396

NNR AIR CARGO SERVICE
Hook Creed Blvd. & 145th Avenue
Valley Stream, NY 11581

NORTEL TECHNOLOGY
London Road
Harlow, ESSEX, CM17 9NA UK

PENN STATE UNIVERSITY LIB.
Pattee Library
University Park, PA 16802

PHILIPS RESEARCH LAB LIBRARY
Cross Oak Lane, Salfords
Redhill, SURREY, RH1 5HA UK

QUEEN MARY & WESTFIELD COLL
Mile End Road
London E1 4NS UK

QUEENSLAND CENTER, LIBRARY
2643 Moggill Road
Brisbane, Qld, 4069 AUSTRALIA

RADIO FREQUENCY
36 Garden Street
Kilsyth, VIC 3137 AUSTRALIA

RAND AFRIKAANS UNIVERSITY
PO Box 524, Aucklandpark
Johannesburg, 2006 S AFRICA

READMORE ACADEMIC SVCS.
LIBRARY
901 Route 168
Turnersville, NY 08012

SALISBURY DSTO
PO Box 830701
Birmingham, AL 35283-0701

SESTRA STRADA,CRS4
BIBLIOTECA
Casella Postale
Uta, ITALY 09010

SONY CORPORATION
174 Fujitsukacho, Hodogaya Ku
Yokohama MZ, 240 JAPAN

SOUTHWEST RESEARCH INST.
6220 Culebra Road
San Antonio, TX 78238

SPIKE TECH
1 Chestnut Street
Nashua, NH 03060

SWETS SUBSCRIPTION SERVICE
440 Creamery Way, Suite A
Exton, PA 19341

T NOVA DEUTSCHE
Am Kavalleriesa
Darmstadt, 64295 GERMANY

TECHNISCHE UNIV. DELFT
Mekelweg 4, Delft
HOLLAND, 2628 CD
NETHERLANDS

TELSTRA RES. LABS LIBRARY
770 Blackburn Road
Clayton, VIC, 3168 AUSTRALIA

UNIV OF CENTRAL FLORIDA LIB.
PO Box 162440
Orlando, FL 32816-2440

UNIVERSITY OF WARWICK
Gibbet Hill Road
Coventry, CV4 7AL UK

US ARMY COLD REGION RES, LIB.
72 Lyme Road
Hanover, NH 03775-1290

US COAST GUARD ACADEMY
15 Mohegan Avenue
New London, CT 06320-4195

VECTOR FIELDS LTD.
24 Bankside Kidlington
Oxford, OX5 1JE UK

VTT, TECHNICAL RESEARCH.
CTR.
PO Box 1202
Espoo, FIN-02044 FINLAND

ACES COPYRIGHT FORM

This form is intended for original, previously unpublished manuscripts submitted to ACES periodicals and conference publications. The signed form, appropriately completed, MUST ACCOMPANY any paper in order to be published by ACES. PLEASE READ REVERSE SIDE OF THIS FORM FOR FURTHER DETAILS.

TITLE OF PAPER:

AUTHORS(S)

PUBLICATION TITLE/DATE:

RETURN FORM TO:
Dr. Richard W. Adler
Naval Postgraduate School
Code EC/AB
833 Dyer Road, Room 437
Monterey, CA 93943-5121 USA

PART A - COPYRIGHT TRANSFER FORM

(NOTE: Company or other forms may not be substituted for this form. U.S. Government employees whose work is not subject to copyright may so certify by signing Part B below. Authors whose work is subject to Crown Copyright may sign Part C overleaf).

The undersigned, desiring to publish the above paper in a publication of ACES, hereby transfer their copyrights in the above paper to The Applied Computational Electromagnetics Society (ACES). The undersigned hereby represents and warrants that the paper is original and that he/she is the author of the paper or otherwise has the power and authority to make and execute this assignment.

Returned Rights: In return for these rights, ACES hereby grants to the above authors, and the employers for whom the work was performed, royalty-free permission to:

1. Retain all proprietary rights other than copyright, such as patent rights.
2. Reuse all or portions of the above paper in other works.
3. Reproduce, or have reproduced, the above paper for the author's personal use or for internal company use provided that (a) the source and ACES copyright are indicated, (b) the copies are not used in a way that implies ACES endorsement of a product or service of an employer, and (c) the copies per se are not offered for sale.
4. Make limited distribution of all or portions of the above paper prior to publication.
5. In the case of work performed under U.S. Government contract, ACES grants the U.S. Government royalty-free permission to reproduce all or portions of the above paper, and to authorize others to do so, for U.S. Government purposes only.

ACES Obligations: In exercising its rights under copyright, ACES will make all reasonable efforts to act in the interests of the authors and employers as well as in its own interest. In particular, ACES REQUIRES that:

1. The consent of the first-named author be sought as a condition in granting re-publication permission to others.
2. The consent of the undersigned employer be obtained as a condition in granting permission to others to reuse all or portions of the paper for promotion or marketing purposes.

In the event the above paper is not accepted and published by ACES or is withdrawn by the author(s) before acceptance by ACES, this agreement becomes null and void.

AUTHORIZED SIGNATURE — TITLE (IF NOT AUTHOR)

EMPLOYER FOR WHOM WORK WAS PERFORMED — DATE FORM SIGNED

PART B - U.S. GOVERNMENT EMPLOYEE CERTIFICATION

(NOTE: If your work was performed under Government contract but you are not a Government employee, sign transfer form above and see item 5 under Returned Rights).

This certifies that all authors of the above paper are employees of the U.S. Government and performed this work as part of their employment and that the paper is therefore not subject to U.S. copyright protection.

AUTHORIZED SIGNATURE — TITLE (IF NOT AUTHOR)

NAME OF GOVERNMENT ORGANIZATION — DATE FORM SIGNED

PART C - CROWN COPYRIGHT

(Note: ACES recognizes and will honor Crown Copyright as it does U.S. Copyright. It is understood that, in asserting Crown Copyright, ACES in no way diminishes its rights as publisher. Sign only if *ALL* authors are subject to Crown Copyright.

This certifies that all authors of the above Paper are subject to Crown Copyright. (Appropriate documentation and instructions regarding form of Crown Copyright notice may be attached).

AUTHORIZED SIGNATURE — TITLE OF SIGNEE

NAME OF GOVERNMENT BRANCH — DATE FORM SIGNED

Information to Authors

ACES POLICY

ACES distributes its technical publications throughout the world, and it may be necessary to translate and abstract its publications, and articles contained therein, for inclusion in various compendiums and similar publications, etc. When an article is submitted for publication by ACES, acceptance of the article implies that ACES has the rights to do all of the things it normally does with such an article.

In connection with its publishing activities, it is the policy of ACES to own the copyrights in its technical publications, and to the contributions contained therein, in order to protect the interests of ACES, its authors and their employers, and at the same time to facilitate the appropriate re-use of this material by others.

The new United States copyright law requires that the transfer of copyrights in each contribution from the author to ACES be confirmed in writing. It is therefore necessary that you execute either Part A-Copyright Transfer Form or Part B-U.S. Government Employee Certification or Part C-Crown Copyright on this sheet and return it to the Managing Editor (or person who supplied this sheet) as promptly as possible.

CLEARANCE OF PAPERS

ACES must of necessity assume that materials presented at its meetings or submitted to its publications is properly available for general dissemination to the audiences these activities are organized to serve. It is the responsibility of the authors, not ACES, to determine whether disclosure of their material requires the prior consent of other parties and if so, to obtain it. Furthermore, ACES must assume that, if an author uses within his/her article previously published and/or copyrighted material that permission has been obtained for such use and that any required credit lines, copyright notices, etc. are duly noted.

AUTHOR/COMPANY RIGHTS

If you are employed and you prepared your paper as a part of your job, the rights to your paper initially rest with your employer. In that case, when you sign the copyright form, we assume you are authorized to do so by your employer and that your employer has consented to all of the terms and conditions of this form. If not, it should be signed by someone so authorized.

NOTE RE RETURNED RIGHTS: Just as ACES now requires a signed copyright transfer form in order to do "business as usual", it is the intent of this form to return rights to the author and employer so that they too may do "business as usual". If further clarification is required, please contact: The Managing Editor, R.W. Adler, Naval Postgraduate School, Code EC/AB, Monterey, CA, 93943, USA (408)656-2352.

Please note that, although authors are permitted to re-use all or portions of their ACES copyrighted material in other works, this does not include granting third party requests for reprinting, republishing, or other types of re-use.

JOINT AUTHORSHIP

For jointly authored papers, only one signature is required, but we assume all authors have been advised and have consented to the terms of this form.

U.S. GOVERNMENT EMPLOYEES

Authors who are U.S. Government employees are not required to sign the Copyright Transfer Form (Part A), but any co-authors outside the Government are.

Part B of the form is to be used instead of Part A only if all authors are U.S. Government employees and prepared the paper as part of their job.

NOTE RE GOVERNMENT CONTRACT WORK: Authors whose work was performed under a U.S Government contract but who are not Government employees are required to sign Part A-Copyright Transfer Form. However, item 5 of the form returns reproduction rights to the U.S. Government when required, even though ACES copyright policy is in effect with respect to the reuse of material by the general public.

APPLIED COMPUTATIONAL ELECTROMAGNETICS SOCIETY JOURNAL

INFORMATION FOR AUTHORS

PUBLICATION CRITERIA

Each paper is required to manifest some relation to applied computational electromagnetics. **Papers may address general issues in applied computational electromagnetics, or they may focus on specific applications, techniques, codes, or computational issues.** While the following list is not exhaustive, each paper will generally relate to at least one of these areas:

1. Code validation. This is done using internal checks or experimental, analytical or other computational data. Measured data of potential utility to code validation efforts will also be considered for publication.

2. Code performance analysis. This usually involves identification of numerical accuracy or other limitations, solution convergence, numerical and physical modeling error, and parameter tradeoffs. However, it is also permissible to address issues such as ease-of-use, set-up time, run time, special outputs, or other special features.

3. Computational studies of basic physics. This involves using a code, algorithm, or computational technique to simulate reality in such a way that better or new physical insight or understanding is achieved.

4. New computational techniques, or new applications for existing computational techniques or codes.

5. "Tricks of the trade" in selecting and applying codes and techniques.

6. New codes, algorithms, code enhancement, and code fixes. This category is self-explanatory but includes significant changes to existing codes, such as applicability extensions, algorithm optimization, problem correction, limitation removal, or other performance improvement. **Note: Code (or algorithm) capability descriptions are not acceptable, unless they contain sufficient technical material to justify consideration.**

7. Code input/output issues. This normally involves innovations in input (such as input geometry standardization, automatic mesh generation, or computer-aided design) or in output (whether it be tabular, graphical, statistical, Fourier-transformed, or otherwise signal-processed). Material dealing with input/output database management, output interpretation, or other input/output issues will also be considered for publication.

8. Computer hardware issues. This is the category for analysis of hardware capabilities and limitations in meeting various types of electromagnetics computational requirements. Vector and parallel computational techniques and implementation are of particular interest.

Applications of interest include, but are not limited to, antennas (and their electromagnetic environments), networks, static fields, radar cross section, shielding, radiation hazards, biological effects, electromagnetic pulse (EMP), electromagnetic interference (EMI), electromagnetic compatibility (EMC), power transmission, charge transport, dielectric and magnetic materials, microwave components, MMIC technology, remote sensing and geophysics, communications systems, fiber optics, plasmas, particle accelerators, generators and motors, electromagnetic wave propagation, non-destructive evaluation, eddy currents, and inverse scattering.

Techniques of interest include frequency-domain and time-domain techniques, integral equation and differential equation techniques, diffraction theories, physical optics, moment methods, finite differences and finite element techniques, modal expansions, perturbation methods, and hybrid methods. This list is not exhaustive.

A unique feature of the Journal is the publication of unsuccessful efforts in applied computational electromagnetics. Publication of such material provides a means to discuss problem areas in electromagnetic modeling. Material representing an unsuccessful application or negative results in computational electromagnetics will be considered for publication only if a reasonable expectation of success (and a reasonable effort) are reflected. Moreover, such material must represent a problem area of potential interest to the ACES membership.

Where possible and appropriate, authors are required to provide statements of quantitative accuracy for measured and/or computed data. This issue is discussed in "Accuracy & Publication: Requiring quantitative accuracy statements to accompany data", by E.K. Miller, *ACES Newsletter*, Vol. 9, No. 3, pp. 23-29, 1994, ISBN 1056-9170.

EDITORIAL REVIEW

In order to ensure an appropriate level of quality control, papers are refereed. They are reviewed both for technical correctness and for adherence to the listed guidelines regarding information content. Authors should submit the initial manuscript in draft form so that any suggested changes can be made before the photo-ready copy is prepared for publication.

JOURNAL COPY INFORMATION

March issue	Copy deadline 13 January
July issue	Copy deadline 25 May
November issue	Copy deadline 25 September

STYLE FOR CAMERA-READY COPY

The ACES Journal is flexible, within reason, in regard to style. However, certain requirements are in effect:

1. The paper title should NOT be placed on a separate page. The title, author(s), abstract, and (space permitting) beginning of the paper itself should all be on the first page. The title, author(s), and author affiliations should be centered (center-justified) on the first page.

2. An abstract is REQUIRED. The abstract should state the computer codes, computational techniques, and applications discussed in the paper (as applicable) and should otherwise be usable by technical abstracting and indexing services.

3. Either British English or American English spellings may be used, provided that each word is spelled consistently throughout the paper.

4. Any commonly-accepted format for referencing is permitted, provided that internal consistency of format is maintained. As a guideline for authors who have no other preference, we recommend that references be given by author(s) name and year in the body of the paper (with alphabetical listing of all references at the end of the paper). Titles of Journals, monographs, and similar publications should be in boldface or italic font or should be underlined. Titles of papers or articles should be in quotation marks.

5. Internal consistency shall also be maintained for other elements of style, such as equation numbering. As a guideline for authors who have no other preference, we suggest that equation numbers be placed in parentheses at the right column margin.

6. The intent and meaning of all text must be clear. For authors who are NOT masters of the English language, the ACES Editorial Staff will provide assistance with grammar (subject to clarity of intent and meaning).

7. Unused space should be minimized. Sections and subsections should not normally begin on a new page.

MATERIAL, SUBMITTAL FORMAT AND PROCEDURE

The preferred format for submission and subsequent review, is 12 point font or 12 cpi, double line spacing and single column per page. Four copies of all submissions should be sent to the Editor-in-Chief (see inside front cover). Each submission must be accompanied by a covering letter. The letter should include the name, address, and telephone and/or fax number and/or e-mail address of at least one of the authors.

Only camera-ready original copies are accepted for publication. The term **"camera-ready" means that the material is neat, legible, and reproducible**. The preferred font style is Times Roman 10 point (or equivalent) such as that used in this text. A double column format similar to that used here is preferred. **No author's work will be turned down once it has been accepted because of an inability to meet the requirements concerning fonts and format.** Full details are sent to the author(s) with the letter of acceptance.

There is NO requirement for India ink or for special paper; any plain white paper may be used. However, faded lines on figures and white streaks along fold lines should be avoided. Original figures - even paste-ups - are preferred over "nth-generation" photocopies. These original figures will be returned if you so request.

While ACES reserves the right to re-type any submitted material, this is not generally done.

PUBLICATION CHARGES

ACES members are allowed 12 pages per paper without charge; non-members are allowed 8 pages per paper without charge. Mandatory page charges of $75 a page apply to all pages in excess of 12 for members or 8 for non-members. Voluntary page charges are requested for the free (12 or 8) pages, but are NOT mandatory or required for publication. A priority courtesy guideline, which favors members, applies to paper backlogs. Full details are available from the Editor-in-Chief.

COPYRIGHTS AND RELEASES

Each primary author must sign a copyright form and obtain a release from his/her organization vesting the copyright with ACES. Forms will be provided by ACES. Both the author and his/her organization are allowed to use the copyrighted material freely for their own private purposes.

Permission is granted to quote short passages and reproduce figures and tables from an ACES Journal issue provided the source is cited. Copies of ACES Journal articles may be made in accordance with usage permitted by Sections 107 or 108 of the U.S. Copyright Law. This consent does not extend to other kinds of copying, such as for general distribution, for advertising or promotional purposes, for creating new collective works, or for resale. The reproduction of multiple copies and the use of articles or extracts for commercial purposes require the consent of the author and specific permission from ACES. Institutional members are allowed to copy any ACES Journal issue for their internal distribution only.